Title
The Role of PLOD3 in Tumorigenesis of Head and Neck Squamous Cell Carcinoma

Author
Cui, Li

Publication Date
2018

Peer reviewed|Thesis/dissertation

UNIVERSITY OF CALIFORNIA

Los Angeles

The Role of PLOD3 in Tumorigenesis of Head and Neck Squamous Cell Carcinoma

A dissertation submitted in partial satisfaction of the

requirements for the degree Doctor of Philosophy

in Oral Biology

by

Li Cui

2018

ABSTRACT OF THE DISSERTATION

The Role of PLOD3 in Tumorigenesis of

Head and Neck Squamous Cell Carcinoma

by

Li Cui

Doctor of Philosophy in Oral Biology

University of California, Los Angeles, 2018

Professor Shen Hu, Chair

Metabolic remodeling is now widely regarded as a hallmark of cancer. However, the role of metabolic enzymes in the tumorigenesis of head and neck squamous cell carcinoma (HNSCC) is poorly known. We have identified many novel differentially expressed genes/metabolic enzymes and metabolites between HNSCC and adjacent normal tissues by using transcriptomic and metabolomic analyses. Here, procollagen-lysine, 2-oxoglutarate 5-dioxygenase 3 (PLOD3) was found to be significantly upregulated in HNSCC tumor tissues and cell lines. Patients with higher PLOD3 expression suffered poorer tumor differentiation and worse long term overall survival. This observation was also found in many other types of human cancers. PLOD3 downregulation

inhibited cancer cell proliferation, migration and invasion *in vitro* and tumor growth *in vivo,* and ectopic expression of PLOD3 potentiated (promoted) cancer cell proliferation, migration and invasion *in vitro* and tumor growth *in vivo.* In addition, we explored the potential molecular mechanisms accounting for the pro-carcinogenic role of PLOD3 in HNSCC. MiR-124-3p was demonstrated to be an upstream regulator of PLOD3. Overexpression of miR-124-3p suppressed the proliferation, migration and invasion capacity of HNSCC cells, whereas underexpression of miR-124-3p led to the opposite results. More importantly, PLOD3 overexpression partially rescued the tumor suppressive effect of miR-124-3p, indicating that miR-124-3p was a functional modulator of PLOD3. RNA sequencing (RNA-Seq) was performed to screen the potential downstream effectors of PLOD3. Functional analysis revealed the differentially expressed genes were enriched in actin cytoskeleton regulation and focal adhesion. Furthermore, we observed that PLOD3 downregulation changed the morphology of cancer cells, which failed to attach the surface of the petri dish. Therefore, we hypothesized that focal adhesion kinase (FAK) might be a potential downstream effector of PLOD3. PLOD3 downregulation suppressed the phosphorylation of FAK, PI3K and AKT, and *vice versa*. Furthermore, FAK inhibition significantly suppressed the tumor-promoting role of PLOD3 in HNSCC. In conclusion, our results have revealed a miR-124-3p-PLOD3-FAK/PI3K/AKT regulatory axis that contributes to the tumorigenesis of HNSCC and PLOD3 might represent a therapeutic target for HNSCC treatment.

The dissertation of Li Cui is approved.

Guoping Fan

Diana V Messadi

Kang Ting

Fariba S Younai

Shen Hu, Committee Chair

University of California, Los Angeles

2018

TABLE OF CONTENT

Chapter 1

Chapter 2

Chapter 3

LIST OF FIGURES

ACKNOWLEDGEMENTS

This dissertation would not have been possible without the generous support and help from the many people throughout my doctorate program. First and foremost, I would like to express my gratitude to Dr. Shen Hu for his mentorship, advice, guidance, insight as well as all the help. I would like to thank my committee members Dr. Guoping Fan, Dr. Diana Messadi, Dr. Kang Ting and Dr. Fariba Younai for their thoughtful advice, guidance, and encouragement. It is my great honor to have them as my committee members, and it is with much hope that I may have the opportunity to continually interact with them in the coming future.

Many thanks to Ms. Megan Scott and Mr. Matthew Dingman at the Oral Biology department for helping me dealing with the administrative situations. I want to thank all the current and past members of Hu Lab for their kind support. Lastly, I would like to acknowledge my family for their accommodation and support during my PhD studies. This would not have been possible without all your help.

BIOGRAPHICAL SKETCH	
NAME	**POSITION TITLE**
Li Cui	Graduate Student Researcher (GSR) in Division of Oral Biology and Medicine

EDUCATION/TRAINING

INSTITUTION AND LOCATION	DEGREE or Position	Completion Date MM/YYYY	FIELD OF STUDY
Sun Yat-sen University	D.D.S.	06/2010	Dentistry
Southern Medical University	M.S.	06/2013	Dentistry
University of California, Los Angeles	GSR	*in progress*	Oral Biology

Awards

Medical Scientific Research Grant of Guangdong Province (PI)

Outstanding paper award of 1st international conference for Cancer Metabolism and Treatment

Publications

1 **Cui L**, Liu J, Yan X, Hu S. Identification of metabolite biomarkers for gout using capillary ion chromatography with mass spectrometry. Anal Chem 2017; 89:11737-11743.
2 **Cui L**, Zhao X, Hu S. Determination of autoantibodies to salivary gland antigens by immunoblotting. Methods Mol Biol (Accepted).
3 **Cui L**, Xu SM, Ma DD, Gao J, Liu Y, Yue J, Wu BL. The role of integrin-a5 in the proliferation and odontogenic differentiation of human dental pulp stem cells. J Endod 2014; 40(2):235-40.
4 **Cui L**, Xu SM, Ma DD, Wu BL. The effect of TRPM7 suppression in the proliferation, migration and osteogenic differentiation of human dental pulp stem cells. Int Endod J 2014; 47:583-593.
5 Zhao X, Sun S, Zeng X, **Cui L***. Expression profiles analysis identifies a novel three-mRNA signature to predict overall survival in oral squamous cell carcinoma. Am J Cancer Res 2018; 8(3):450-461. (*Corresponding author)
6 Zhao X, Liang M, Li X, Qiu X, **Cui L***. Identification of key genes and pathways associated with osteogenic differentiation of adipose stem cells. J Cell Physiol 2018 [Epub ahead of print]. (*Corresponding author)
7 Xu SM, Ma DD, Zhuang R, Sun WJ, Liu Y, Wen J, **Cui L***. DJ-1 is upregulated in oral squamous cell carcinoma and promotes oral cancer cell proliferation and invasion. J Cancer 2016; 7:1020-1028. (*Correspondence author)

8 Chen H, Liu X, Jin Z, Liang M, **Cui L***, Zhao X. A three miRNAs signature for predicting the transformation of oral leukoplakia to oral squamous cell carcinoma. Am J Cancer Res 2018; 8:1403-1413 (*Corresponding author).
9 Chen H, Zhao X, Qiu Y, Xu D, **Cui L***, Wu B. The tubular penetration depth and adaption of four sealers: a scanning electron microscopic study. Biomed Res Int 2017; 2017: 2946524. (*Corresponding author).
10 Elzakra N, **Cui L***, Liu T, Li H, Huang J, Hu S. Mass Spectrometric analysis of SOX11-binding proteins in head and neck cancer cells demonstrates the interaction of SOX11 and HSP90α. J Proteome Res 2017; 16:3961-3968 (*Co-first author).
11 Ji EH*, **Cui L***, Yuan X*, Cheng S, Messadi D, Yan X, Hu S. Metabolomic analysis of human oral cancer cells with adenylate kinase 2 or phosphorylate glycerol kinase 1 inhibition. J Cancer. 2017; 8:298-304. (*Co-first author)
12 Liu Y*, **Cui L***, Huang JW, Ji EH, Chen W, Messadi D, Hu S. SOX4 promotes progression in OLP-associated squamous cell carcinoma. J Cancer 2016; 7:1534-1540. (*Co-first author)
13 Ma DD*, **Cui L***, Gao J, Yan WJ, Liu Y, Xu SM, Wu BL. Proteomic analysis of mesenchymal stem cells from normal and deep carious dental pulp. PLoS One 2014; 9:e97026. (*Co-first author).
14 Liu J*, **Cui L***, Yan X, Zhao X, Cheng J, Gao Q, Ye X, Hu S. Analysis of oral microbiota revealed high abundance of Prevotella intermedia in gout patients. Cell Physiol Biochem 2018; 49:1804-1812
15 **Cui L**, Cheng S, Liu X, Messadi D, Yang Y, Hu S. Syntenin-1 is a promoter and prognostic marker of head and neck squamous cell carcinoma invasion and metastasis. Oncotarget 2016; 7: 82634-82647.
16 **Cui L**, Elzakra N, Xu S, Xiao GG, Yang Y, Hu S. Investigation of three potential autoantibodies in Sjogren's syndrome and associated MALT lymphoma. Oncotarget 2017; 8:30039-30049.
17 Xu SM*, **Cui L***, Ma DD, Sun WJ, Wu BL. Effect of ITGA5 down-regulation on the migration capacity of human dental pulp stem cells. Int J Clin Exp Pathol 2015; 8: 14425-32. (*co-first author)
18 **Cui L**, Xu SM, Ma DD, Wu BL. Response to the “Letter to the Editor by Xu JL”. Int Endod J 2014; 47:1000.
19 Liu Y, Gao Y, Zhan XL, **Cui L**, Xu SM, Ma DD, Yue J, Wu BL, Gao J. TLR4 activation by lipopolysaccharide and Streptococcus mutants induces differential regulation of proliferation and migration in human dental pulp stem cells. J Endod 2014; 40:1375-1381.

Book Chapter
Cui L, Zhao X, Hu S. SOX genes and cancer. 2018. DOI: 10.5772/intechopen.

CHAPTER 1: Transcriptomics and metabolomics profiling of head and neck squamous cell carcinoma and matched adjacent normal tissues

1 INTRODUCTION

1.1 Head and neck squamous cell carcinoma (HNSCC)

1.1.1 Prevalence of HNSCC

Head and neck cancer (HNC) is the sixth most common cancer worldwide, accounting for approximately 630,000 new cases diagnosed and 350,000 cancer deaths every year[1]. Head and neck squamous cell carcinoma (HNSCC) is by far the most common type of HNC[2]. It encompasses epithelial malignancies that arise in the mucosal linings of the upper airway and food passages (paranasal sinuses, nasal cavity, oral cavity, pharynx, and larynx)[3,4]. The incidence rates of HNSCC increase with age. Males generally have a higher incidence rate than females, with the ratio ranges from 2:1 to 4:1[5]. Wide geographical variation exists in incidence around the world. High risk region of HNSCC includes Indian subcontinent, Australia, France, Brazil, and Southern Africa[6]. The decline in tobacco product use has contributed to the decreasing incidence of oral squamous cell carcinoma and laryngeal SCC in the developed countries[7]. However, in developed world there is a huge surge in the incidence of oropharyngeal squamous cell carcinoma (OPSCC) which is caused by human papilloma virus (HPV) infection[8-10]. HNSCC incidence rate is even various in the different ethnic groups in a specific geographical region. For instance, increased incidence of HNSCC was reported in black as compared to white male Americans. In addition, higher percentage of advanced staged, poor prognosis HNSCC was observed in black than white patients [11,12].

1.1.2 Risk factors of HNSCC

Tobacco and alcohol consumption are the major risk factors for HNSCC. They account for about 75% of all cases and have a multiplicative combined effect[13]. Smokeless tobacco products such as betel quid are important risk factors for oral cancer[14]. Virus infections is another recognized major risk factor for HNSCC. Human papillomavirus (HPV), mainly HPV type 16 and type 18, is detected in approximately 25% of all HNSCC[15]. HPV positive HNSCC are more commonly found in OPSCC (tonsillar and base of tongue) compared with other regions such as oral cavity and laryngeal. Other contributing risk factors include genetic factors, family history of HNSCC, older age, sun exposure, poor dental hygiene and dietary habits[6,16].

1.1.3 Diagnosis and staging of HNSCC

Early detection of HNSCC is extremely important for improving the prognosis[17]. However, currently there is no proven screening method. A thorough history inquiry and combination of inspection, palpation, indirect mirror examination, or direct flexible laryngoscopy contribute to the initial assessment of the primary tumor. Computed tomography (CT), magnetic resonance imaging (MRI), positron emission tomography (PCT) and integrated PCT/CT are valuable for assessing the degree of local infiltration, involvement of regional lymph nodes, and presence of distant metastases or second primary malignancies. Confirmed diagnosis of HNSCC is based on histology of the biopsy from the primary site. However, suspicious lesions are often relatively inaccessible for histological assessment. Fine needle aspiration (FNA) biopsy might be performed instead. FNA biopsy is also often used for an initial tissue diagnosis of HNSCC when a patient presents with a neck mass without an obvious primary tumor.

Accurate staging is an important guidance for therapeutic decision making. The tumor, node, metastases (TNM) staging system of the American Joint Committee on Cancer (AJCC) and the Union for International Cancer Control (UICC) is widely used to classify HNSCC[18]. "T" describes the extent of primary tumor (T), "N" refers to absence or presence and extent of metastatic regional lymph node(s), and "M" indicates the absence or presence of distant metastasis. One significant shortcoming of TNM system is that it does not include pathological or biological parameters. Therefore, molecular staging has become a relatively new concept in the past decade. Combination of TNM staging system and molecular staging might be helpful to guide precise medicine in the coming future.

1.1.4 Molecular events of HNSCC carcinogenesis

Sustaining proliferative signaling, evading growth suppressors, resisting cell death, enabling replicative immortality, inducing angiogenesis, activating invasion and metastasis, deregulating cellular energetics, genome instability and mutation, avoiding immune destruction and tumor promoting inflammation are regarded as ten hallmarks of cancer[19] . The epidermal growth factor receptor (EGFR) is a growth factor receptor that plays a crucial role in regulating growth and cell survival[20]. EGFR is overexpressed in up to 90 % of HNSCC[21]. Transforming growth factor-α (TGF-α), a primary autocrine ligand of EGFR, is also highly increased in HNSCC[22]. Activation of TGF-α-EGFR axis is important for maintaining the sustaining proliferative capacity of HNSCC cells. Cancer cells also inhibit the tumor growth suppression signaling. *TP53* is the most frequently mutated tumor suppressor gene in HNSCC. About 70.4% of HNSCC cases from The Cancer Genome Atlas (TCGA) database have *TP53* mutation[23]. P53 functions as a transcriptional factor and exerts a tumor suppressive role by regulating a number of

downstream target genes involved in cell-cycle arrest, apoptosis, antioxidant response, cell senescence, DNA repair, and metabolism[24,25]. Another major tumor suppressor is retinoblastoma protein (RB). RB is a central regulator of cell cycle entry by inhibiting the E2F family of DNA-binding transcription factors (E2F)[26]. Resistance to cell death is a feature of cancer cells. Loss of p53 function and an increase in EGFR signaling help HNSCC cells resist to apoptosis. Phosphoinositide 3-kinase (PI3K)-protein kinase B (PKB, also known as AKT) signaling pathway is a downstream effector of EGFR and commonly overexpressed in HNSCC[27]. Telomerase is a reverse transcriptase that synthesizes *de novo* telomeric repeats, which counteracts terminal DNA sequences loss from chromosomes ends and maintains the proliferative capacity of stem cells[28]. Telomerase is aberrantly active in HNSCC, which ensures the replicative immortality of cancer cells[29]. Angiogenesis is important for tumor growth, as it only provides the required oxygen and nutrients, but also facilitates to remove metabolic wastes and carbon dioxide. Cancer cells can send the signal to the adjacent tissues and activate the growth factors, which contribute the formation of new blood vessels. Under hypoxia condition, the expression levels of pro-angiogenic factors, such as vascular endothelial growth factor (VEGF), platelet-derived growth factor (PDGF), fibroblast growth factors (FGF 1 and 2) and epidermal growth factor (EGF). VEGF is overexpressed in HNSCC, and upregulation of VEGF is closely associated with poor prognosis of HNSCC[30]. Epithelial to mesenchymal transition (EMT) is a dynamic and complex cellular process that plays an essential role in the development of metastatic disease[31]. Cancer cells must degrade the basement membrane and the structure of extracellular matrix to promote invasion and metastasis. Upregulation of matrix metalloproteinases MMP-2 and MMP-9 is important for increasing the invasion and metastasis capacity of HNSCC cells[32]. An emerging feature of cancer is the abnormal tumor metabolism.

For instance, normal differentiated cells primarily generate the cellular energy through mitochondrial oxidative phosphorylation. However, most cancer cells rely on aerobic glycolysis instead. This phenomenon is called "the Warburg effect"[33]. Oncometabolites refers to metabolites whose upregulation can promote the tumorigenesis. A couple of oncometabolites such as fumarate, succinate, 2-hydroxyglutarate (2-HG) have been discovered so far[34]. Our group also has demonstrated that the levels of metabolites in aerobic glycolysis pathway were significantly overexpressed in the oral cancer stem cells compared to non-cancer stem cells[35]. An efficient cytotoxic T lymphocytes (CTLs) response is important for activating the immune system. Cell surface leukocyte antigen (HLA) class I molecules is necessary for the presentation of peptide antigens to activating CTLs. However, the expression level of HLA class I was down-regulated in about 50 % of HNSCC, which might help the cancer cells evade immune destruction[36]. Genomic instability refers to an increased frequency of genome alteration during cell division, which is a feature of cancer cells. *PIK3CA, EGFR, CCND2, KDM5A, ERBB2, PMS1, FGFR1* and *WHSCIL1* were commonly amplified, and *CDKN2A, SMAD4, NOTCH2, NRAS* and *TRIM33* were frequently deleted in both HNSCC cell lines and tumors[37]. Various immune cells include neutrophils, monocytes, macrophages, mast cells, dendritic cells, lymphocytes and fibroblasts are found in tumor microenvironment. Inflammatory mediators and inflammatory cells[38]. Upregulation of inflammatory cytokines and mediators such as prostaglandin E2 (PGE2) and interleukin-1 (IL-1) in HNSCC promotes tumor growth, invasion, angiogenesis and metastasis[39].

1.1.5 Treatment approaches for HNSCC

Surgery is the major treatment option for primary and recurrent HNSCC. In most cases, various treatment methodologies include surgery, radiation, and chemotherapy are combined for the management of HNSCC[40]. For early stage HNSCC, the patients are usually treated with surgery and radiotherapy. For the advanced stage HNSCC, chemotherapy is commonly required. Cisplatin remains the cornerstone for treating recurrent and metastatic HNSCC. Administration of cisplatin or other chemotherapeutic drugs such as 5-fluorouracil (5-FU) can significantly enhance the efficiency of radiotherapy[41]. Cetuximab (EGFR monoclonal antibody) in combination with platinum/5-FU has become a new alternative regimen for platinum refractory HNSCC[42].

1.2 Omics approaches in cancer research

High-throughput omics technologies such as genomics, transcriptomics, proteomics, and metabolomics are powerful tools that allow us to dissect the entire phenotypic and functional network of genes, proteins and metabolites present in a cell or organism. Cancer is a heterogeneous disease with unique genomic and phenotypic features. There are great differences among different patients (intertumor heterogeneity) and even within each individual tumor (intratumor heterogeneity) [43,44]. Traditional molecular biology is important for revealing the role of a specific molecule or pathway in tumorigenesis. However, it cannot provide a panoramic view of the deregulated molecules or pathways in the cancer samples from an individual. In addition, it is impossible for traditional molecular biology to investigate how the changes in a specific molecule affects other molecules or pathways in cancer cells globally. Omics techniques are able to discriminate the clinical tumor subtypes among individuals and provide the guidance of personalized cancer management. TCGA and the International Cancer Genome Consortium

(ICGC) provide large-scale genomic, transcriptomic, epigenomic, proteomic data and clinical data for various types of cancers, which have contributed to highlight the similarities and differences of biological information for each cancer and across multiple type[45,46].

Genomics provides the order of DNA in a genome at single base pair resolution[47]. Cancer genomic is the study of the totality of DNA sequence and gene expression differences between tumor cells and normal host cells. With the advancement in the genomics technologies, many novel genetic alterations such as genomic loss or amplification, mutations in coding regions, chromosomal rearrangements, aberrant methylation, and expression profiles have been discovered in various types of cancers. The representative technologies of genomics include whole genome sequencing (WGS), targeted sequencing and genotyping[48]. Transcriptomics is the study of the complete set of RNA transcripts that are produced by the genome. Based on the difference of the global mRNA profile between tumor and normal samples, transcriptomics is widely applied in cancer diagnosis, prognosis predication and drug discovery and development [49]. In addition to mRNA, non-coding RNAs such as microRNAs (miRNAs), long non coding RNAs (lncRNAs) and circular RNAs (or circRNAs) have been demonstrated to play a crucial role in tumorigenesis [50-52]. The representative technologies of transcriptomics include microarray and RNA sequencing (RNA-seq). Proteomics is defined as the large-scale study of proteins produced in an organism, system, or biological context. Proteins are the active key players maintaining normal cellular functions. Poor association between mRNA and abundance and corresponding protein levels are very common, indicating genetic abnormalities in tumor cells do not accurately portray the situation at the protein levels[53]. Proteomics has wide applications for the discovery of diagnostic, prognostic and predictive biological markers as well as novel drug

targets in human cancer. The representative technologies of proteomics include two-dimensional gel electrophoresis (2-DE), 2-D difference gel electrophoresis (DIGE), liquid chromatography–mass spectrometry (LC-MS), surface-enhanced laser desorption/ionization time-of-flight (SELDI-TOF)-MS, isotope-coded affinity tag technology, reverse-phase protein arrays, and antibody microarray[54,55]. Metabolomics is the systematic study of small molecule profiles in the context of physiological stimuli or disease states. It has emerged as a powerful analytical methodology for studying metabolic pathways, gene networks, and systems biology. With the development of MS and nuclear magnetic resonance (NMR) spectroscopy methods, metabolomics has played an important role for screening novel biomarkers for cancer diagnosis, prognosis, or treatment efficacy monitoring. Due to the highly complex nature and wide concentration range of the small molecules, separation science is crucial for achieving a comprehensive profiling analysis [56]. Various separation techniques such as capillary electrophoresis, gas chromatography (GC), or LC have greatly enhanced the strength of MS-based metabolomics. The representative technologies of metabolomics include NMR-based metabolomics, GC-MS-based metabolomics, LC-MS-based metabolomics and UPLC-MS-based metabolomics[57,58].

2 MATERIALAS AND METHODS

RNA-seq library preparation and sequencing

Disruption and homogenization of the frozen tissues were achieved by using pestle and QIA shredder (QIAGEN, Hilden, Germany). Then RNeasy Mini Kit (Qiagen) was employed to isolate the total RNA from tissue samples based on manufacturer's instructions. DNase I was used to degrade the DNA contaminant in the samples. RNA molecules were further purified

with oligo (dT)-attached magnetic beads. The RNA intensity was evaluated using a 2,100 Bioanalyzer (Agilent Technologies Inc, Santa Clara, CA, USA) and only tissue samples with an RNA Integrity Number (RIN) value greater than or equal to 7 were selected for constructing the sequencing library. Purified RNA was then fragmented using RNA fragmentation reagents. First-strand cDNA was generated using random hexamer-primed reverse transcription, then was followed by a second-strand cDNA synthesis. The synthesized cDNA was subjected to end-repair and then was 3' adenylated. Adaptors were ligated to the ends of these 3′ adenylated cDNA fragments and PCR was used to amplify the cDNA fragments. The amplified products were purified with the solid phase reversible immobilization (SPRI) beads, and dissolved in EB solution. The PCR products were denatured by heating and circularized in the presence of the splint oligo sequence. After PCR enrichment and purification of adapter-ligated fragments, the concentration of DNA with adapters was determined with Applied Biosystems 7500 Fast Real-Time PCR System (Applied Biosystems, Foster City, CA, USA) using primers QP1 5′-AATGATACGGCGACCACCGA-3′ and QP2 5′- CAAGCAGAAGACGGCATACGAGA-3′. The length of the DNA fragment was measured using a 2,100 Bioanalyzer (Agilent Technologies Inc).

DNA nanoballs (DNBs) were generated with the ssDNA circle by rolling circle replication (RCR). The DNBs were load into the patterned nanoarray and single-end read of 50 base pair were read through on the BGISEQ-500 platform. Base-calling was performed by the BGISEQ-500 software version 0.3.8.1111.

Data filtering

The reads which contain the sequence of adaptor, high content of unknown bases and low quality reads were removed before further analysis. The steps for filtering are as follows:

Firstly, the FastQC v0.11.5 software was employed to evaluate the quality of the RNA-seq Then, the reads were chosen based on the following parameters: (1) trimming and cleaning reads that aligned to primers and/or adaptors, (2) deleting reads with over 50% of low-quality bases (quality value ≤5) in one read, and (3) reads with over 10% unknown bases (N bases). After filtering, the remaining reads are called 'clean reads' and stored as FASTQ format.

Ingenuity pathway analysis (IPA)

Identified metabolic enzymes at significantly differential expression levels (a corrected p value less than 0.05 and a fold change value more than 2) were subjected to IPA analysis (Ingenuity System, Redwood City, CA, USA). Accession numbers of detected metabolic enzymes (Gene ID) were listed in MS Excel and imported into IPA to map the canonical pathways. Data were submitted as fold change values (ratios) calculated against the control group (HNSCC tissues/adjacent normal tissues) and p values. Downstream metabolic pathways were scored in accordance to the ontology support using Ingenuity Knowledge Base (http://www.ingenuity.com/science/knowledge-base).

Pathway analysis

Gene Set Enrichment Analysis (GSEA) was used to identify groups of genes enriched in either the HNSCC tissues or adjacent normal tissues. The GSEA analysis tool (version 3.0) was downloaded from the Broad Institute website (http://www.broadinstitute.org/gsea/index.jsp). Curated gene sets of Kyoto Encyclopedia of Genes and Genomes (KEGG) pathways were downloaded from the Broad Institute's Molecular Signatures Database. Pathways with no

correlation with HNSCC were excluded. Both small (< 5 genes) and large (> 500 genes) gene sets were excluded from the analysis. Heatmap was generated using Morpheus software from the Broad Institute (https://software.broadinstitute.org/morpheus/).

Metabolite extraction

The steps for metabolites were as follows: 1) 40 μl liquid sample was added into 96-well plate. 2) 120 μl methyl alcohol (-20 °C) was added to the well above and vortex mixed. 3) Stored overnight at -20 °C for 30 minutes. 4) Centrifuged at 4000g for 20 minutes at 4°C. 5) Collected supernatants to new tube until LC-MS analysis. The supernatants (5μl from every sample) of all the studied samples were pooled as the quality control (QC). The QC sample was injected regularly throughout the run (after every 10 samples) to monitor the stability of the analytical platform. This QC sample was also used to condition the column at the beginning of the UPLC /MS run, because the first injections of a batch are often not reproducible.

UPLC-MS/MS Analysis

All chromatographic separations were performed using an UPLC system (Waters, Milford, MA, USA). An ACQUITY UPLC BEH C18 column (100mm*2.1mm, 1.7μm, Waters) was used for the reversed phase separation. The column oven was maintained at 50 °C. The flow rate was 0.4 ml/min and the mobile phase consisted of solvent A (water + 0.1% formic acid) and solvent B (acetonitrile+ 0.1% formic acid). The following gradient elution conditions were used to elute metabolites: 0～2 min，100% phase A; 2~12 min 0% to 100% B; 11~13 min, 100% B; 13～15 min, 100% A. The injection volume for each sample was 10 μl. A high-resolution tandem mass spectrometer SYNAPT G2 XS QTOF (Waters) was used to detect metabolites eluted form the column. The Q-TOF was operated in both positive and negative ion modes. For positive ion

mode, the capillary and sampling cone voltages were set at 2 kV and 40 V, respectively. The mass spectrometry data were acquired in Centroid MSE mode. The TOF mass range was from 50 to 1200 Da and the scan time was 0.2 s. For the MS/MS detection, all precursors were fragmented using 20-40 eV, and the scan time was 0.2 s. During data acquisition, the signal was gained every 3 s for real-time quality correction. A quality control sample (equal pool of all samples) was acquired after every 10 samples to evaluate the stability of the instrument during measurements.

Peak peaking & identification

Peak peaking is achieved primarily through the Progenesis QI (version 2.2), which includes steps such as peak alignment, peak extraction, normalization, deconvolution, and compound identification. The main parameters for peak extraction and identification are set as below:

Mode	Adducts	Peak alignment	Peak extraction	Normalization	Mass deviation
Positive	[M+H]+ [M+NH_4]+ [M+K]+ [M+Na]+ [M+H-H_2O]+	QC	Default	Default	10ppm
Negative	[M-H]- [M+Cl]-	QC	Default	Default	10ppm

Statistically analysis

For the RNA-seq study, the clean reads were mapped to assembled reference sequence database by software Bowtie2 and then the fragment for each unigene was calculated from the mapping results. The relative levels of the unigenes were counted by dividing the unigene's FPKM value in cancer tissue samples with the same unigene FPKM value in the adjacent normal tissue samples. Differentially expressed genes (DEGs) were filtered to satisfy both *P*-value and fold-change criteria simultaneously ($|\log_2 (\text{Fold change})| \geq 1$ and FDR<0.05). The *P*-values were obtained using the unpaired Student's *t*-test and the false discovery rate (FDR) was controlled by the Benjamini and Hochberg algorithm. For the metabolomics study, the raw data were converted into CDF format using the Masslynx version 4.1 (Waters Corp., Manchester, UK) and import into the Progenesis QI software (version 2.0), which allowed the generation of a data matrix with retention time (RT), mass-to-charge ratio (m/z) values, and peak intensity. The main parameters were at default settings. The low weight ion (RSD > 30%) was removed from the extracted data, and the QC-RLSC (Quality control-based robust LOESS signal correction) method was adopted to correct the data. Differential metabolites were identified based on q-values (adjusted p-values using Benjamini-Hochberg procedure) and false discovery rate (FDR) of ≤ 0.05, FC ≥ 1.2 or ≤ 0.833, and variable importance in projection (VIP) score ≥ 1 from the PLS-DA model.

3 RESULTS

3.1 The DEGs between HNSCC and adjacent normal tissues

A volcano plot was generated to visualize the distribution of expressed genes between HNSCC and paired adjacent normal tissues. Red or blue dots in the plots represented significantly

upregulated or downregulated genes respectively (Figure 1A). In total, 10,811 (6,653 upregulated and 4,158 downregulated) significantly changed genes were identified. Heat maps were generated based on the expression levels of DEGs. Each column represents a biological sample and each row in the heat map represents a gene. The color indicates the expression levels of genes between HNSCC tissues and adjacent normal tissues **(Figure 1B)**.

3.2 GSEA analysis of the DEGs

The nominal p-value of <0.05 and false-discovery rate (FDR) q-value of <0.25 were set as the cutoff value. The top enriched pathways in the malignant samples included cell cycle, DNA replication, homologous recombination, purine metabolism, pyrimidine metabolism, snare interactions in vesicular transport, spliceosome, proteasome, basic transcriptional factors, and N-glycan biosynthesis **(Figure 2A-2J)**. The top pathways in non-malignant samples included citrate TCA cycle, oxidative phosphorylation, fatty acid metabolism, PPAR signaling pathway, calcium signaling pathway, propanoate metabolism, butanoate metabolism, tryptophan metabolism, alanine and aspartate and glutamate pathway, and valine leucine and isoleucine degradation. **(Figure 3A-3J)**

3.3 Global profiling of tissue metabolites in HNSCC and adjacent normal tissues

To discover potential metabolite biomarkers, we first profiled samples from 39 HNSCC tissues and 39 paired adjacent normal tissues with UPLC-MS/MS. In total, 14941 (positive ion mode: 9151; negative ion mode: 5790) metabolic features were found to be present in the study groups. UPLC-MS/MS with the Progenesis QI software allow to detect 4,538 significantly changed metabolic features (2,706 upregulated and 1,832 downregulated) between HNSCC tissues and

adjacent normal tissues **(Figure 4A)**. The heat maps exhibited the different distribution patterns of metabolites between HNSCC tissues and adjacent normal tissues **(Figure 4B)**. The PLS-DA scores plot showed that the cancer tissues cluster distinctly to the left; whereas the adjacent normal tissues cluster distinctly to the right with little overlapping with the cancer tissues. The PLS-DA analysis showed a high degree of segregation between cancer tissues and adjacent normal tissues in the positive and negative electrospray ionization modes **(Figure 4C).**

3.4 The differentially expressed metabolites between HNSCC and adjacent normal tissues

To further identify potential metabolites, both HMDB (http://www.hmdb.ca/) and Metlin (https://metlin.scripps.edu/) databases were searched using accurate mass and mass spectrometric fragmentation patterns. The expression levels of various acylcarnitines (2-hydroxymyristoyl carnitine, 2-methylbutyroyl carnitine, 3-hydroxypenta decanoyl carnitine, 3-hydroxyl undecanoyl carnitine, 12-hydroxy-12-octadecanoylcarnitine, arachidyl carnitine, cervonyl carnitine, cis-5-tetradecenoyl carnitine, clupanodonyl carnitine, dodecanoylcarnitine, heptadecanoyl carnitine, hydroxyvaleryl carnitine, L-palmitoylcarnitine, methylmalonyl carnitine, stearoylcarnitine, succinylcarnitine, tetracosatetraenoyl carnitine and tetradecanoyl carnitine) were all significantly increased in HNSCC tissues **(Figure 5A-5B)**. Another significantly upregulated pathway in HNSCC tissues was sphingosine-1-phosphate (S1P) pathway. The levels of metabolites in the S1P pathway (ceramides, sphingosine, S1P, phosphonoethanolamine, palmitaldehyde and hexadecenal) were higher in the cancer tissues **(Figure 6)**. Interestingly, various types of DNA damage markers including 1-methyladenine, 8-hydroxyadenine, FAPy-adenine, 5-methycytosine, 8-Oxo-dGMP, 3'-O-methylguanine, 8-hydroxyguanine and 8-hydroxyl-deoguanine were upregulated in the HNSCC tissues compared with the adjacent normal tissues

(Figure 7). The biosynthesis of specific bases (adenine, cytosine, guanine and uracil), nucleoside (guanosine), amino acid (L-asparagine, L-aspartic acid, L-glutamic acid, L-valine, L-proline and L-serine), and nucleotide derivatives (adenosine monophosphate, cytodine monophosphate, cytidine 2',3'-cyclic phosphate and uridine 2',3'-cyclic phosphate) and pyrimidine nucleotide sugars (UDP-N-acetyl-alpha-D-galactosamine, uridine diphosphate-N-acetylglucosamine and uridine diphosphategalactose) were also increased in the tumor tissues **(Figures 8-9)**. The lipid metabolism was also remarkably altered HNSCC tissues. For instance, CE (20:4(5Z, 8Z, 11Z, 14Z), CE (20:2(6Z, 9Z)), PC (14:0/16:0), PIP (16:0/20:4(5Z, 8Z, 11Z, 14Z)), PE (16:1(9Z)/18:2 (9Z, 12Z)), PE (18:1(11Z)/18:2(9Z, 12Z)), PE(14:0/20:2(11Z,14Z)), PE(18:1(11Z)/20:5(5Z,8Z,11Z,14Z,17Z)), and PE(18:1(9Z)/22:5(4Z,7Z,10Z,13Z,16Z)) and PE(14:0/14:0) were increased in cancer tissues **(Figure 10)**. The metabolites in the melatonin pathways (L-tryptophan, 5-hydroxytryptophan, N-acetylserotonin, melatonin, cyclic melatonin, 6-sulfatoxymelatonin and 6-hydroxymelatonin glucuronide) were downregulated in HNSCC tissues **(Figure 11)**. The levels of several metabolites in the vitamin D pathway (vitamin D3, calcidiol and 24-hydroxycalcitriol), coenzyme Q10 pathway (ubiquinone-2 and coenzyme Q10), and retinoic acid pathway (4-oxo-retinoic acid and 4-hydroxyretinoic acid) were decreased in cancer tissues **(Figure 12A-12C)**. The levels of some interesting metabolites such as hippuric acid, N-butyrylglycine and ganglioside GM3 (d18:0/12:0) were also found to be reduced in the HNSCC samples **(Figure 13)**. Finally, many lipids such as DG(20:5n3/0:0/22:6n3), LysoPE(20:5(5Z,8Z,11Z,14Z,17Z)/0:0), LysoPC(10:0), PS(MonoMe(11,3)/MonoMe(11,5)), PC(22:5(4Z,7Z,10Z,13Z,16Z)/22:6(4Z,7Z,10Z,13Z,16Z,19Z))), PS(18:0/18:0), , PE(16:0/22:6(4Z,7Z,10Z,13Z,16Z,19Z)), PS(18:0/18:1(9Z)), MG(18:4(6Z,9Z,12Z,15Z)/0:0/0:0),

PS(20:3(8Z,11Z,14Z)/20:3(8Z,11Z,14Z)), and were downregulated in tumor samples **(Figure 14)**.

3.5 IPA analysis of the differentially expressed metabolic enzymes between cancer and adjacent normal tissues

A total of 721 differentially expressed metabolic enzymes (403 upregulated and 318 downregulated) were detected between HNSCC and adjacent normal tissues. The heat map exhibited the different distribution patterns of metabolic enzymes between HNSCC and adjacent normal tissues **(Figure 15A)**. IPA analysis showed that the glycolysis, pyrimidine deoxyribonucleotides de novo biosynthesis I, and pyrimidine ribonucleotides de novo biosynthesis etc. were upregulated in cancer tissues, while tRNA splicing, oxidative phosphorylation and fatty acid oxidation etc. were downregulated in tumor samples **(Figure 15B)**.

4 DISCUSSION

In the RNA-seq study, we have identified many consistently altered genes between HNSCC and the adjacent normal control tissues. GSEA revealed many meaningful pathways that are closely associated with carcinogenesis. GSEA is a very powerful platform for interpreting gene expression data, such as microarray and RNA seq data. The advantage of GSEA over single-gene methods with individual genes is that it performs the analysis of whole sets of functionally related groups of genes. It is less likely that a group of genes were falsely perturbed at the same time than a single gene was. Therefore, it exhibits better performance for detecting biologically significant changes. In addition, when the members from the same gene set have strong

correlation, GSEA can enhance the signal-to-noise ratio and boost the possibility to detect modest changes in individual genes[59].

Cell cycle and DNA replication were the top gene sets enriched in HNSCC tissues. Cell homeostasis is regulated by a balance among proliferation, growth arrest and apoptosis[60]. Cell cycle machinery controls cell proliferation and uncontrolled cell proliferation is one of the main hallmarks of cancer. Cyclin-dependent kinases (CDKs) are serine/threonine kinases and plays an important role in regulating the progression of the cell cycle in eukaryotes[61,62]. The expression levels of *CDK1, CDK2, CDK4, CKD6* and *CDK7* were all significantly increased in cancer tissues compared with the normal controls. Cyclins are the regulatory subunits of CDKs and promote cell cycle progression by activating CDKs. Similarly, the levels of cyclins encoded genes (*CCNA2, CCNB1, CCNB2 CCND1, CCND2, CCND3* etc) were remarkably upregulated in HNSCC tissues. However, the inhibitor of CDKs (*CDKN1C*) was downregulated in cancer tissues. Based on the heat map data, we also found some oncogenes were significantly increased in HNSCC tissues. For instance, Myc is a master regulator which controls almost every aspect of the oncogenic processes such as proliferation, survival, apoptosis, differentiation, and metabolism[63,64]. PLK1 regulates the initiation, maintenance, and completion of mitosis. Its overexpression has been reported in a variety of human cancers and was associated with unfavorable clinical outcome[65]. The rate of DNA replication is higher in cancer cells to ensure the rapid growth of tumor. DNA polymerase delta consists of 4 subunits: POLD1, POLD2, POLD3, and POLD4, plays an important role in DNA replication and repair[66]. Our results showed that the expression levels of *POLD1, POLD2 and POLD3* were higher in HNSCC tissues compared to adjacent normal tissues. Proliferating cell nuclear antigen (PCNA) is a highly-conserved protein found in all eukaryotic species as well as in Archaea. It serves as a

processivity factor for DNA polymerase δ and is essential for replication[67]. The level of *PCNA* was also significantly higher in HNSCC tissues. Loss of heterozygosity (LOH) is one of the most frequent genetic alteration in cancer cells, which indicates that the genetic information at a chromosomal locus is from only one parental chromosome rather than from both parental chromosomes. Elevated levels of homologous recombination might accelerate the frequency of LOH[68]. Purines and pyrimidines are the most abundant metabolic substrates for all living organisms. They are the building blocks for DNA and RNA as well as provide the necessary energy and cofactors to promote cell survival and proliferation[69]. High concentration of purines and pyrimidines have been observed in tumor cells. Thymidine phosphorylase encoded by TYMP is a nucleoside metabolism enzyme that catalyzes the conversion of thymidine to thymine and 2-deoxy-α-D-ribose-1-phosphate (dRib-1-P). TP is widely overexpressed in human cancers and is correlated with unfavorable prognosis. Upregulation of TP promotes metastasis, invasion, angiogenesis and cell death evasion[70]. Soluble N-ethylmaleimide-sensitive factor (NSF) attachment protein receptors (SNAREs) are key proteins which various cellular processes such as synaptic vesicle fusion, membrane fusion and transmitter release. Certain members of SNARES have been shown to be closely associated with tumor progression[71]. For instance, our results showed that YKT6 was increased in HNSCC tissues. Cancer cells derived exosomes are not only involved in tumor growth, metastasis and chemoresistance, but also served as key players for the intercellular communication between cancer cells and stromal cells[72]. YKT6 is a SNARE protein and has been shown to control the exosome release in lung cancer cells[73]. Alternative splicing of mRNA precursor is important for proteomic diversity and gene expression. However, accumulation of certain alternatively spliced products might be associated with cancer development[74,75]. Serine/arginine-rich splicing factor 3 (SRSF3) is the smallest member of

serine/arginine-rich (SR) family of proteins and plays important roles in RNA metabolism and functions such as regulation of alternative RNA splicing, mRNA export from nucleus, pri-miRNA processing and cap-independent translation. SRSF3 is upregulated in various types of cancers and acts as a promoter in tumorigenesis[76]. The proteasome is a multicatalytic proteinase complex involving in the degradation of most intracellular proteins, which plays a critical role in regulating cellular function and maintaining homeostasis[77]. The proteasome beta-4 subunit (PSMB4) is indispensable for the assembly of 20S proteasome complex which is a crucial part of the ubiquitin–proteasome system (UPS). Recent studies have reported that PSMB4 is overexpressed in various tumors and positively regulate carcinogenesis[78]. Transcription factors (TFs) are commonly deregulated in tumorigenesis. In cancer cells, genes encoding TFs are often amplified, deleted, rearranged via chromosomal translocation, or subjected to point mutations that lead to a gain- or loss-of-function[79]. For instance, both TAF2 copy number and mRNA were significantly overexpressed in 73% of high-grade serous ovarian cancers (HGSC)[80]. Glycosylation is the most complex post-translational modification step for protein biosynthesis, which leads to various functional changes of glycoproteins[81]. Alterations in the sugar chains contribute to the malignant phenotypes of cancer cells. Ribophorin II (RPN2) is a highly conserved glycoprotein and is part of an N-oligosaccharyl transferase complex. RPN2 promotes the oncogenic phenotypes of breast cancer cells by enhancing the glycosylation of CD63[82].

The gene sets oxidative phosphorylation and citric tricarboxylic acid (TCA) cycle were enriched in adjacent normal tissues. Normal cells primarily use mitochondrial oxidative phosphorylation (OXPHOS) to generate ATP for energy. However, the metabolic activities of tumor cells preferentially rely on glycolysis over OXPHOS for glucose-dependent ATP production[83]. The succinate dehydrogenase (SDH) complex is consisted of five proteins encoded by SDHA,

SDHB, SDHC, SDHD, and SDHAF2. Loss of SDHA by mutation has been found in various types of cancers such as paraganglioma, pheochromocytoma and gastrointestinal stromal tumors [84,85]. Decreased in SDHA levels might result in accumulation of succinate acid, which is regarded as an oncometabolite[86]. Our results showed that the expression level of SDHA was consistently downregulated in HNSCC tissues compared with the normal controls, further studies are needed to explore whether SDHA is mutated in HNSCC. There is increasing evidence that cancer cells frequently exhibit specific alteration in fatty acid metabolism. Acyl-CoA synthetase 1 (ACSL1) is important for converting free long-chain fatty acids into fatty acyl-CoA esters. It may play a potential oncogenic role in colorectal and breast cancer and acts as a tumor suppressive gene in lung cancer[87], indicating the role of ACSL1 in tumorigenesis might be dependent on cancer types. Peroxisome proliferator-activated receptors (PPARs) are ligand-dependent transcription factors that are activated by fatty acids and their derivatives. The PPAR family comprises three members, PPARα, PPARβ/δ, and PPARγ. PPARα agonist could significantly lead to reductions in tumor growth and vascularization[88]. Our results showed that PPARα was downregulated in HNSCC, indicating that it might play a tumor suppressive role in tumorigenesis. The intracellular calcium ions (Ca^{2+}) as a second messenger is required for the regulation of many cellular processes such as gene transcription, cell proliferation, differentiation and survival[89]. Intracellular Ca^{2+} homeostasis is altered in cancer cells, which is closed associated with tumor initiation, angiogenesis, progression and metastasis. Deficiency of propionyl-CoA carboxylase subunit alpha (PCCA) might lead to propionic academia. Gut microbiota-derived propionate inhibited the proliferation of cancer cells[90]. In addition, propionate generated either by bacteria or during cellular metabolism exhibited immunoregulatory function and may contribute to cancer prevention[91]. The downregulation of

PCCA in HNSCC tissues might lead to decreased level of propionate, and its reduction might promote tumor development. Butyrate is a bacterial metabolite mainly found in the large intestine lumen, and it can inhibit the proliferation of human colon carcinoma cells[92]. Similar to intestine, oral cavity is also home to microbial communities. Overwhelming body of study has showed there were close association between bacterial and HNSCC development[93]. We speculate that downregulation of propionate metabolism in HNSCC might promote carcinogenesis. Several amino acid metabolism including tryptophan metabolism, alanine and aspartate and glutamate pathway, and valine leucine and isoleucine degradation were found to be enriched in adjacent normal tissues. Further studies are needed to explore their role in carcinogenesis of HNSCC.

Cancer cells can reprogram their metabolism to generate the energy and the biosynthetic intermediates to survive in the harsh and hypoxic environment. Although altered metabolism is recognized as a hallmark of cancers, it remains unclear which pathways are crucial in regulating metabolic plasticity. In this metabolomics study, we have demonstrated that UPLC with Orbitrap MS is a powerful method for separation and identification of the dysregulated metabolites in cancer tissues and adjacent normal tissues. The identified metabolites not only include known biomarkers of HNSCC but also encompass a set of novel biomarkers that might be associated with the disease progression of HNSCC.

Accumulation of acylcarnitine species is one of the most changed pathway in HNSCC tissues. The deregulated fatty acid oxidation (FAO) might be one possibility accounting for our observation of increased acylcarnitines in HNSCC patients' tissues. Carnitine palmitoyltransferase I (CPTI) and CPTII are the key enzymes for FAO. CPTI catalyzes the rate-limiting step of FAO by converting acyl-CoAs into acylcarnitines, while CPTII is responsible for converting acylcarnitine back into acyl-CoAs[94]. Therefore, upregulation of CPTI

and/downregulation of CPTII in HNSCC tissues might be responsible for the increased acylcarnitine species. Another possibility is that acylcarnitines seem to be a signature of branched-chain amino acid (BCAA) metabolism[95]. It is reasonable to speculate that tumor cells require more nutrients including BCAAs for their proliferation. Consistent with our findings, the expression level of acylcarnitines was significantly increased in HCC tissues and in the serum of high fat diet-fed mice[96]. Similarly, the urinary levels of acylcarnitines were higher in renal cell carcinoma (RCC) patients in compared with the matched control patients[97]. Sphingosine-1-phosphate (S1P) pathway was significantly upregulated in HNSCC tissues. S1P is formed by phosphorylation of sphingosine using ATP and this process is catalysed by two sphingosine kinase isoforms (SK1 and SK2)[98]. S1P plays an important role in cancer progression and regulated many cellular processes such as inflammation, cell transformation, survival, metastasis and tumor microenvironment neovascularization[99]. Various types of DNA base damage were found in HNSCC tissues. Living organisms are evolved to efficiently repair DNA damage to protect the genome for survival. DNA can be damaged from both endogenous sources and exogenous sources. The common endogenous DNA damage are hydrolysis, oxidation, alkylation, and mismatch of DNA bases. Exogenous sources of DNA damage include ionizing radiation (IR), ultraviolet (UV) radiation, and various chemicals agents[100,101]. DNA damage is the major reason responsible for the initiation and development of human cancers. DNA damage caused genomic instability is a hallmark of cancer. The levels of three nucleobases including adenine, cytosine, and guanine were significantly increased in cancer tissues. The increased synthesis of these basic substance is important for the rapid proliferation of cancer cells. The 20 standard proteinogenic amino acids are important for both the building blocks for protein synthesis and intermediate metabolites which fuel other biosynthetic reactions[102,103]. It is no

wonder to observe that tumor cells exhibit increased demand for specific amino acids for maintaining proliferation. Uridine diphospho-N-acetylglucosamine (UDP-GlcNAc) and UDP-N-acetyl-alpha-D-galactosamine (UDP-GalNAc) are the end products of hexosamine biosynthesis pathway. They are both important donor molecules for glycosylation reactions. Glycosylation is the most common posttranslational modification of proteins which is crucial for determining three-dimensional structures of these macromolecules[104]. UDP-GlcNAc and UDP-GalNAc was accumulated in human colon cancer cells only in those cells that did not differentiate *in vitro*[105]. UDP-GlcNAc is important for the production of β1, 6-branched oligosaccharides which have been shown to be closely associated with tumor progression and metastasis[106]. We also observed that a number of fatty acid molecules were upregulated or downregulated in HNSCC tissues. Lipid metabolism plays an essential role in membrane biosynthesis, energy storage and the generation of signaling molecules. Changes in lipid metabolism might confers the aggressive properties of cancer cells[107,108].

Melatonin related pathway is significantly downregulated in HNSCC tissues. Melatonin is a metabolite secreted primarily by the pineal gland of human and mammals in response to darkness[109]. In recent years, an overwhelming amount of research have demonstrated melatonin exhibited oncostatic properties in various types of cancer[110]. Exogenous melatonin exerts the tumor suppressive mechanism mainly through antimitotic and antioxidant activity. However, this is first time to show that the endogenous level of melatonin in HNSCC tissues was downregulated, indicating reduced melatonin might be an important mechanism responsible for the carcinogenesis of HNSCC. Vitamin D3 is the precursor of calcitriol (1, 25 dihydroxyvitamin D3 (1, 25(OH) 2D3)) which regulates a number of downstream genes. Accumulating studies have shown that vitamin D deficiency is associated with increased risk of developing cancer

[111,112]. Calcidiol and 24-Hydroxycalcitriol are the inactive prohormone and end products for calcitriol respectively. Although the level of calcitriol was not detected, we speculate that it is decreased in HNSCC. Coenzyme Q10 is an essential component of the electron transport chain and an effective antioxidant for the prevention of oxidative damage and inflammatory responses [113]. Its downregulation in HNSCC tissues might aggravate the oxidative stress, which promotes the cancer initiation and development. Retinoic acid (RA) not only can induce differentiation and/or apoptosis in cancer cells, but also exhibits anti-proliferative and anti-oxidant activity. These tumor suppressive effects are mediated through the RA receptors (RARs) and the retinoid X receptors (RXRs). 4-oxo-retinoic acid and 4-hydroxyretinoic acid could significantly suppressed the proliferation of breast cancer cells[114,115]. In addition, we also detected some novel downregulated metabolites such as hippuric acid, N-butyryglycine and 3-O-Sulfogalactosylceramide (d18:1/16:0). Further studies are warranted to reveal their roles in tumorigenesis of HNSCC.

Interestingly, there were some overlapped signal pathways detected by the metabolomics study and the IPA analysis of the differentially expressed metabolic enzymes. For instance, the nucleotide biosynthesis, lipid metabolism, amino acid metabolism, melatonin pathway etc. were found to be deregulated using both methodologies. One limitation of our metabolomics study is that we were only able to confirm a subset of deregulated metabolites. This is probably due to most data analysis software for metabolomics available today still needing further development to fulfill complicated metabolomics data processing and metabolite identification. In addition, there is no comprehensive spectral library available containing the complete entries of the MS/MS spectra for human metabolites so that metabolites can be confidently identified by searching the comprehensive metabolite MS/MS database.

In conclusion, our study has revealed significantly changed genes and metabolites between HNSCC and adjacent normal tissues. These novel molecules might be closely associated with the initiation and development of HNSCC, and might have clinical utility for the diagnosis and prognosis prediction in HNSCC. With these potential biomarkers, it is possible that we can diagnose HNSCC at the very early stage. Moreover, combination of these biomarkers might stratify the HNSCC patients with low risk and high risk for cancer progression and recurrence, which will provide useful guidance for personalized and precision therapy.

CHAPTER 2: The role of PLOD3 in HNSCC

1 INTRODUCTION

1.1 Location and structure of PLOD3

Currently three members have been discovered in procollagen-lysine, 2-oxoglutarate 5-dioxygenase (PLOD) family, namely PLOD1, PLOD2 and PLOD3[116]. The gene encoding the PLOD3 is located in human 7q22 chromosome, which is distinct from the locations of PLOD1 (1p36) and PLOD2 (3q24)[117,118]. The different location of the three PLODs isoforms indicate they are different metabolic enzymes and might not be able to compensate for one another. All three PLOD isoforms have similar structure of 19 exons. The introns of PLOD3 contains many contain many Alu repeats, but it is markedly shorter than PLOD1 and PLOD2, indicating that PLOD1 and PLOD2 may have lengthened introns during vertebrate evolution[119]. Human PLOD3 has 738 amino acids and its molecular weight is 85 kDa. The amino acid sequence of three PLODs are similar and all contain a signal sequence at the amino-terminus. There are about 60% similarity for the amino acid sequence between PLOD1 and PLOD3 or PLOD2 and PLOD3 [120].

1.2 Physiological functions of PLOD3

Collagen is a group of extracellular matrix proteins that play versatile roles in cellular physiology, ranging from structural support to mediating cell signaling[121]. Currently there are 28 known collagen types. All types of collagen contain at least one triple helical domain formed by repeating Gly-X-Y (where X and Y can be any amino acid) sequences[122]. Collagen is synthesized in endoplasmic reticulum as a precursor, then undergoes various post-translational modifications (PTMs) before being secreted out of the cell. One of the most important PTM for

forming mature collagen is hydroxylation of many lysine residues into and hydroxylysine (Hyl)[123]. Hyl can serve as an attachment site for carbohydrates, leading to the subsequent galactosylhydroxylysine (GHyl) or glucosylgalactosylhydroxylysine (GGHyl). PLODs are metabolic enzymes that play an important role in catalyzing the hydroxylation of specific lysine residues in proteins especially in collagen. Some of these Hyl residues play an essential role in forming certain covalent cross links in collagen, which predominate in bone, cartilage, ligament, most tendons, embryonic skin, and most major internal connective tissues of the body. In addition to collagen, PLODs can also modify the proteins which have the collagenous like structure (Gly-X-Y). All three PLODs need to form homodimers for lysyl hydroxylase activity. Interestingly, PLOD3 also can form a heterodimer with PLOD1. Dimerization is required for the LH activity of PLOD3, whereas it is dispensable for glycosyltransferase activities. The dimerization process is mainly mediated by the amino acids 541-547 in PLOD3[124]. Mutations in PLOD3 led to a 30% lower Hyl levels of collagens IV and V, while no such decrease was observed in collagen I and III, indicating PLOD3 is important for the lysyl hydroxylation of collagens IV and V[125]. In addition, loss of PLOD3 prevents the intracellular tetramerization of type VI collagen and leads to impaired secretion of type IV and VI collagens[126]. The gene mutated in the Ehlers-Danlos syndromes (EDS) type VIA patients is PLOD1. The triple-helical regions of collagen I and III were hydroxylated abnormally in patients with EDS-VIA, suggesting that PLOD1 is important for hydroxylation of lysine in collagen I and III[127]. Other studies also indicated that PLOD3 is important for the maturation of collagen I in osteoblast. PLOD3 is crucial for the formation of glucosylate galactosylhydroxylysine residues in type I collagen and its downregulation significantly affects type I collagen fibrillogenesis[128,129]. PLOD2 is mainly involved in the lysyl hydroxylation of the N- and C-telopeptides[130]. The

difference of PLODs in hydroxylation of lysine in different types of collagen further support that their biological functions cannot be compensate for one another.

In addition to LH activity, PLOD3 also have collagen glucosyltransferase (GGT) and galactosyltransferase (GT) activities. These two enzymes are required for forming the unique 2-O-α-D-glucopyranosyl-O-β-D-galactopyranosyl hydroxylysyl residues typical of collagens and of other proteins with collagenous domains. Both PLOD3 knockout embryos and the fibroblastic cells from the PLOD3 knockout embryos showed a significant reduction in GGT activity, suggesting that PLOD3 is the key molecule accounting for the GGT activity[131]. As GGT activity is highly sensitive and specific for PLOD3, measuring the GGT activity in the biological samples can reflect the expression level of PLOD3. The GT activity is not exclusive to PLOD3, and many GTs have GT activities[117]. A conserved cysteine at position 144 and a leucine at position 208 as well as the aspartates of a DXD-like motif crucial are crucial for maintaining the GGT activity [132].

Just as mentioned above, the major target of PLOD3 *in vivo* is collagen type IV. PLOD3 was demonstrated to be an important regulator for the biosynthesis, secretion and activity of adiponectin, which has crucial roles in glucose and lipid metabolism and inflammation. Adiponectin has collagenous region, and hydroxylation and glycosylation of the lysine residues of adiponectin can enhance its biological function[133]. PLOD3 is important for catalyzing formation of the glucosylgalactosylhydroxylysines of mannan-binding lectin (MBL), which is a component of lectin pathway of complement activation. Mice lacking LH activity had reduced levels of circulating MBL[134].

As PLOD3 is an important enzyme, it is no wonder that PLOD3 is ubiquitously expressed in cells. PLOD3 is manly located in the ER, and it is found extracellularly in serum, the

extracellular space and on cellular membrane[135]. It is the only secreted PLOD isoform. The glycosyltransferase domain of PLOD3 rather than the LH domain is responsible for secretion of PLOD3 into the cell medium. Two pathways have been proposed for the secretion of PLOD3 from the ER; one is Golgi dependent and the other is Golgi independent. PLOD3 secreted in the cell medium is Golgi dependent and relies on the glycosyltransferase activity. However, the PLOD3 expressed on the cellular membrane is secreted in a Golgi independent manner. The secretion of PLOD3 into extracellular space indicates that it might be important for the extracellular matrix (ECM) remodeling[136]. PLOD3 is indispensable for development, as the PLOD3 knockout embryos leads to embryonic lethality at E9.5. Downregulation of GGT activity in PLOD3 knockout mice is the major reason responsible for the embryonic lethality, which can disrupts the type IV collagen location and subsequent basement membrane formation[137]. Lack of PLOD3 also significantly affects the normal organization of the extracellular matrix (ECM) and cytoskeleton[131]. PLOD3 plays a critical role in regenerative growth and guidance of axons of the dorsal nerve branch by partially regulated it functional substrate collagen alpha-5(IV) chain [138]. Neural stem cell with PLOD3 deletion failed to transition from a sheet to a stream, indicating that changes in modification and distribution of ECM components due to PLOD3 deletion can significantly influence the signals required for the migration capacity of neural crest cells[139]. MMP-9 secreted by tumor cells and leukocytes can be recruited to the fibroblast surface through its FNII repeats or collagen-binding domain and PLOD3 is responsible for the docking of MMP-9 to fibroblast surface. In addition, PLOD3 mediated MMP-9 recruitment stimulates the activation of transforming growth factor beta 1 (TGF-β), which subsequently promotes the differentiation of fibroblast into myofibroblasts[140].

1.3 Regulation of PLOD3

Currently the molecular mechanisms that regulate PLOD3 activities are poorly unknown. MiR-663 was demonstrated to be a direct regulator of PLOD3. Ectopic expression of miR-663 could inhibit the PLOD3 expression, leading to reduced type IV collagen biosynthesis, indicating miR-663 might be functional modulator of PLOD3[141]. In addition to miRNAs, transcriptional factors are the major potential regulators of PLOD3. Further studies are urgently to reveal the upstream regulators and downstream effectors of PLOD3.

1.4 Deregulation of PLOD3 in diseases

Recessive dystrophic epidermolysis bullosa (RDEB) is a disease caused by reduced or absent type VII collagen. The expression level of PLOD3 was significantly reduced in basement membrane of RDEB patient skin compared to the normal skin, indicating that PLOD3 at the basement membrane might be important for the disease progression of RDEB[142]. Mutation of *PLOD3* leads to an inherited syndrome of congenital malformations with various connective tissues disorder, which significantly affects the normal function of many tissues and organs[143]. The copy number of *PLOD3* was remarkably increased in patients with gastric cancer, indicating PLOD3 might be a tumor promoter of gastric cancer[144]. Another study demonstrated that the expression level of PLOD3 was significantly upregulated in colorectal cancer tissues in comparison with the normal tissues[145]. The levels of PLOD3 were also found to be upregulated in the secretome from pancreatic cancer cell lines compared with the normal pancreatic cells[146], indicating PLOD3 might be important for the cell to cell communication in the tumor microenvironment. A recent also reported that PLOD3 was overexpressed in glioblastoma (GBM) tissues and cell lines. Downregulation of PLOD3 inhibited the oncogenic activities of GBM cells[147]. Although there are some studies revealing the potential oncogenic role of PLOD3 in cancer, the concrete molecular mechanisms are poorly investigated. In addition, the role of

PLOD3 in HNSCC is unknown. Therefore, the aim of this project was to determine the potential clinical significance of PLOD3 in HNSCC.

2 MATERIALS AND METHODS

Cell culture

SCC1, SCC23, SCC17, UM5, UM6, UM1 and UM2 HNSCC cell lines were cultured in the Dulbecco's modified eagle medium (DMEM) supplemented with 10% fetal bovine serum, penicillin (100 U/mL), and streptomycin (100 μg/mL). Normal human oral keratinocytes (NHOKs) and normal human epidermal keratinocytes (NHEKs) were cultured in EpiLife media supplemented with the human keratinocyte growth supplement (Invitrogen, Carlsbad, CA, USA). The cells were maintained at 37°C, 5% CO_2 in a humidified cell culture incubator and passaged when they reached 90–95% confluence.

Immunohistochemistry

For immunohistochemistry analyses, formalin-fixed paraffin-embedded sections were deparaffinized by sequential washing with xylene, 100% ethanol, 95% ethanol, 80% ethanol and PBS. The sections were incubated with 0.3% H_2O_2 in methanol for 5 min to quench the endogenous peroxidase activity. The slides were blocked in PBS with 5% BSA for 30 min and then incubated overnight with a 1:100 dilution of anti-PLOD3 primary antibody (Proteintech, Chicago, IL, USA) at 4 °C. After sections were rinsed with PBS, they were incubated with horseradish peroxidase (HRP)-conjugated goat anti-rabbit IgG (Invitrogen) for 2 h at room temperature.

MTT assay

After 24 h of serum starvation, the cells were seeded into a 96-well plate at a density of 3000 cells/well. At the indicated time points, 20μL of MTT (Sigma-Aldrich, St. Louis, MO, USA) dissolved in PBS at 5 mg/ml was added to each culture well. Following by incubation for 4 h at 37°C, the supernatant was then discarded and the precipitate dissolved in 200 μl of dimethyl sulfoxide (DMSO, Sigma). The absorbance of each well was measured using a Synergy HT microplate reader (BioTek Instruments, Winooski, VT, USA) at 570 nm.

5-ethynyl-2′-deoxyuridine assay

The 5-ethynyl-2′-deoxyuridine (EdU) detection kit (Invitrogen) was used to evaluate cell proliferation. According to the manufacturer's instructions, the cells were treated with 10 μmol/L EdU for 2 h at 37°C and fixed with 3.7% formaldehyde for 15 min. After cells were washed with 3% BSA in PBS, they were treated with 0.5% Triton X-100 (Sigma-Aldrich) for 20 min and stained with 1 × Click-iT reaction cocktail for 30 minutes at room temperature. After PBS wash, Hoechst 33342 dye was used to stain the cell nucleus at room temperature for 30 min. Images were captured under a confocal laser scanning microscope (Carl Zeiss, Jena, Germany).

Cell colony formation assay

The cells were seeded into a 6-well plate at a density of 3000 cells/well in 2 mL medium. After incubation at 37°C for 14 days, the cells were washed three times with PBS and stained with 0.5% crystal violet for 30 min.

Migration assay

The migration assays were performed with the Transwell Chambers (BD Biosciences. Bedford, MA, USA). Following 24 h serum starvation, trypsinized cells (1 × 105 cells /well) were re-suspended in DMEM containing 0.1% FBS and added to upper chamber of transwell inserts. DMEM supplemented with 10% FBS was used in the lower chamber to act as a chemoattractant. After 24 h, cells that had migrated through the membrane were fixed and stained with the crystal violet. The percentage of migrated area per field under light microscopy (Carl Zeiss) in four random fields were calculated by using Image J (FijiVersion, National Institutes of Health, Bethesda, MD, USA).

Transwell Matrigel invasion assay

The invasion assays were performed with the Transwell Matrigel Invasion Chambers (BD Biosciences. Bedford, MA, USA). Following 24 h serum starvation, trypsinized cells (5 × 105 cells /well) were resuspended in DMEM containing 0.1% FBS and added to upper chamber of transwell inserts. DMEM supplemented with 10% FBS was used in the lower chamber to act as a chemoattractant. After 48 h, cells that had invaded through the membrane were fixed and stained with the crystal violet. The percentage of invaded area per field under light microscopy in four random fields were calculated by using Image J.

Real-time PCR

Total RNA was isolated from cancer cells using the Quick-RNA™ kit (Zymo Research Corp, Irvine, CA, USA) according to the manufacturer's instructions. First-strand complementary DNA synthesis was performed using the SuperScript III Reverse Transcriptase (Invitrogen). The complementary DNA levels were amplified with Light Cycler 480@ SYBR Green I MasterMix (Roche, Applied Science, Indianapolis, IN, USA) using the CFX96 Real-Time PCR detection

system (Bio-Rad Laboratories Inc., Hercules, CA, USA). GADPH and U6 were used as the internal controls for mRNA and miRNA analysis respectively.

Western blotting

The protein samples were loaded and separated on a 4-12% Bis-Tris NuPAGE gel (Invitrogen) and transferred onto a nitrocellulose membrane using a Trans-blot SD semi-dry transfer cell (Bio-Rad). The membranes were blocked for 2 h at room temperature in TBST buffer containing 5% nonfat milk (Santa Cruz Biotech), and incubated with first primary antibodies overnight at 4 °C, followed by HRP-linked secondary antibodies (GE Healthcare). Signal detection was performed with the ECL-Plus Western blotting reagent kit (GE Healthcare).

SiRNA transfection

Cancer cells were transfected with double-stranded siRNAs using the RNAiMAX transfection regent (Invitrogen) according to the manufacturer's instruction. SiPLOD3 (siRNA1 and siRNA2) was mixed with the transfection reagent respectively and then added to the cell culture. SiRNA control (siCTRL) was used as negative control. After overnight incubation, the siRNAs were removed and the cells were further cultured in fresh media for 48 h before any additional experiments.

Production of PLOD3 recombinant lentiviral vectors

PLOD3 was cloned into the pGCL-GFP vector and constructs were confirmed by sequencing. Recombinant lentiviral vectors and packaging vectors were then transfected into 293T cells. The supernatant liquor containing lentiviruses was harvested 72 h after transfection. The lentiviruses were then purified by ultracentrifugation, and the titer of lentiviruses was determined. The empty

vector was packaged as a negative control. The cancer cells were infected with the lentiviruses at a multiplicity of infection of 40.

Analysis of PLOD3 gene expression in tumor samples from existing tumor databases

The normalized datasets comparing the gene expression profiles between HNSCC and normal controls were downloaded from NCBI GEO databases. The accession number was GSE663, GSE37991, GSE23558, GSE25099, GSE85514 and GSE30784 respectively.

The clinical information and RNASeq V2 datasets of cancer patients were obtained from The Cancer Genome Atlas (TCGA) database (https://tcga-data.nci.nih.gov/tcga) to determine the clinical significance of PLOD3 in cancers. Briefly the mRNA expression levels were log2-transformed and X tile software (https://medicine.yale.edu/lab/rimm/research/software.aspx) was used to find out the best cutoff point to divide the cancer patients into high/low PLOD3 expression groups. Kaplan–Meier overall survival curves were generated for patients whose follow-up data were available. The log-rank test was used to analyze survival differences between the two groups.

Xenograft mouse model

Male athymic nude mice (BALB/C-nu/nu, 4–5 weeks old) were used for the *in vivo* studies. Before injection, cancer cells were re-suspended in a 1:1 mixture of Matrigel (BD Biosciences) and PBS. A 100-μl cell suspension containing 2 x 10^6 PLOD3 knockdown or PLOD3 overexpression cells was subcutaneously injected into the dorsal flank of each mouse. For the control groups, mice received 100 μl injections of the respective control cells in corresponding concentrations. The tumor diameters and weight were measured and recorded.

3 RESULTS

3.1 PLOD3 is overexpressed in HNSCC tissues and cell lines

We used seven publicly available expression profiling data sets downloaded from the Gene Expression Omnibus (GEO) and the Cancer Genome Atlas (TCGA) Data Portal. Our results revealed that the expression of PLOD3 was significantly increased in HNSCC cancer tissues compared with normal control tissues. Interestingly, in GSE85514 and GSE30784, the expression level of PLOD3 was significantly higher in tumor tissues than that in oral precancerous lesions. In addition, HNSCC patients in the high PLOD3 expression group suffered a significantly lower overall survival than those in the low PLOD3 expression group **(Figure 16)**.

We also analyzed PLOD3 expression in other types of cancers by using the data from TCGA database. The expression level of PLOD3 was significantly increased in cancer tissues including acute myeloid leukemia (AML), bladder urothelial carcinoma (BLCA), breast cancer (BRCA), colon adenocarcinoma (COAD), cholangiocarcinoma (CHOL), esophageal carcinoma (ESCA), glioblastoma(GBM), kidney chromophobe (KICH), kidney renal clear cell carcinoma(KIRC), kidney renal papillary cell carcinoma (KIRP), liver hepatocellular carcinoma(LIHC), lung adenocarcinoma(LUAD), lung squamous cell carcinoma(LUSC), prostate adenocarcinoma(PRAD), rectum adenocarcinoma(READ), stomach adenocarcinoma(STAD), stomach and esophageal carcinoma(STES) and thyroid carcinoma(THCA) compared to their respective adjacent normal tissues **(Figure 17A-17B)**. In addition, the cancer patients with higher expression of PLOD3 had poorer long-term overall survival rates in many other types of cancers including GBM, KIRC, LIHC, LUSC, low grade

glioma (LGG), LUAD, ovarian cancer (OV), cervical squamous cell carcinoma (CESC), THCA and sarcoma (SARC) **(Figure 18)**.

To assess the potential involvement of PLOD3 in HNSCC development and progression, we investigated the expression levels of PLOD3 in the HNSCC cell lines, UM1, UM2, UM5, UM6, SCC17, SCC1 and SCC23 as well as in normal cell lines, NHOK and NHEK.
In comparison with the control normal cell lines, the results of western blot analysis showed that the expression of PLOD3 was upregulated in all HNSCC cell lines. In addition, PLOD3 was higher in high invasive oral cancer cell lines UM1 and UM5 compared to low invasive oral cancer cell lines UM2 and UM6 **(Figure 19A-19B)**. Then, the protein expression levels of PLOD3 were examined in fourteen paired tumor and non-tumor tissue samples. As predicted, PLOD3 expression levels were significantly increased in tumor tissues compared to non-tumor tissues **(Figure 19C-19D)**. PLOD3 expression was further examined in paraffin-embedded sections of 144 HNSCC and 20 normal specimens by IHC. The results revealed the staining intensity of PLOD3 was gradually increased in normal tissues, well-differentiated tumor, moderately differentiated tumor and poorly differentiate tumor **(Figure 20A-20B)**.

3.2 PLOD3 plays pro-carcinogenic roles in HNSCC

The significant upregulation of PLOD3 in HNSCC cell lines and tissues implied that PLOD3 may have a pro-carcinogenic role in HNSCC tumorigenesis. To test this hypothesis, depletion of PLOD3 was achieved by transfecting siRNA oligos (siRNA1 and siRNA2) against PLOD3 into SCC1 cells (a cell line derived from tongue squamous cell carcinoma and SCC23 cells (a cell line derived from laryngeal squamous cell carcinoma). Significant losses of PLOD3 at both

mRNA and protein levels were achieved by siPLOD3-treated cells with respect to control (siCTRL) transfection **(Figure 21A-21C)**. Cell proliferation was then assessed by MTT assay, which showed a drastic decrease of proliferative capacity after siPLOD3-treatment with respect to siCTRL treatment **(Figure 21D)**. This was supported by the results of the colony formation: as significantly less number of colonies formed in siPLOD3-treated group than those in siCTRL treated group **(Figure 21E)**. In addition, the percentage of EdU positive cells was significantly lower in the cells with siPLOD3 transfection when compared to those with siCTRL transfection **(Figure 21F)**. The mobility of cancer cells was significantly decreased upon PLOD3 knockdown as indicated by a transwell migration assay, demonstrating significantly fewer number of cells penetrated the pores of the membrane than siCTRL treated group **(Figure 21G)**. Matrigel invasion assay measurement showed that knockdown of PLOD3 also significantly suppressed the invasive ability of HNSCC cells **(Figure 21H)**. Notably, we observed that the knockdown of PLOD3 in SCC1 and SCC23 significantly decreased xenograft tumor volume and weight compared with the controls **(Figure 22)**.

Then we constructed PLOD3 overexpressing lentiviruses (PLOD3 OV) and control lentiviruses (CTRL). Cancer cells were successfully infected with lentiviral particles and the expression level of PLOD3 protein was remarkably increased after lenti-PLOD3 infection **(Figure 23A-23B)**. The results showed that the cells with PLOD3 overexpression had higher proliferative capacity and stronger colony forming ability compared with cells infected with the control lentiviruses **(Figure 23C-23D)**. In addition, PLOD3 overexpression led to a higher percentage of EdU positive cells **(Figure 23E)**. SCC1 and SCC23 cells with PLOD3 overexpression were more proficient than control lentivirus-infected cells at migrating through the membrane. PLOD3

upregulation also significantly enhanced the invasive capacity of cancer cells **(Figure 23F-23G)**. Overexpression of PLOD3 in SCC1 and SCC23 significantly increased xenograft tumor volume and weight compared with the controls **(Figure 24)**.

4 DISCUSSION

The carcinogenesis of HNSCC is a multistep process during which cells undergo profound metabolic and behavioural changes, leading them to proliferate in an uncontrolled way[148,149]. However, the underlying molecular mechanisms remain unclear. In this chapter, we demonstrated that PLOD3 is overexpressed in HNSCC cell lines and tissues compared with the controls. In addition, HNSCC patients with higher PLOD3 suffered unfavorable clinicopathological parameters and overall survival. This finding was also observed in many other types of cancers based on the TCGA data. Moreover, downregulation of PLOD3 suppressed the proliferation, migration and invasion of cancer cells *in vitro* and tumor growth *in vivo*, and upregulation of PLOD3 promoted the malignant phenotypes of HNSCC cells, indicating that PLOD3 functions as a tumor promoter in HNSCC tumorigenesis.

The Gene Expression Omnibus (GEO, http://www.ncbi.nlm.nih.gov/geo/) is an international public repository that archives and freely distributes microarray, next-generation sequencing, and other forms of high-throughput functional genomic data sets[150,151]. TCGA is a large-scale cancer genome project which provides researchers with multi-dimensional maps of the key genomic changes and clinical information in 33 types of cancer (http://cancergenome.nih.gov/)[152]. Both GEO and TCGA have significantly increased our understanding of cancer. Interestingly, PLOD3 was found to be overexpressed in HNSCC tissues in comparison with normal tissues in many

independent studies, indicating PLOD3 upregulation is a common phenomenon during the HNSCC carcinogenesis. In addition, PLOD3 levels in oral precancerous legions were higher than normal mucosa while lower than HNSCC tissues, indicating PLOD3 might promote the tumorigenesis of HNSCC at the very early stage. Based on the expression and clinical data obtained from TCGA database, PLOD3 is overexpressed in almost 20 cancer types. Moreover, HNSCC patients with higher PLOD3 expression experienced a significantly lower long term overall survival than those with lower PLOD3 expression. This phenomenon again was found in many other types of cancers, indicating PLOD3 upregulation is common event in cancers and its overexpression generally might lead to unfavorable clinical outcome.

The expression level of PLOD3 was significantly overexpressed in all HNSCC cell lines compared to the normal epithelial cells. In addition, its level was higher in HNSCC cell lines (UM1 and UM5) with high metastasis capacity compared with that in the cancer cell lines with low metastasis potential (UM2 and UM6). These observations indicate that upregulation of PLOD3 might enhance the malignant behaviours of HNSCC cells. Our IHC findings demonstrated that the PLOD3 staining intensity was higher in HNSCC tissues compared to the normal tissues, and it was positively associated with worse tumor differentiation, which further implicated the tumor promoting role of PLOD3 in HNSCC. PLOD3 downregulation inhibited cell proliferation, migration and invasion *in vitro* and tumor growth *in vivo*, and ectopic expression of PLOD3 potentiated cell proliferation, migration and invasion *in vitro* and tumor growth *in vivo*. To the best of our knowledge, this is the first study to explore the role of PLOD3 in HNSCC.

Consistently with our current findings, a study compare mRNA profiles of 1,454 metabolic enzymes across 1,981 tumours spanning 19 cancer types to identify the consistently differentially expressed enzymes, and PLOD3 was demonstrated to be one of the top deregulated metabolic enzymes[153]. PLOD3 was found to be overexpressed in hepatocellular carcinoma (HCC) tissues in comparison with control tissues. In addition, PLOD3 showed good performance for the diagnosis of early-stage HCC. Moreover, PLOD3 inhibition suppressed the *in vitro* and *in vivo* liver tumorigenesis by selectively targeting epithelial-mesenchymal transition and cell-cycle proteins [154]. A recent finding reported that PLOD3 knockdown suppressed the proliferation and migration of lung cancer cells, and vice versa. Also, GATA Binding Protein 3 was shown to be an upstream regulator of PLOD3[155]. Tsai et al showed that PLOD3 was overexpressed in glioma tissues, and inhibition of PLOD3 could suppress the oncogenic activities of glioma cells[147]. Also, PLOD3 depletion could sensitized lung cancer cells to radiotoxicity and additively enhancing radiation-induced apoptosis[156], suggesting that PLOD3 might be important for maintaining the radio-resistance of cancer cells. Although there are three members in PLOD family, their function seems not redundant for one another. Firstly, only PLOD3 has the GT and GGT activities. In addition, the GCT activities was demonstrated to be crucial for cellular survival. Secondly, mice with PLOD3 knockout failed to survive[137], suggesting that PLOD3 was indispensable for development. One interesting finding is that PLOD3 seems to be essential for maintaining the oncogenic behaviors for the HNSCC cells, as cells with PLOD3 depletion almost lost the proliferation, migration and invasion capacity completely. These findings suggest that PLOD3 might be a powerful gene for promoting tumorigenesis in HNSCC.

CHAPTER 3: MiR-124-3p-PLOD3-FAK/PI3K/AKT pathway is important for the tumorigenesis of HNSCC

1 INTRODUCTION

1.1 MicroRNAs overview

1.1.1 MicroRNAs

MicroRNAs (miRNAs) are an abundant class of evolutionarily conserved, short non-coding RNAs of 20-24 nucleotides that play important roles in virtually all biological pathways throughout the plant and animal kingdoms[157]. The first miRNA, lin4, was discovered in 1993 on *Caenorhabditis elegans*[158,159]. Currently there are more than 2600 human mature miRNAs based on data from the miRBase (http://www.mirbase.org/). The main function of miRNAs is to negatively regulate protein expression by binding of fully or partially complementary sequences to the 3'- untranslated region (UTR) of target messenger RNAs (mRNAs), resulting in translation inhibition or/and mRNA degradation[160,161]. The microRNA-mRNA binding site is relatively short (6-8 base pairs), and therefore each mature miRNA can control the expression of a number of target mRNAs[162]. In addition, each mRNA might be regulated by various miRNAs.

1.1.2 Mechanism of miRNAs regulation

MiRNAs can be originated from either intergenic or coding-intronic[163,164]. Intergenic miRNAs are transcribed by RNA polymerase II or III to generate a primary transcript named pri-miRNA [165]. Then pri-miRNA is cleaved into pre-miRNA in the nucleus by the core components (Drosha and DGCR8) of the microprocessor complex[166]. MiRNA within introns depends on the RNA splicing machinery for their biogenesis. Pre-miRNAs are exported to the cytoplasm by Exportin 5 and Ran-GTP. The pre-miRNAs are cleaved by a complex including the RNase Dicer, AGO2 (Argonaute 2), and TRBP (trans-activation-responsive RNA-binding protein) to form mature

miRNAs. These mature miRNAs are loaded into the RNA-induced silencing complex (RISC), then bind to the 3' UTR of the targeted mRNAs[167,168]. The fate of miRNAs is determined by the binding. Perfect complementarity between miRNA and target mRNA leads to targeting the mRNA transcript degradation, while imperfect complementarity results in translation inhibition [161].

1.1.3 The role of miRNAs in cancer

MiRNAs have been demonstrated to potentially regulate every aspect of cellular activities including cell growth, proliferation, differentiation, and motility[169,170]. Deregulation of miRNAs has been reported in many human diseases such as cardiovascular diseases, inflammatory diseases neurodevelopmental diseases and cancer[171,172]. It is now well documented that miRNAs are aberrantly expressed in various human cancers. MiRNAs may function as either oncogene or tumor suppressor during the tumorigenesis. MiRNAs have shown great promise for clinical application. MiRNA expression pattern is associated with tumor subtypes, which might help facilitate tumor classification. For instance, only 48 miRNA markers can discriminate the cancers from various tumor origin with an overall accuracy of approximately 90%, indicating miRNA expression signature is effective for tracing the tissue of origin of cancers[173]. MiRNAs are also closely associated with the chemoresistance of cancer cells, indicating that miRNAs can be used for monitoring therapeutic response. For instance, overexpression of miR-449b in nasopharyngeal carcinoma increased cisplatin resistance by targeted transforming growth factor beta-induced (TGFBI) directly[174]. Interestingly, single-nucleotide polymorphisms (SNPs) is existed in the miRNA binding site, which might be closely associated with cancer risk and susceptibility[175]. MiRNAs are highly stable in the biofluids such as serum, plasma, urine and saliva. Thus, they serve as promising non-invasive biomarkers for early detection and prognostic

prediction of various diseases including cancer[176,177]. For instance, the expression level of miR-31 was significantly increased in the saliva samples from oral cancer patients compared with those from patients with oral verrucous leukoplakia or healthy controls. In addition, its levels dropped significantly following excision[178].

MiRNAs have been shown to play a crucial role in tumorigenesis of HNSCC. The expression level of miR-134 was significantly upregulated in HNSCC compared to the normal mucosa. In addition, high miR-134 expression was associated with adverse clinicopathological parameters and worse survival. Furthermore, ectopic expression of miR-134 promoted the oncogenic phenotypes of cancer cells both *in vitro* and *in vivo*, and opposite results were observed when miR-134 was downregulated. These data indicated that miR-134 might serve as a tumor promoter in HNSCC[179]. MiR-135b overexpression promoted the proliferation, migration, and colony formation *in vitro* and enhanced tumor growth *in vivo*. In addition, hypoxia-inducible factor-1α (HIF-1α) was demonstrated to be a downstream target of miR-135b[180]. Most miRNAs play a tumor suppressive role in the carcinogenesis. For instance, the expression level of miR-874 was significantly downregulated in HNSCC. In addition, miR-874 overexpression remarkably inhibited proliferation and induced G2/M arrest and cell apoptosis. Histone deacetylase 1 (HDAC1) was a downstream target of miR-874[181]. Based on miRNA profiling, miR-125b was found to be decreased in HNSCC tissues and cell lines. Loss of miR-125b might be partially result from the hypermethylation of its promoter. In addition, miR-125b might exert its tumor suppressive role by deregulating TACSTD2 and mitogen-activated protein kinase pathway[182]. Taken together, MiRNAs are powerful molecules that play an essential role in the tumorigenesis of various types of cancers including HNSCC. They are attractive as biomarkers for the cancer detection, diagnosis, and prognosis assessment, which is very important for

therapeutic guidance. However, currently there are a number of candidate miRNAs emerging as promising biomarkers. From a clinical and practical view, it is impossible to test these miRNAs simultaneously. Therefore, well designed prospective clinical trials with large patient groups are urgently needed to explore the most powerful miRNAs for clinical applications.

1.2 FAK in cancer

FAK is encoded by *PTK2*, which is localized at chromosome 8q24.3, a region with frequent chromosomal abnormalities in human cancers[183,184]. FAK contains four domains: the catalytic kinase core, the N-terminal four-point-one, ezrin, radixin, moesin (FERM) domain, an unstructured proline-rich area and a C-terminal focal adhesion targeting (FAT) domain[185]. Several tyrosine phosphorylated residues are important for maintaining the biological functions of FAK. Tyrosine residue 397 is the major site of FAK autophosphorylation and serves as the binding site for various proteins such as Src, Shc and the regulatory subunit of PI3K[186]. The tyrosine residue 925 is docking site for the Src homology 2 (SH2) domain of Grb2[187]. Phosphorylation of tyrosine 925 can activate the rat sarcoma (RAS)-mitogen-activated protein kinase (MAPK) signaling pathway, which is important for angiogenesis and cell proliferation. FAK has been demonstrated to play a central role in promoting cancer growth and metastasis by mediating various cellular processes such as cell survival, proliferation, migration, invasion, epithelial-mesenchymal transition, angiogenesis and regulation of cancer stem cell activities[185]. Due to the importance of FAK in carcinogenesis, many FAK inhibitors such as PF-00562271 and GSK2256098 have been developed for chemotherapeutics, and promising results are obtained from the clinical trials[188,189]. FAK was overexpressed in various types of cancers including HNSCC. For instance, the expression level of FAK was overexpressed in HPV negative HNSCC cell lines and tissues. Patients with *PTK2* amplification was significantly

associated with worse disease-free survival. In addition, suppression of FAK led to significant radiosensitization enhancements in HNSCC cells[190]. FAK is upstream regulator of phosphatidylinositol 3-kinase (PI3K)-protein kinase B (AKT). PI3K-AKT signaling pathway is considered to be the most frequently altered oncogenic pathway in HNSCC[191].

2 MATERIALS AND METHODS

MiRNA mimic/inhibitor transfection

Cancer cells were transfected with miR-124-3p mimic/inhibitor using the RNAiMAX transfection regent (Invitrogen) according to the manufacturer's instruction. MiR-124-3p mimic/inhibitor was mixed with the transfection reagent respectively and then added to the cell culture. Scrambled miRNA control was used as negative control. After overnight incubation, the medium was removed, and the cells were further cultured in fresh media for 48 h before any additional experiments.

3′-UTR luciferase reporter assay

For dual luciferase reporter assays, cancer cells were co-transfected with 3′-UTR-PLOD3 vector constructs (SwitchGear Genomics, Carlsbad, CA, USA), and either miR-124-3p mimic or scramble miRNA using RNAiMAX reagent. Luciferase activity was measured at 48 h after transfection using the Dual-Luciferase Reporter Assay System (SwitchGear Genomics), according to the manufacturer’s protocol. Firefly luciferase activity was normalized to Renilla luciferase activity.

3 RESULTS

3.1 MiR-124-3p directly targets PLOD3 by binding to 3′ UTR region

Multiple miRNA target prediction programs showed that miR-124-3p was a conserved and powerful regulator of PLOD3 (data not shown). Thus, we investigated potential direct interaction between miR-124-3p and 3′-UTR PLOD3 by luciferase assay. As shown in **Figure 25A**, PLOD3 3′-UTR shows high complementarity to the seed sequence of miR-124-3p. In addition, the 3′-UTR PLOD3 sequence that miR-124-3p targeted was highly conserved across different species **(Figure 25B)**. Luciferase assays showed that the miR-124-3p mimic significantly suppressed relative luciferase activity compared to the scramble control **(Figure 25C)**, suggesting that miR-124-3p directly targets 3′-UTR mRNA of PLOD3. In addition, miR-124-3p mimic remarkably reduced PLOD3 expression at the protein level **(Figure 25D-25E)**.

3.2 MiR-124-3p plays a tumor suppressive role in HNSCC

The qRT-PCR analysis confirmed that transfection of miR-124-3p mimic resulted in miR-124-3p upregulation in SCC1 and SCC23 cells **(Figure 26A)**. MTT, colony formation and EdU assays indicated that miR-124-3p overexpression apparently suppressed proliferation of both SCC1 and SCC23 cells **(Figure 26B-26D)**. Migration assay also displayed that miR-124-3p upregulation markedly prohibited CRC cell migration **(Figure 26E)**. Additionally, overexpression of miR-124-3p led to decrease of invasion ability in both SCC1 and SCC23 cells **(Figure 26F)**. Conversely, downregulation of miR-124-3p was successfully achieved by transfecting the cells with miR-124-3p inhibitor **(Figure 27A)**. Our results showed downregulation of miR-124-3p promoted the proliferation, migration and invasion capacity of both SCC1 and SCC23 cells **(Figure 27B-27F)**.

3.3 Overexpression of PLOD3 partially rescues the suppression of miR-124-3p

To elucidate whether the suppressive effect of miR-124-3p was mediated by repression of PLOD3 in HNSCC cells, we evaluated whether ectopic expression of PLOD3 could rescue the suppressive effect of miR-124-3p. We transfected miR-124-3p mimic into cancer cells infected with PLOD3 overexpressing lentiviruses or control lentiviruses and WB results showed that the levels of PLOD3 were higher in cells infected with PLOD3 overexpressing lentivirus following miR-124-3p mimic transfection **(Figure 28A)**. MTT, colony formation and EdU assays showed that PLOD3 overexpression could partially abrogate the effects mediated by miR-124-3p in both SCC1 and SCC23 cells **(Figure 28B-28D)**. At the same time, the migration and invasion assays showed that PLOD3 upregulation could partially restore the migration and invasion activity compared with the cells infected with control lentivirus **(Figure 28E-28F)**.

3.4 RNA-seq analysis reveals potential downstream pathways regulated by PLOD3

To understand the PLOD3-mediated molecular events in HNSCC cells, we conducted a genome-wide analysis to globally characterize PLOD3-regulated transcriptome changes. Total RNAs of SCC1 and SCC23 cells treated with siCTRL or siPLOD3 oligos were subjected to transcriptomic sequencing. Compared with the siCTRL-treated cells, a total of 3275 (1631 upregulated and 1644 downregulated) and 3146 (1497 upregulated and 1649 downregulated) transcripts were found to be significantly aberrantly expressed in siPLOD3-treated SCC1 and SCC23 cells respectively **(Figure 29A-29B)**. In addition, most deregulated genes were overlapped between SCC1 and SCC23 **(Figure 29C)**. GSEA showed that the differentially expressed genes in both cell lines were enriched in pathways including cell cycle, homologous recombination, purine and pyrimidine metabolism, focal adhesion, regulation of actin cytoskeleton, chemokine signaling pathway, spliceosome and ubiquitin mediated proteolysis **(Figure 30A-30H)**. Interestingly, we

observed the morphology of cancer cells became round following PLOD3 downregulation **(Figure 31)**. As focal adhesion kinase (FAK) is closely involved in cellular adhesion and spreading processes, we hypothesized that FAK might be deregulated following PLOD3 suppression.

3.5 FAK phosphorylation (pFAK) is important for the pro-oncogenic role PLOD3 in HNSCC

WB analysis showed that the expression level of pFAK, pPI3K and pAKT was significantly downregulated following PLOD3 downregulation, while their levels were upregulated when PLOD3 was overexpressed **(Figure 32)**. To explore whether the tumor promoting role of PLOD3 was mediated by phosphorylation of FAK in HNSCC cells, we evaluated whether suppression of FAK phosphorylation could inhibited the tumor promoting of PLOD3. We transfected siFAK or siCTRL into cancer cells infected with PLOD3 overexpressing lentivirus. The expression levels of FAK and pFAK were both significantly reduced following siFAK transfection **(Figure 33A)**. MTT, colony formation and EdU assays showed that knockdown of FAK could significantly inhibited the proliferation of PLOD3 overexpression cancer cells **(Figure 33B-33D)**. Furthermore, the migration and invasion assays showed that FAK silencing repressed the migration and invasion capacities of PLOD3 overexpression cancer cells **(Figure 33E-33F)**.

4 DISCUSSION

In this chapter, we demonstrated that miR-124-3p directly bound to the 3' UTR region of PLOD3. Upregulation of miR-124-3p significantly suppressed the proliferation, migration and invasion capacity of HNSCC cells, while downregulation of miR-124-3p promoted the

oncogenic activities of cancer cells, indicating miR-124-3p might play a tumor suppressive role in HNSCC. More importantly, overexpression of PLOD3 could partially restore the proliferation, migration and invasion capacity of cancer cells following miR-124-3p upregulation, suggesting that miR-124-3p is a powerful and functional upstream regulator of PLOD3. RNA seq analysis revealed that PLOD3 downregulation affected many important pathways such as cell cycle, regulation of the actin cytoskeleton and focal adhesion. In addition, the morphology of cancer cell became round following PLOD3 inhibition. Moreover, FAK-PI3K-AKT pathway was demonstrated to be an important downstream effector for the oncogenic role of PLOD3 in HNSCC.

Accumulating evidence has shown that miRNAs play a crucial role in the initiation and progression of cancers[192,193]. MiR-124 was firstly identified by cloning studies in mice[194]. It is derived from three independent genes (*miR-124-1*, *miR-124-2*, and *miR-124-3*), whose chromosome locations are distinct from one another[195]. Like many other miRNAs, the nucleotide sequence of miR-124 precursors is different across different species. However, the sequences of mature miR-124 is highly conserved[196]. However, knock-out of miR-124-1 gene not only led to the downregulation of mature miR-124 levels, but also resulted in defective neuronal survival and axonal outgrowth as well as smaller brain size[197], indicating that the functional compensation among *miR-124-1*, *miR-124-2*, and *miR-124-3* might be not strong. MiR-124 family is highly expressed in the adult brain of vertebrates and plays an important role in neurogenesis by facilitating neural differentiation[198-200]. Overexpression of miR-124 remarkably suppressed the proliferative capacity of vascular smooth muscle cells (VSMCs) by regulating S100 calcium-binding protein A4 (S100A4). S100A4 is known inducer of VSMC proliferation and migration, suggesting miR-124 might be an important regulator for the development of neointimal

proliferation[201]. MiR-124 was demonstrated to be a negative regulator of osteogenic and myogenic differentiation[202,203]. Sun et al reported that miR-124 was a crucial mediator for the cholinergic anti-inflammatory action. Upregulation of miR-124 decrease IL-6 and TNF- α production by downregulating signal transducer and activator of transcription 3 (STAT3) and TNF-α converting enzyme (TACE) respectively[204]. MiR-124 is also important for the maintaining the homeostasis of immune system. Deregulation of miR-124 has been shown to be closely associated with various immunological disorders such as inflammatory bowel diseases, rheumatoid arthritis and ankylosing spondylitis[205].

Consistent with our findings, miR-124-3p was demonstrated to function as a tumor suppressor in HNSCC. The expression level of miR-124 was significantly reduced in HNSCC tissues compared to the normal controls. Upregulation of miR-124 suppressed the malignant phenotypes of cancer cells both *in vitro* and *in vivo* by downregulating sphingosine kinase 1 (SPHK1)[206]. MiR-124 levels were reported to be reduced in cancer associated fibroblasts (CAFs) and oral cancer cells (OCCs) compared to the normal fibroblasts. In addition, ectopic expression of miR-124 in CAFs-OCCs co-culture system could significantly attenuate the proliferation and migration of OCCs[207]. In addition to HNSCC, miR-124 plays a tumor suppressive role in various types of cancers. For instance, the expression level miR-124 was downregulated in bladder cancer tissues compared to the normal controls. miR-124 overexpression significantly abrogated the proliferation, migration, invasion and vasculogenic mimicry *in vitro* and tumor growth *in vivo* by regulating ubiquitin like with PHD and ring finger domains 1 (UHRF1)[208]. MiR-124 was significantly decreased in metastatic bone tissues from breast cancers. Reduced miR-124 expression was correlated with unfavorable clinical characteristics and worse bone metastasis-free survival and overall survival. Restoration of miR-124 inhibited the bone

metastasis of breast cancer cells *in vivo*, and opposite results were observed when miR-124 was inhibited[209]. Similarly, the expression level of miR-124-3p was downregulated in glioblastoma multiforme (GBM) tissues in comparison with normal brain tissues based on the high-throughput sequencing. In addition, miR-124-3p overexpression significantly inhibited GBM cell proliferation, migration and tumor angiogenesis by regulating Neuropilin-1[210]. In most cases, a specific miRNA might function as an oncogene or a tumor suppressor in the different types of cancer or even in the same type of cancers. The regulatory role of miRNAs in cancer seems to be closely associated with the cancer types and the tumor microenvironments. However, to the best of our knowledge, currently all the studies consistently demonstrated that miR-124 was a tumor suppressor gene in the tumorigenesis. In combination with our findings, miR-124 downregulation is an important molecular event for the initiation and development of HNSCC. One possible mechanism accounting for miR-124 downregulation in HNSCC is methylation. Further studies are warranted to verify this hypothesis.

Our results showed that miR-124-3p was an upstream regulator of PLOD3, and overexpression of PLOD3 partially rescued the tumor suppressive effects of miR-124-3p, indicating that PLOD3 is a functional downstream effector of miR-124-3p. As we have demonstrated PLOD3 played a tumor promoting role in HNSCC, the downregulation of miR-124-3p in HNSCC might result in the PLOD3 overexpression, which subsequently enhance carcinogenesis.

We then performed RNA-seq to investigate the downstream pathways regulated by PLOD3. It was not surprising to observe that cell cycle was one of the most significantly deregulated pathways following PLOD3 suppression in both HNSCC cell lines, which was in line with our phenotype studies. Other interesting affected pathways included homologous recombination, purine and pyrimidine metabolism, focal adhesion, regulation of actin cytoskeleton, chemokine

signaling pathway, spliceosome and ubiquitin mediated proteolysis. Homologous recombination might exert a fundamental role in carcinogenesis. HR might serve as an errant DNA repair mechanism that can lead to loss of heterozygosity or genetic rearrangements[211]. Purines and pyrimidines serve as the building blocks of DNA and RNA. In addition, they are important for energy conservation and transport, coenzymes synthesis and phospholipid and carbohydrate metabolism[212,213]. Therefore, defective in purine and pyrimidine metabolism significantly affect any system in a cell. Adhesion of cells to the ECM is crucial for maintaining the normal cellular morphology, migration, proliferation, survival, and differentiation. One interesting finding was that the cells with PLOD3 knockdown gradually became round and died. In addition, most of the siPLOD3 treated cancer cells failed to re-attach to the plates when they were passaged. As PLOD3 is indispensable for the collagen synthesis, it was reasonable to observe that PLOD3 deletion affected the adhesion of cancer cells. Furthermore, the functional analysis showed that focal adhesion and regulation of actin cytoskeleton were the most influenced pathways following PLOD3 downregulation. Focal adhesions are multi-protein complexes that are essential for cell contact with the extracellular matrix (ECM) and cellular communication between the ECM and the cell cytoplasm[214,215]. Chemokines are soluble factors which are critical for regulating immune cell recruitment during inflammatory responses and defense against foreign pathogens. Deregulated chemokine signaling pathways have been implicated in cancer development[216]. The spliceosome is a ribonucleoprotein complex involved in RNA splicing, namely removing non-coding introns from precursor messenger RNA. Deregulated alternative splicing might affect many biological processes such as cell cycle control, signal transduction, angiogenesis, motility and invasion and the metastasis and apoptosis[75]. Ubiquitin mediated proteolysis plays a major role in many basic cellular processes such as regulation of cell cycle, modulation of the immune

and inflammatory responses, control of signal transduction pathways, development and differentiation[217].

FAK is a non-receptor tyrosine kinase that acts as a central regulator in signaling networks arising from focal adhesions. As focal adhesion and regulation of actin cytoskeleton were significantly affected after PLOD3 suppression, we hypothesized that FAK might be a downstream target of PLOD3. Our results showed that PLOD3 inhibition suppressed the expression level of pFAK in both cell lines, while pFAK was increased when PLOD3 was overexpressed, indicating PLOD3 was an upstream regulator of pFAK. In addition, targeted inhibition of FAK significantly abrogated the tumor promoting effects of PLOD3. Activation of FAK has been demonstrated to play a pivotal role in promoting cancer progression and metastasis. It is important for cell adhesion, motility, proliferation, and survival in many cell types[218,219]. PI3K-AKT is a downstream signaling pathway of FAK. Interestingly, the expression levels of pPI3K-pAKT were significantly decreased following PLOD3 inhibition, and *vice versa*, indicating PLOD3 downregulation significantly suppressed FAK-PI3K-AKT signaling pathway. The PI3K-AKT signaling pathway is frequently deregulated in almost all types of cancers including HNSCC[220,221].

Based on the current findings, we propose the following model which might play an important role in the tumorigenesis of HNSCC. Firstly, methylation of miR-124-3p leads to the downregulation of miR-124-3p in HNSCC. The expression level of PLOD3 increases significantly without the suppressive effects of miR-124-3p. Finally, upregulation of PLOD3 promotes the tumorigenesis of cancer cells by partially activating FAK-PI3K-AKT signaling pathway.

5 CONCLUSIONS AND OUTLOOK

In this project, we have identified many novel genes/metabolic enzymes or metabolites that might contribute to the tumorigenesis of HNSCC. Future studies are warranted to evaluate their potential clinical significance for early detecting and prognosis prediction for HNSCC. MiR-124-3p-PLOD3-FAK/PI3K/AKT is demonstrated to be an important signaling pathway for HNSCC carcinogenesis, and this might offer a novel therapeutic target for HNSCC. In addition, our preliminary studies have demonstrated PLOD3 is a powerful regulator for HIF1a, which is a central modulator of cellular metabolism. Future studies are needed to explore the underlying molecular mechanisms for the oncogenic role of PLOD3 in HNSCC.

FIGURES AND FIGURE LEGENDS

Figure 1 The differentially expressed genes (DEGs) between HNSCC and adjacent normal tissues. Volcano plot was generated to visualize DEGs, and red or blue dots in the plots indicated significantly upregulated or downregulated genes respectively **(Figure 1A)**. Heat map was generated with based on the expression levels of DEGs. Each column represented a biological sample and each row in the heat map represents a gene **(Figure 1B).**

Figure 2 The top enriched pathways in HNSCC tissues. Gene set enrichment analysis (GSEA) showed that the top enriched pathway in the HNSCC included cell cycle, DNA replication, homologous recombination, purine metabolism, pyrimidine metabolism, snare interactions in vesicular transport, spliceosome, proteasome, basic transcriptional factors, and N-glycan biosynthesis **(Figure 2A-2J)**.

Figure 3 The top enriched pathways in adjacent normal tissues. Pathways including citrate TCA cycle, oxidative phosphorylation, fatty acid metabolism, PPAR signaling pathway, calcium signaling pathway, propanoate metabolism, butanoate metabolism, tryptophan metabolism, alanine and aspartate and glutamate pathway, and valine leucine and isoleucine degradation were enriched in adjacent normal tissues **(Figure 3A-3J)**.

Figure 4 The differentially expressed metabolites between HNSCC and adjacent normal tissues. Volcano plots of metabolic features that were significantly different between HNSCC tissues and adjacent normal tissues. Y-axis indicated the p values (log-scaled), whereas the X-axis showed the fold change (log-scaled). Each symbol represented a different metabolic feature, and the red color of the symbol indicated the significantly changed metabolic features **(Figure 4A)**. Heat map analysis of significantly different m/z. Each row represented a different ion, with

each column representing a sample. The different colors indicate different intensities, and the colors range from green to red, indicating a low to high intensity **(Figure 4B)**. PLS-DA scores plots of tissues samples showed there were obvious difference between HNSCC tissues and adjacent normal tissues **(Figure 4C)**.

Figure 5 Acylcarnitines are significantly enriched in HNSCC. The levels of various acylcarnitines including 2-hydroxymyristoyl carnitine, 2-methylbutyroyl carnitine, 3-hydroxypenta decanoyl carnitine, 3-hydroxyl undecanoyl carnitine, 12-hydroxy-12-octadecanoylcarnitine, arachidyl carnitine, cervonyl carnitine, cis-5-tetradecenoyl carnitine, clupanodonyl carnitine **(Figure 5A)**, dodecanoylcarnitine, heptadecanoyl carnitine, hydroxyvaleryl carnitine, L-palmitoylcarnitine, methylmalonyl carnitine, stearoylcarnitine, succinylcarnitine, tetracosatetraenoyl carnitine and tetradecanoyl carnitine **(Figure 5B)** were remarkably upregulated in HNSCC tissues.

Figure 6 Sphingosine-1-phosphate metabolic pathway is upregulated in HNSCC. The levels of metabolites in sphingosine-1-phosphate metabolic pathway including ceremides sphingosine, sphingosine-1-phosphate, phosphonoethanolamine, palmitaldehyde and hexadecenal were increased in HNSCC.

Figure 7 DNA damage related metabolites are increased in HNSCC. Various types of DNA damage associated metabolites including 1-methyladenine, 8-hydroxyadenine, FAPy-adenine, 5-methycytosine, 8-Oxo-dGMP, 3'-O-methylguanine, 8-hydroxyguanine and 8-hydroxyl-deoguanine were elevated in HNSCC **(Figure 7)**.

Figure 8 Nucleotide associated metabolites are increased in HNSCC. The levels of various bases (adenine, cytosine, guanine and uracil), nucleoside (guanosine), and nucleotide derivatives

(adenosine monophosphate, cytodine monophosphate, cytidine 2',3'-cyclic phosphate and uridine 2',3'-cyclic phosphate) were increased in HNSCC.

Figure 9 The levels of pyrimidine nucleotide sugars and amino acids are increased in HNSCC. The levels of pyrimidine nucleotide sugars (UDP-N-acetyl-alpha-D-galactosamine, uridine diphosphate-N-acetylglucosamine and uridine diphosphategalactose) **(Figure 9A)** and amino acids (L-asparagine, L-aspartic acid, L-glutamic acid, L-valine, L-proline and L-serine) were higher in the tumor tissues compared with adjacent normal tissues **(Figure 9B)**.

Figure 10 The representative upregulated lipids in HNSCC. Various lipids such as CE (20:4(5Z, 8Z, 11Z, 14Z), CE (20:2(6Z, 9Z)), PC (14:0/16:0), PIP (16:0/20:4(5Z, 8Z, 11Z, 14Z)), PE (16:1(9Z)/18:2 (9Z, 12Z)), PE (18:1(11Z)/18:2(9Z, 12Z)), PE(14:0/20:2(11Z,14Z)), PE(18:1(11Z)/20:5(5Z,8Z,11Z,14Z,17Z)), and PE(18:1(9Z)/22:5(4Z,7Z,10Z,13Z,16Z)) and PE(14:0/14:0) were increased in tumor samples.

Figure 11 Melatonin pathway is downregulated in HNSCC. The metabolites in the melatonin pathways including L-tryptophan, 5-hydroxytryptophan, N-acetylserotonin, melatonin, cyclic melatonin, 6-sulfatoxymelatonin and 6-hydroxymelatonin glucuronide were decreased in HNSCC tissues.

Figure 12 Vitamin D pathway, coenzyme 10 and retinoic acids are downregulated in HNSCC. The levels of several metabolites in the vitamin D pathway (vitamin D3, calcidiol and 24-hydroxycalcitriol) **(Figure 12A)**, coenzyme Q10 pathway (ubiquinone-2 and coenzyme Q10) **(Figure 12B)**, and retinoic acid pathway (4-oxo-retinoic acid and 4-hydroxyretinoic acid) **(Figure 12C)** were reduced in HNSCC.

Figure 13 Interested downregulated metabolites in HNSCC. Various metabolites such as Gamma-linolenic acid, 9,10-DiHODE, dodecanedioic acid, L-phenylalanine, N-butyrylglycine, hippuric acid, 3-O-sulfogalactosyl ceramide (d18:1/16:0), ganglioside GM3 (d18:0/12:0) and 13-HOTE were also found to be reduced in the tumor samples.

Figure 14 The representative downregulated lipids in HNSCC. Many lipids such as LysoPE(20:5(5Z,8Z,11Z,14Z,17Z)/0:0), PS(MonoMe(11,3)/MonoMe(11,5)), LysoPC(10:0), PC(22:5(4Z,7Z,10Z,13Z,16Z)/22:6(4Z,7Z,10Z,13Z,16Z,19Z))), PS(18:0/18:0), DG(20:5n3/0:0/22:6n3), PE(16:0/22:6(4Z,7Z,10Z,13Z,16Z,19Z)), PS(18:0/18:1(9Z)) MG(18:4(6Z,9Z,12Z,15Z)/0:0/0:0) and PS(20:3(8Z,11Z,14Z)/20:3(8Z,11Z,14Z)) were downregulated in tumor samples.

Figure 15 The differentially expressed metabolic enzymes between HNSCC and adjacent normal tissues. IPA analysis of the differentially expressed metabolic enzymes to reveal the altered metabolic pathways in HNSCC **(Figure 15A)**. Heat map was used to visualize the distribution of differentially expressed metabolic enzymes between HNSCC tissues and adjacent normal tissues **(Figure 15B)**.

Figure 16 PLOD3 is increased in HNSCC tissues based on GEO data and TCGA. The levels of PLOD3 were higher in HNSCC tissues compared with the normal tissues in various independent studies (GSE6631, GSE37991, GSE23558, GSE25099, GSE30784 and TCGA). In addition, PLOD3 levels were higher in HNSCC tissues compared to oral precancerous lesions (GSE85514 and GSE30784). HNSCC patients with higher PLOD3 suffered worse long term overall survival.

Figure 17 PLOD3 is increased in various types of cancers. Based on the data available from TCGA database, we found that the expression level of PLOD3 was significantly increased in cancer tissues including acute myeloid leukemia (AML), bladder urothelial carcinoma (BLCA), breast cancer (BRCA), colon adenocarcinoma (COAD), cholangiocarcinoma (CHOL), esophageal carcinoma (ESCA), glioblastoma(GBM), kidney chromophobe (KICH), kidney renal clear cell carcinoma(KIRC) **(Figure 17A)**, kidney renal papillary cell carcinoma (KIRP), liver hepatocellular carcinoma(LIHC), lung adenocarcinoma(LUAD), lung squamous cell carcinoma(LUSC), prostate adenocarcinoma(PRAD), rectum adenocarcinoma(READ), stomach adenocarcinoma(STAD), stomach and esophageal carcinoma(STES) and thyroid carcinoma(THCA) **(Figure 17B)**.

Figure 18 PLOD3 upregulation is associated with unfavorable overall survival in various types of cancers. Based on the data available from TCGA database, higher PLOD3 expression was associated with poorer long-term overall survival rates in many other types of cancers including GBM, KIRC, LIHC, LUSC, low grade glioma (LGG), LUAD, ovarian cancer (OV), cervical squamous cell carcinoma (CESC), THCA and sarcoma (SARC).

Figure 19 The expression level of PLOD3 in HNSCC cell lines and tissues. The expression levels of PLOD3 were significantly higher in all the HNSCC cell lines compared to the normal cells **(Figure 19A-19B)**. In addition, the expression levels of PLOD3 were upregulated in HNSCC tissues in comparison with the matched adjacent normal tissues **(Figure 19C-19D)**.

Figure 20 Immunohistochemical analysis of PLOD3 staining intensity in HNSCC. The results showed the expression of PLOD3 to increase gradually with the progression of carcinogenesis from normal epithelium, well differentiated HNSCC, moderately differentiated HNSCC to poorly differentiated HNSCC **(Figure 20A-20B)**.

Figure 21 Downregulation of PLOD3 suppresses the malignant phenotypes of HNSCC cells *in vitro*. The expression levels of PLOD3 mRNA and proteins were significantly downregulated following siPLOD3 (siRNA1 and siRNA2) transfection **(Figure 21A-21C)**. Downregulation of PLOD3 inhibited the proliferation, migration and invasion capacity of HNSCC cells *in vitro* **(Figure 21D-21H)**.

Figure 22 Downregulation of PLOD3 suppresses tumor growth of HNSCC cells *in vivo*. The tumor volume and weight were both significantly lower in HNSCC cells with PLOD3 downregulation

Figure 23 Upregulation of PLOD3 promotes the malignant phenotypes of HNSCC cells *in vitro*. The expression levels of PLOD3 mRNA and proteins were significantly upregulated following PLOD3 overexpressing lentiviruses infection **(Figure 21A-21B)**. Downregulation of PLOD3 inhibited the proliferation, migration and invasion capacity of HNSCC cells *in vitro* **(Figure 21C-21G)**.

Figure 24 Ectopic expression of PLOD3 promotes tumor growth of HNSCC cells *in vivo*. The tumor volume and weight were both significantly increased in HNSCC cells with PLOD3 overexpression.

Figure 25 MiR-124-3p directly targets PLOD3 by binding to 3'-UTR region. PLOD3 3'UTR was highly complementary to the seed sequence of miR-124-3p **(Figure 25A)**. In addition, the 3'-UTR PLOD3 sequence that miR-124-3p targeted was highly conserv0ed across different species **(Figure 25B)**. Luciferase assays showed that the miR-124-3p mimic significantly suppressed relative luciferase activity compared to the scramble control **(Figure 25C)**. MiR-124-3p mimic remarkably reduced PLOD3 expression at the protein level **(Figure 25D-25E)**.

Figure 26 Upregulation of miR-124-3p suppresses the malignant phenotypes of HNSCC cells *in vitro*. The expression level of miR-124-3p was significantly increased following miR-124-3p mimic transfection **(Figure 26A)**. Upregulation of miR-124-3p inhibited the proliferation, migration and invasion capacity of HNSCC cells *in vitro* **(Figure 26B-26F)**.

Figure 27 Downregulation of miR-124-3p promotes the malignant phenotypes of HNSCC cells *in vitro*. The expression level of miR-124-3p was significantly decreased following miR-124-3p inhibitor transfection **(Figure 27A)**. Downregulation of miR-124-3p promoted the proliferation, migration and invasion capacity of HNSCC cells *in vitro* **(Figure 27B-27F)**.

Figure 28 PLOD3 overexpression partially rescues the tumor suppressive effects of miR-124-3p. WB results showed that the levels of PLOD3 were higher in HNSCC cells infected with PLOD3 overexpressing lentiviruses following miR-124-3p mimic transfection **(Figure 28A)**. PLOD3 overexpression could partially increase HNSCC cell proliferation, migration and invasion capacity which were inhibited by miR-124-3p upregulation **(Figure 28B-28F).**

Figure 29 RNA-seq analysis the DEGs following PLOD3 downregulation. Compared to the controls, a total of 3275 (1631 upregulated and 1644 downregulated) and 3146 (1497 upregulated and 1649 downregulated) DEGs were found siPLOD3-treated SCC1 and SCC23 cells respectively **(Figure 29A)**. Heap map was used to visualize the distribution of DEGs following PLOD3 inhibition **(Figure 29B)**. In addition, most DEGs were overlapped between SCC1 and SCC23 **(Figure 29C)**.

Figure 30 The top enriched pathways following PLOD3 downregulation. The results showed that the top enriched pathways following PLOD3 knockdown included cell cycle, homologous recombination, purine and pyrimidine metabolism, focal adhesion, regulation of actin

cytoskeleton, chemokine signaling pathway, spliceosome and ubiquitin mediated proteolysis **(Figure 30A-30H)**.

Figure 31 PLOD3 inhibition significantly affects the morphology of HNSCC cells. The morphology of cancer cells became round and the cells were not able to reattach to the plates following PLOD3 downregulation.

Figure 32 PLOD3 is an upstream modulator of FAK-PI3K-AKT signaling pathway. The expression levels of pFAK, pPI3K and pAKT was significantly downregulated following PLOD3 downregulation, while their levels were upregulated when PLOD3 was overexpressed.

Figure 33 The tumor promoting role of PLOD3 is mediated by phosphorylation of FAK in HNSCC cells. The expression levels of FAK and pFAK were both significantly reduced following siFAK transfection **(Figure 33A)**. FAK and pFAK downregulation could significantly inhibit HNSCC cell proliferation, migration and invasion capacity which were promoted by PLOD3 overexpression **(Figure 28B-28F)**.

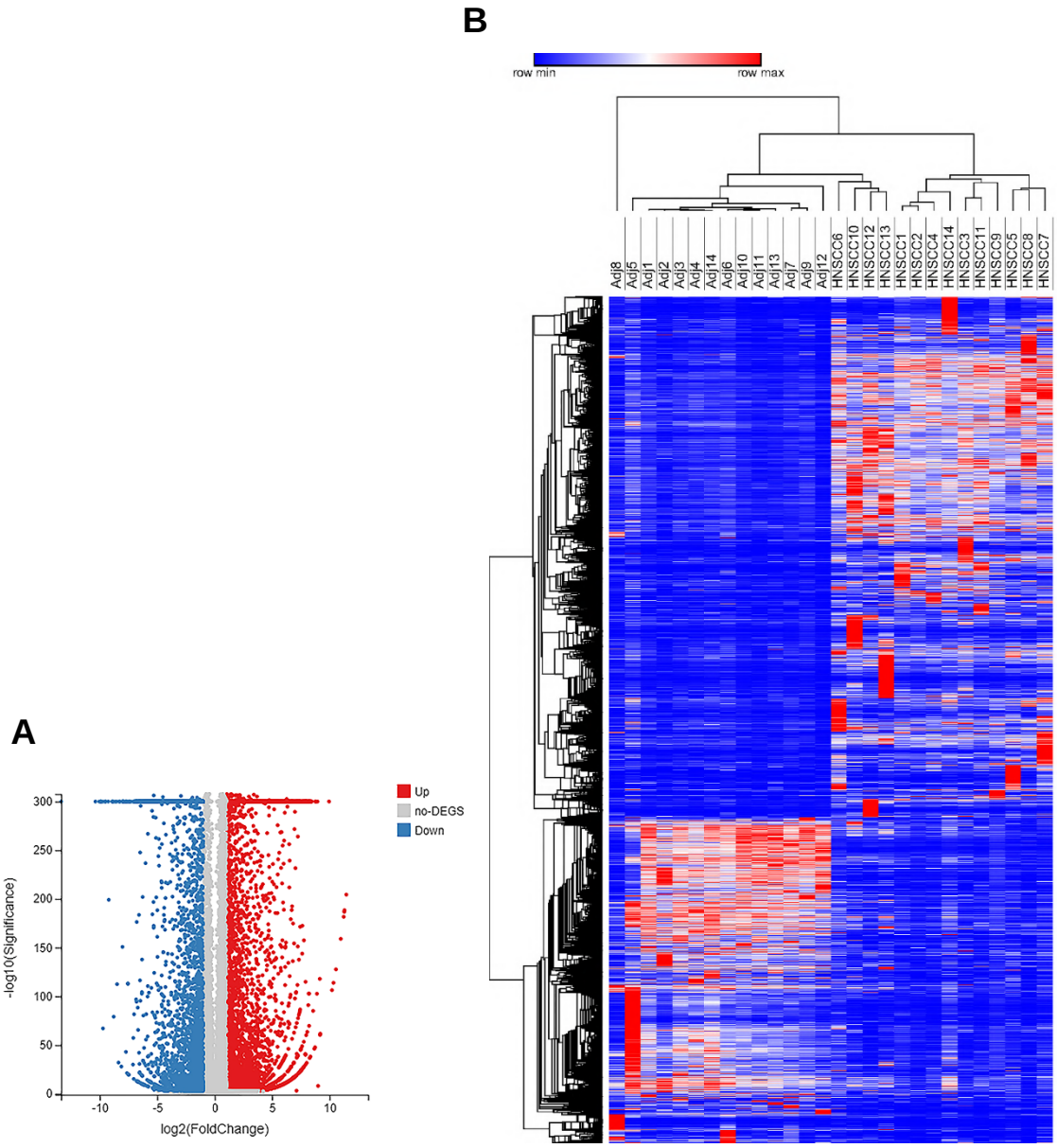
A
B
row min
row max
Adj8
Adj5
Adj1
Adj2
Adj3
Adj4
Adj14
Adj6
Adj10
Adj11
Adj13
Adj7
Adj9
Adj12
HNSCC6
HNSCC10
HNSCC12
HNSCC13
HNSCC1
HNSCC2
HNSCC4
HNSCC14
HNSCC3
HNSCC11
HNSCC9
HNSCC5
HNSCC8
HNSCC7
Up
no-DEGS
Down
-log10(Significance)
log2(FoldChange)
300
250
200
150
100
50
0
-10
-5
0
5
10

Figure 1

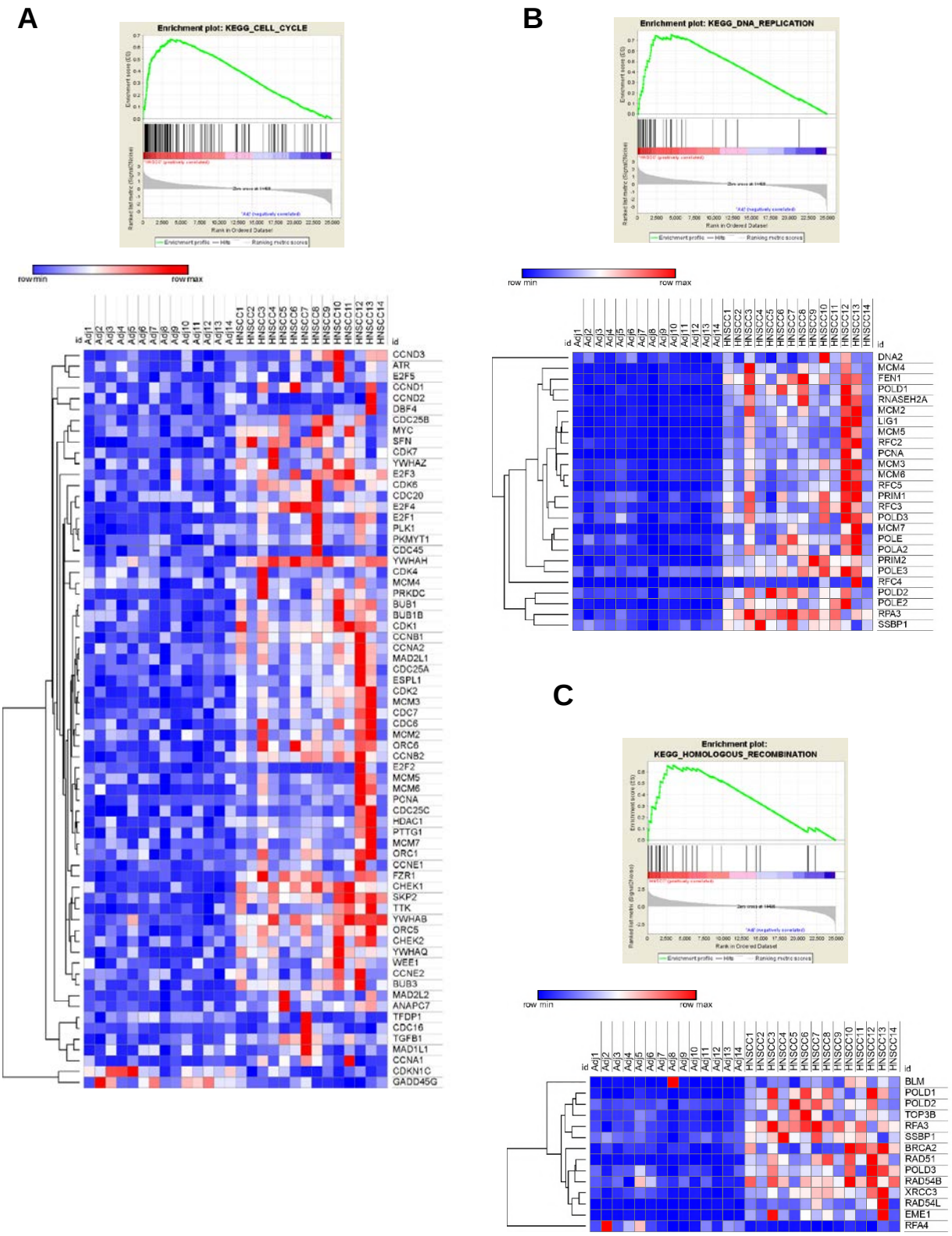
A
Enrichment plot: KEGG_CELL_CYCLE
row min
row max
id
Adj1 Adj2 Adj3 Adj4 Adj5 Adj6 Adj7 Adj8 Adj9 Adj10 Adj11 Adj12 Adj13 Adj14
HNSCC1 HNSCC2 HNSCC3 HNSCC4 HNSCC5 HNSCC6 HNSCC7 HNSCC8 HNSCC9 HNSCC10 HNSCC11 HNSCC12 HNSCC13 HNSCC14
CCND3
ATR
E2F5
CCND1
CCND2
DBF4
CDC25B
MYC
SFN
CDK7
YWHAZ
E2F3
CDK6
CDC20
E2F4
E2F1
PLK1
PKMYT1
CDC45
YWHAH
CDK4
MCM4
PRKDC
BUB1
BUB1B
CDK1
CCNB1
CCNA2
MAD2L1
CDC25A
ESPL1
CDK2
MCM3
CDC7
CDC6
MCM2
ORC6
CCNB2
E2F2
MCM5
MCM6
PCNA
CDC25C
HDAC1
PTTG1
MCM7
ORC1
CCNE1
FZR1
CHEK1
SKP2
TTK
YWHAB
ORC5
CHEK2
YWHAQ
WEE1
CCNE2
BUB3
MAD2L2
ANAPC7
TFDP1
CDC16
TGFB1
MAD1L1
CCNA1
CDKN1C
GADD45G
B
Enrichment plot: KEGG_DNA_REPLICATION
row min
row max
DNA2
MCM4
FEN1
POLD1
RNASEH2A
MCM2
LIG1
MCM5
RFC2
PCNA
MCM3
MCM6
RFC5
PRIM1
RFC3
POLD3
MCM7
POLE
POLA2
PRIM2
POLE3
RFC4
POLD2
POLE2
RPA3
SSBP1
C
Enrichment plot:
KEGG_HOMOLOGOUS_RECOMBINATION
row min
row max
BLM
POLD1
POLD2
TOP3B
RPA3
SSBP1
BRCA2
RAD51
POLD3
RAD54B
XRCC3
RAD54L
EME1
RPA4

Figure 2A-2C

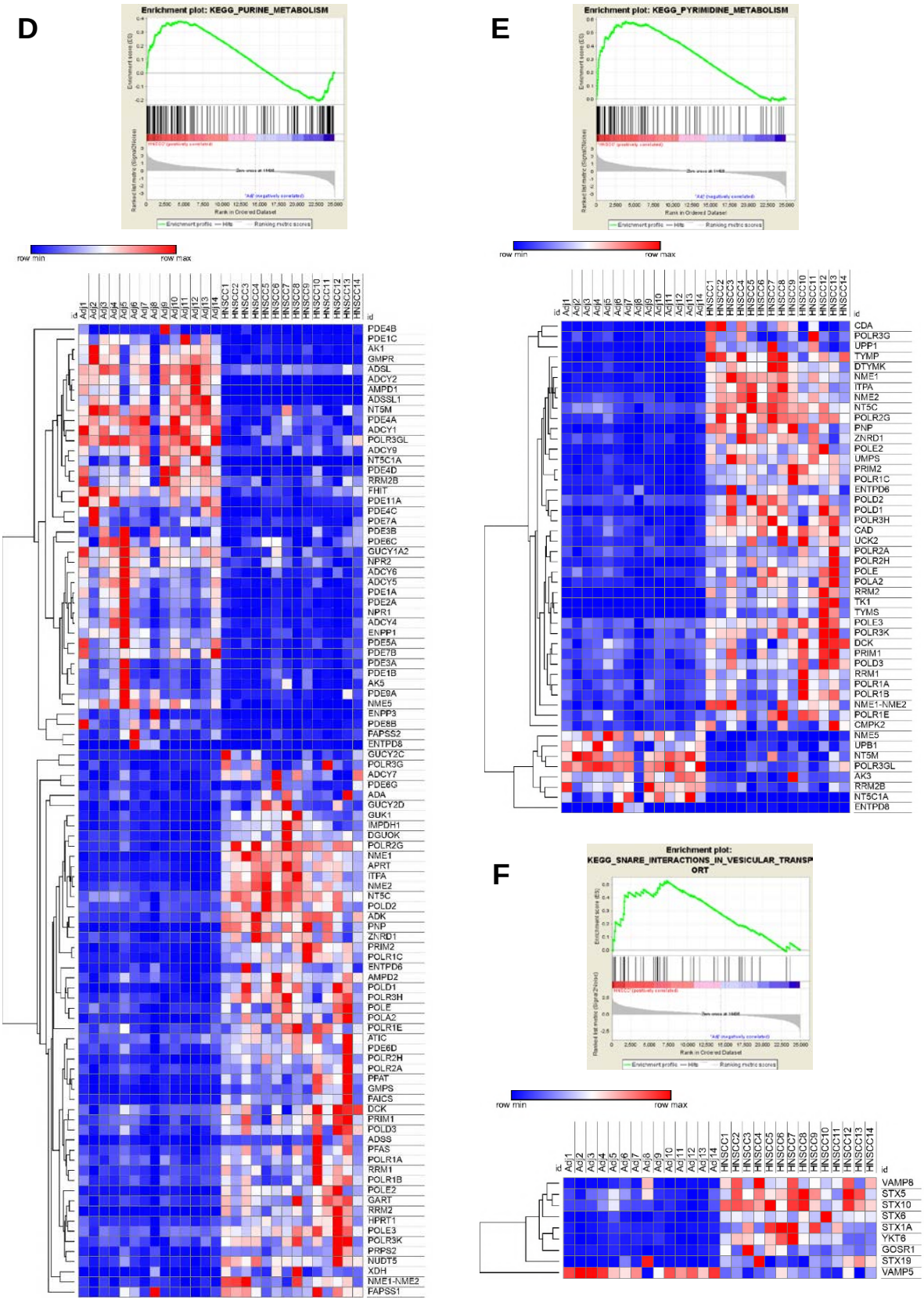
D
Enrichment plot: KEGG_PURINE_METABOLISM
row min
row max
PDE4B
PDE1C
AK1
GMPR
ADSL
ADCY2
AMPD1
ADSSL1
NT5M
PDE4A
ADCY1
POLR3GL
ADCY9
NT5C1A
PDE4D
RRM2B
FHIT
PDE11A
PDE4C
PDE7A
PDE3B
PDE6C
GUCY1A2
NPR2
ADCY6
ADCY5
PDE1A
PDE2A
NPR1
ADCY4
ENPP1
PDE5A
PDE7B
PDE3A
PDE1B
AK5
PDE9A
NME5
ENPP3
PDE8B
PAPSS2
ENTPD8
GUCY2C
POLR3G
ADCY7
PDE6G
ADA
GUCY2D
GUK1
IMPDH1
DGUOK
POLR2G
NME1
APRT
ITPA
NME2
NT5C
POLD2
ADK
PNP
ZNRD1
PRIM2
POLR1C
ENTPD6
AMPD2
POLD1
POLR3H
POLE
POLA2
POLR1E
ATIC
PDE6D
POLR2H
POLR2A
PFAT
GMPS
FAICS
DCK
PRIM1
POLD3
ADSS
PFAS
POLR1A
RRM1
POLR1B
POLE2
GART
RRM2
HPRT1
POLE3
POLR3K
PRPS2
NUDT5
XDH
NME1-NME2
PAPSS1
E
Enrichment plot: KEGG_PYRIMIDINE_METABOLISM
row min
row max
CDA
POLR3G
UPP1
TYMP
DTYMK
NME1
ITPA
NME2
NT5C
POLR2G
PNP
ZNRD1
POLE2
UMPS
PRIM2
POLR1C
ENTPD6
POLD2
POLD1
POLR3H
CAD
UCK2
POLR2A
POLR2H
POLE
POLA2
RRM2
TK1
TYMS
POLE3
POLR3K
DCK
PRIM1
POLD3
RRM1
POLR1A
POLR1B
NME1-NME2
POLR1E
CMPK2
NME5
UPB1
NT5M
POLR3GL
AK3
RRM2B
NT5C1A
ENTPD8
F
Enrichment plot: KEGG_SNARE_INTERACTIONS_IN_VESICULAR_TRANSPORT
row min
row max
VAMP8
STX5
STX10
STX6
STX1A
YKT6
GOSR1
STX19
VAMP5

Figure 2D-2F

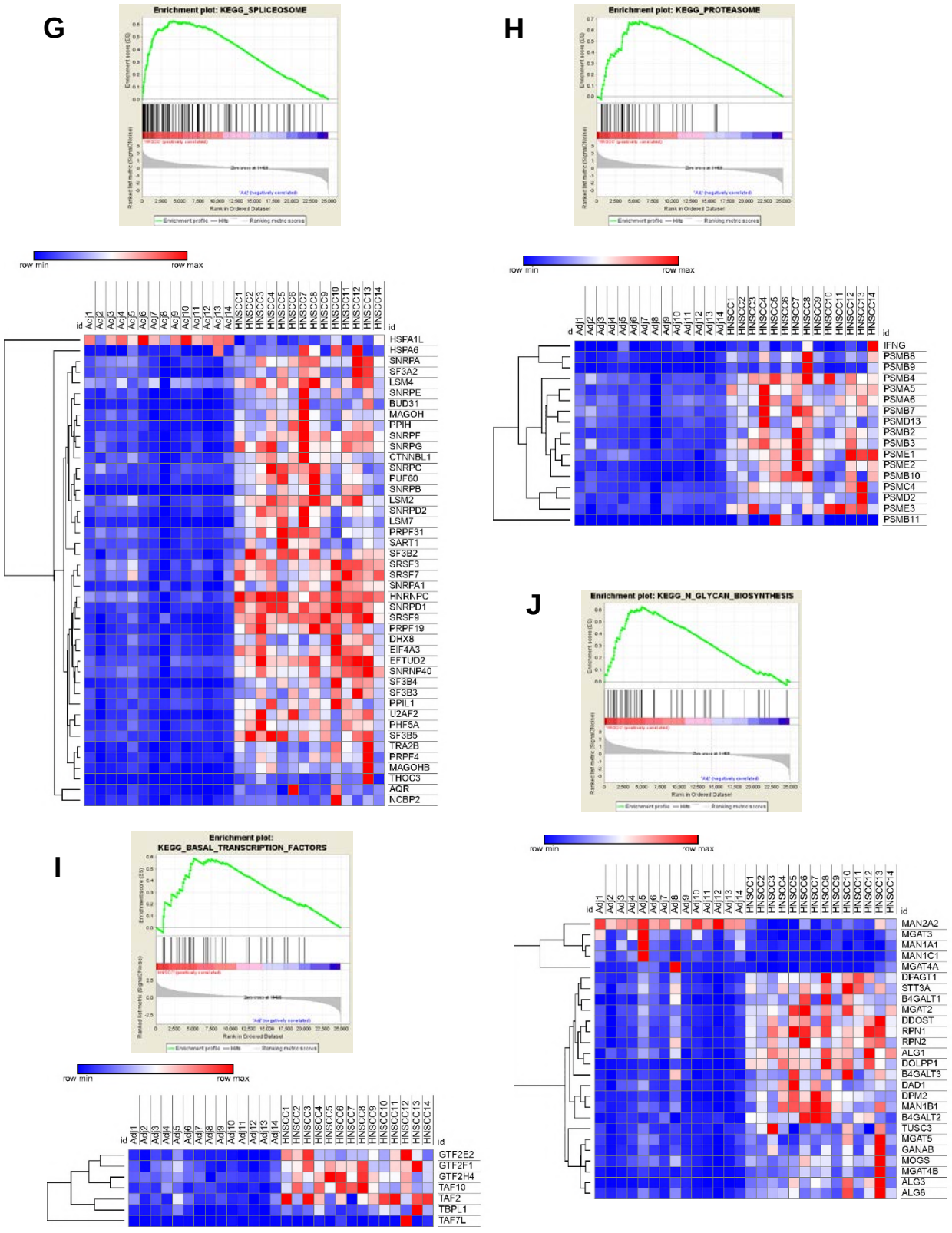
G
Enrichment plot: KEGG_SPLICEOSOME
row min
row max
HSFA1L
HSFA6
SNRFA
SF3A2
LSM4
SNRPE
BUD31
MAGOH
PPIH
SNRPF
SNRPG
CTNNBL1
SNRPC
PUF60
SNRPB
LSM2
SNRPD2
LSM7
PRPF31
SART1
SF3B2
SRSF3
SRSF7
SNRFA1
HNRNPC
SNRPD1
SRSF9
PRPF19
DHX8
EIF4A3
EFTUD2
SNRNP40
SF3B4
SF3B3
PPIL1
U2AF2
PHF5A
SF3B5
TRA2B
PRPF4
MAGOHB
THOC3
AQR
NCBP2
H
Enrichment plot: KEGG_PROTEASOME
row min
row max
IFNG
PSMB8
PSMB9
PSMB4
PSMA5
PSMA6
PSMB7
PSMD13
PSMB2
PSMB3
PSME1
PSME2
PSMB10
PSMC4
PSMD2
PSME3
PSMB11
J
Enrichment plot: KEGG_N_GLYCAN_BIOSYNTHESIS
row min
row max
MAN2A2
MGAT3
MAN1A1
MAN1C1
MGAT4A
DPAGT1
STT3A
B4GALT1
MGAT2
DDOST
RPN1
RPN2
ALG1
DOLPP1
B4GALT3
DAD1
DPM2
MAN1B1
B4GALT2
TUSC3
MGAT5
GANAB
MOGS
MGAT4B
ALG3
ALG8
I
Enrichment plot:
KEGG_BASAL_TRANSCRIPTION_FACTORS
row min
row max
GTF2E2
GTF2F1
GTF2H4
TAF10
TAF2
TBPL1
TAF7L

Figure 2G-2J

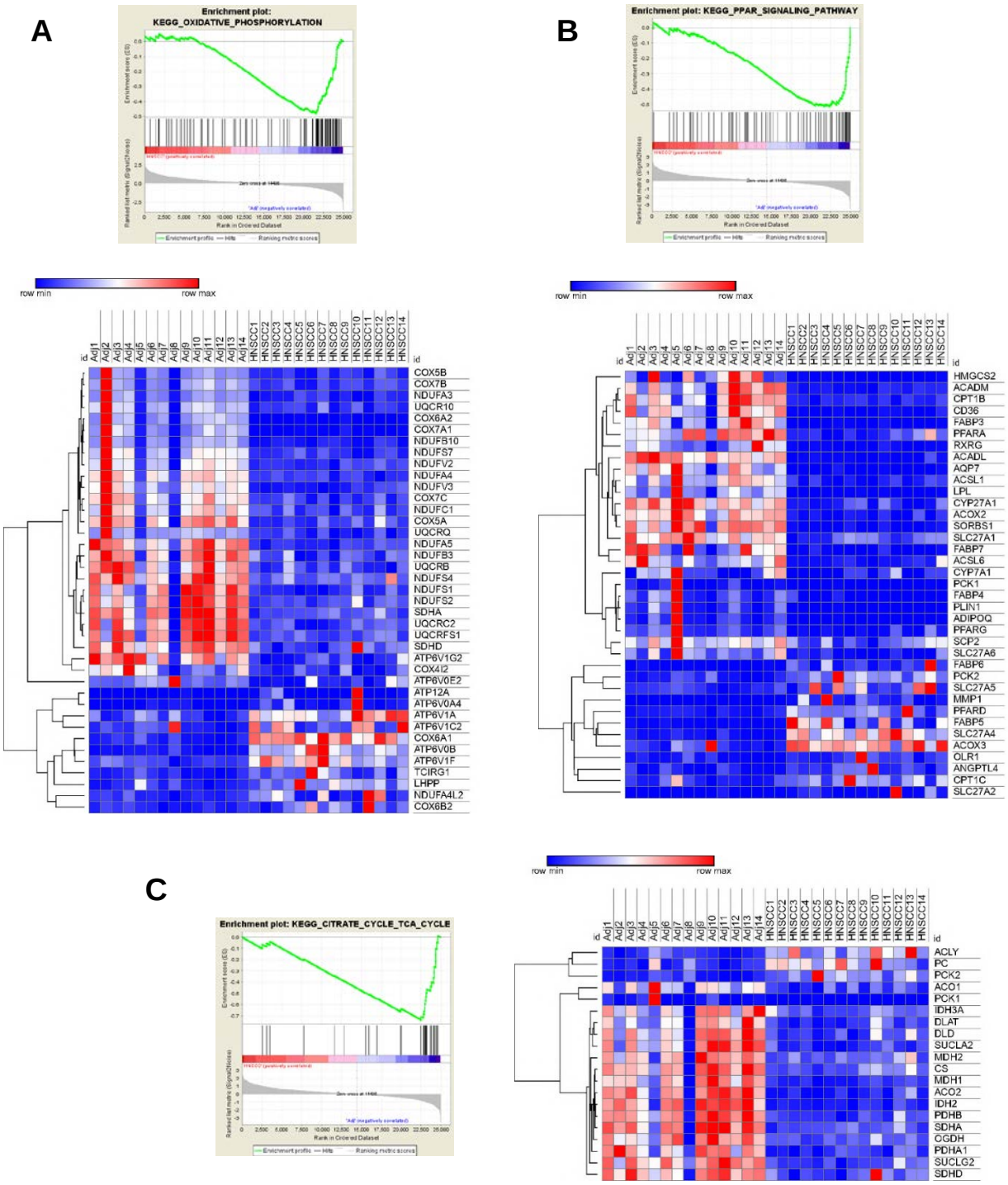
A
Enrichment plot:
KEGG_OXIDATIVE_PHOSPHORYLATION
B
Enrichment plot: KEGG_PPAR_SIGNALING_PATHWAY
row min
row max
id
COX5B
COX7B
NDUFA3
UQCR10
COX6A2
COX7A1
NDUFB10
NDUFS7
NDUFV2
NDUFA4
NDUFV3
COX7C
NDUFC1
COX5A
UQCRQ
NDUFA5
NDUFB3
UQCRB
NDUFS4
NDUFS1
NDUFS2
SDHA
UQCRC2
UQCRFS1
SDHD
ATP6V1G2
COX4I2
ATP6V0E2
ATP12A
ATP6V0A4
ATP6V1A
ATP6V1C2
COX6A1
ATP6V0B
ATP6V1F
TCIRG1
LHPP
NDUFA4L2
COX6B2
HMGCS2
ACADM
CPT1B
CD36
FABP3
PFARA
RXRG
ACADL
AQP7
ACSL1
LPL
CYP27A1
ACOX2
SORBS1
SLC27A1
FABP7
ACSL6
CYP7A1
PCK1
FABP4
PLIN1
ADIPOQ
PPARG
SCP2
SLC27A6
FABP6
PCK2
SLC27A5
MMP1
PFARD
FABP5
SLC27A4
ACOX3
OLR1
ANGPTL4
CPT1C
SLC27A2
C
Enrichment plot: KEGG_CITRATE_CYCLE_TCA_CYCLE
ACLY
PC
PCK2
ACO1
PCK1
IDH3A
DLAT
DLD
SUCLA2
MDH2
CS
MDH1
ACO2
IDH2
PDHB
SDHA
OGDH
PDHA1
SUCLG2
SDHD

Figure 3A-3C

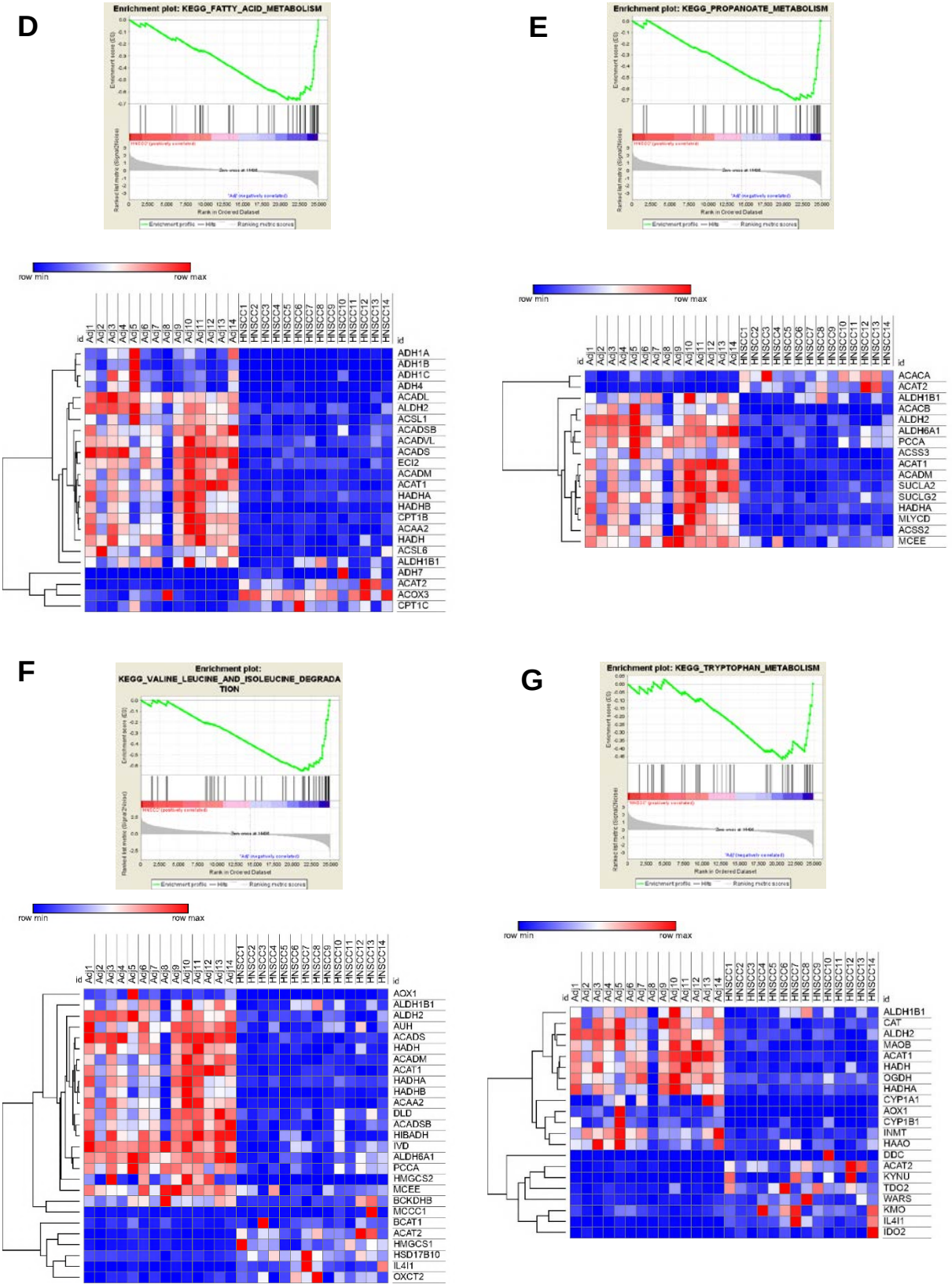
D
Enrichment plot: KEGG_FATTY_ACID_METABOLISM
row min
row max
ADH1A
ADH1B
ADH1C
ADH4
ACADL
ALDH2
ACSL1
ACADSB
ACADVL
ACADS
ECI2
ACADM
ACAT1
HADHA
HADHB
CPT1B
ACAA2
HADH
ACSL6
ALDH1B1
ADH7
ACAT2
ACOX3
CPT1C
E
Enrichment plot: KEGG_PROPANOATE_METABOLISM
row min
row max
ACACA
ACAT2
ALDH1B1
ACACB
ALDH2
ALDH6A1
PCCA
ACSS3
ACAT1
ACADM
SUCLA2
SUCLG2
HADHA
MLYCD
ACSS2
MCEE
F
Enrichment plot: KEGG_VALINE_LEUCINE_AND_ISOLEUCINE_DEGRADATION
row min
row max
AOX1
ALDH1B1
ALDH2
AUH
ACADS
HADH
ACADM
ACAT1
HADHA
HADHB
ACAA2
DLD
ACADSB
HIBADH
IVD
ALDH6A1
PCCA
HMGCS2
MCEE
BCKDHB
MCCC1
BCAT1
ACAT2
HMGCS1
HSD17B10
IL4I1
OXCT2
G
Enrichment plot: KEGG_TRYPTOPHAN_METABOLISM
row min
row max
ALDH1B1
CAT
ALDH2
MAOB
ACAT1
HADH
OGDH
HADHA
CYP1A1
AOX1
CYP1B1
INMT
HAAO
DDC
ACAT2
KYNU
TDO2
WARS
KMO
IL4I1
IDO2

Figure 3D-3G

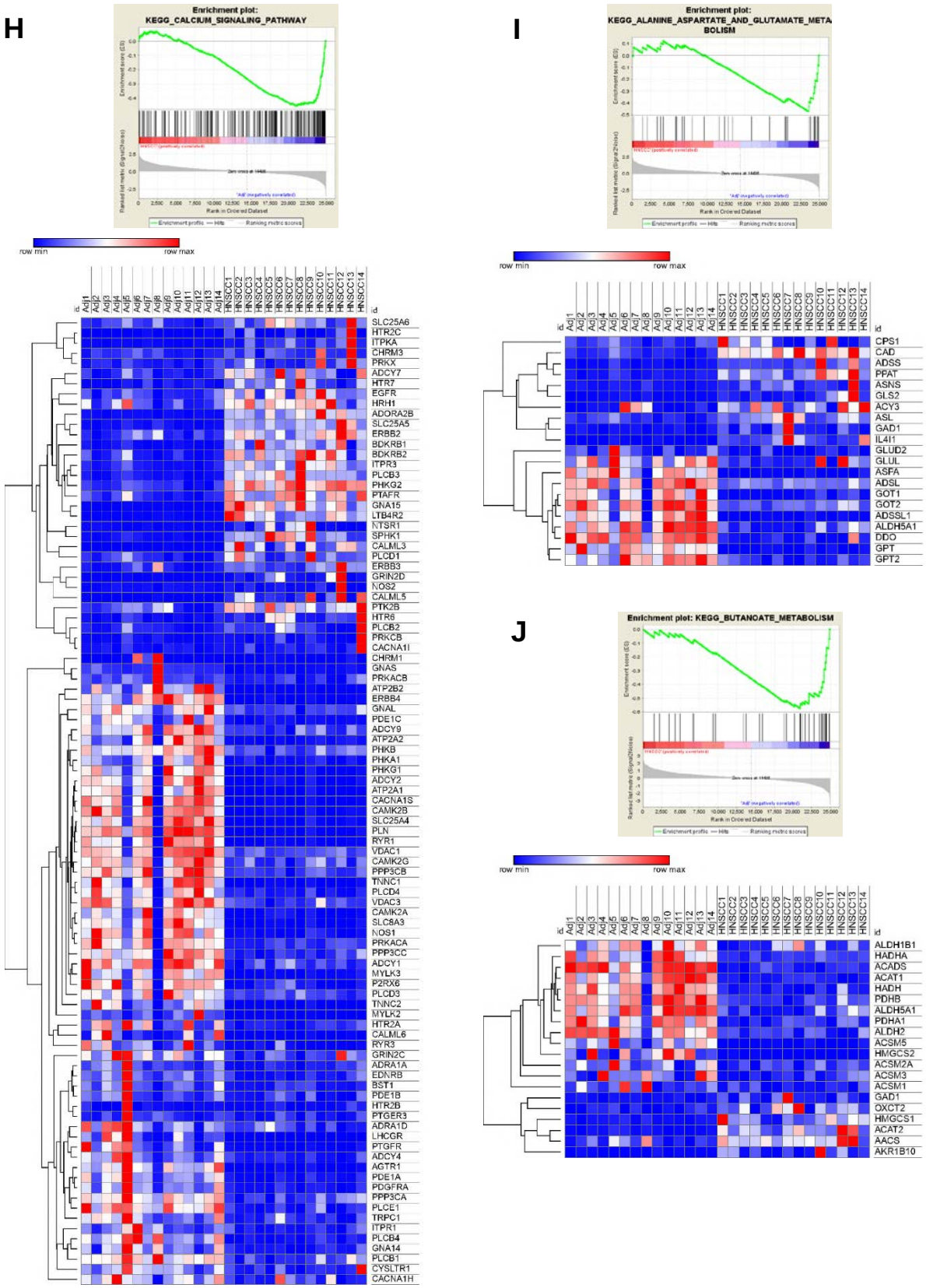
H
Enrichment plot:
KEGG_CALCIUM_SIGNALING_PATHWAY
row min
row max
id
SLC25A6
HTR2C
ITPKA
CHRM3
PRKX
ADCY7
HTR7
EGFR
HRH1
ADORA2B
SLC25A5
ERBB2
BDKRB1
BDKRB2
ITPR3
PLCB3
PHKG2
PTAFR
GNA15
LTB4R2
NTSR1
SPHK1
CALML3
PLCD1
ERBB3
GRIN2D
NOS2
CALML5
PTK2B
HTR6
PLCB2
PRKCB
CACNA1I
CHRM1
GNAS
PRKACB
ATP2B2
ERBB4
GNAL
PDE1C
ADCY9
ATP2A2
PHKB
PHKA1
PHKG1
ADCY2
ATP2A1
CACNA1S
CAMK2B
SLC25A4
PLN
RYR1
VDAC1
CAMK2G
PPP3CB
TNNC1
PLCD4
VDAC3
CAMK2A
SLC8A3
NOS1
PRKACA
PPP3CC
ADCY1
MYLK3
P2RX6
PLCD3
TNNC2
MYLK2
HTR2A
CALML6
RYR3
GRIN2C
ADRA1A
EDNRB
BST1
PDE1B
HTR2B
PTGER3
ADRA1D
LHCGR
PTGFR
ADCY4
AGTR1
PDE1A
PDGFRA
PPP3CA
PLCE1
TRPC1
ITPR1
PLCB4
GNA14
PLCB1
CYSLTR1
CACNA1H
I
Enrichment plot:
KEGG_ALANINE_ASPARTATE_AND_GLUTAMATE_METABOLISM
row min
row max
id
CPS1
CAD
ADSS
PPAT
ASNS
GLS2
ACY3
ASL
GAD1
IL4I1
GLUD2
GLUL
ASPA
ADSL
GOT1
GOT2
ADSSL1
ALDH5A1
DDO
GPT
GPT2
J
Enrichment plot: KEGG_BUTANOATE_METABOLISM
row min
row max
id
ALDH1B1
HADHA
ACADS
ACAT1
HADH
PDHB
ALDH5A1
PDHA1
ALDH2
ACSM5
HMGCS2
ACSM2A
ACSM3
ACSM1
GAD1
OXCT2
HMGCS1
ACAT2
AACS
AKR1B10

Figure 3H-3J

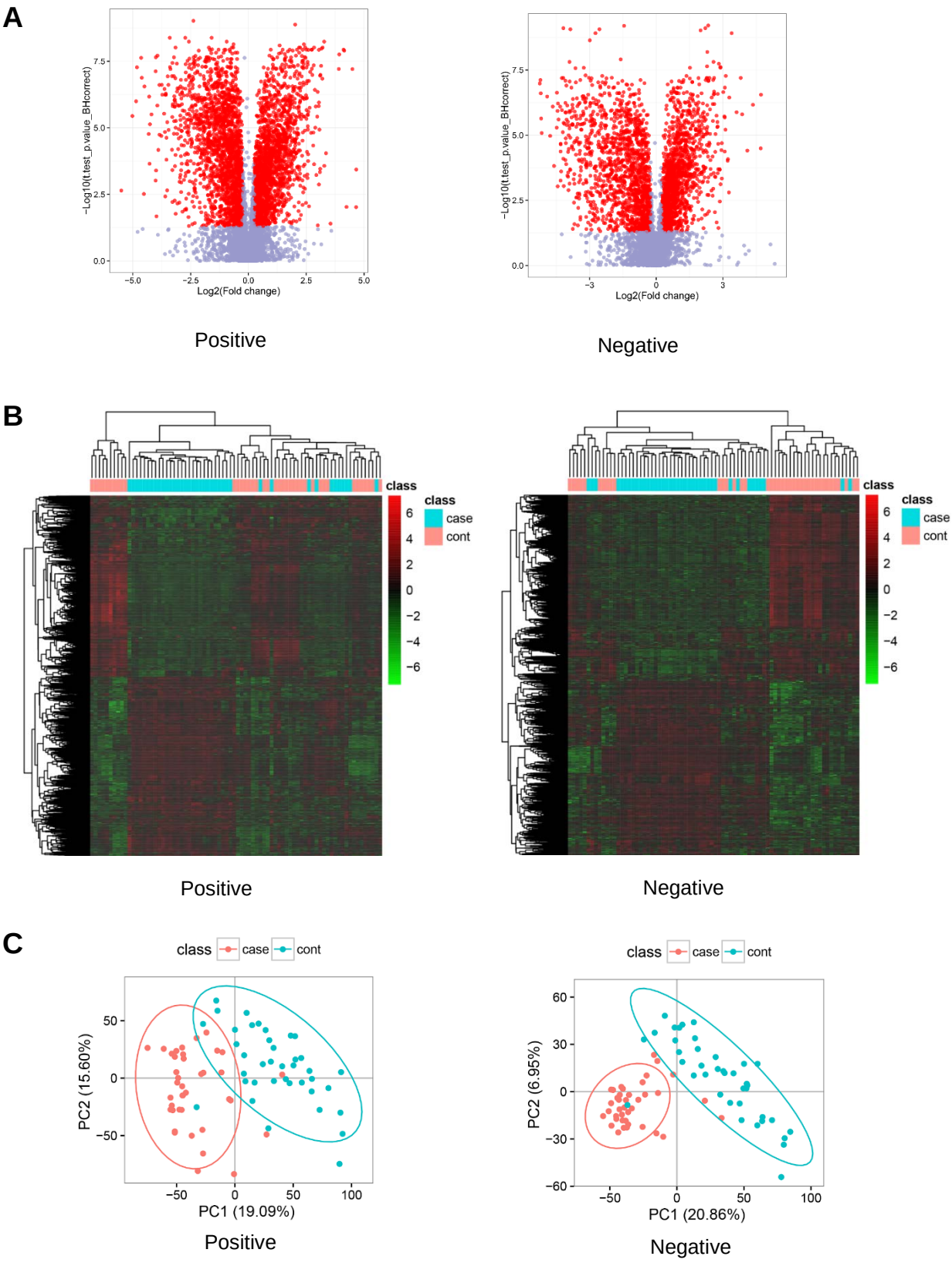
A
−Log10(t.test_p.value_BHcorrect)
Log2(Fold change)
Positive
Negative
B
class
case
cont
Positive
Negative
C
class case cont
PC2 (15.60%)
PC1 (19.09%)
PC2 (6.95%)
PC1 (20.86%)
Positive
Negative

Figure 4A-4C

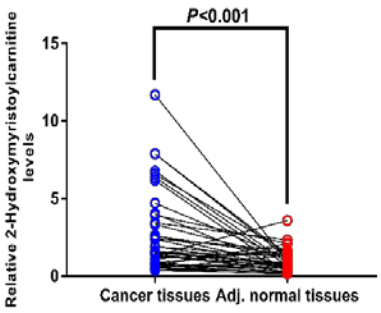

2-Hydroxymyristoyl-carnitine

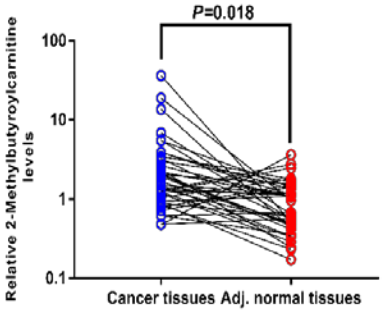

2-Methylbutyroyl-carnitine

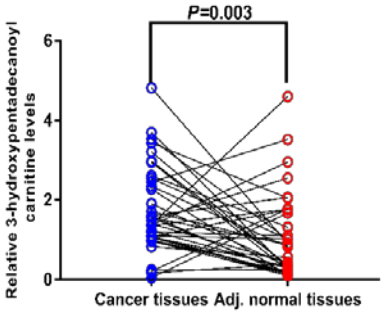

3-hydroxypenta-decanoyl carnitine

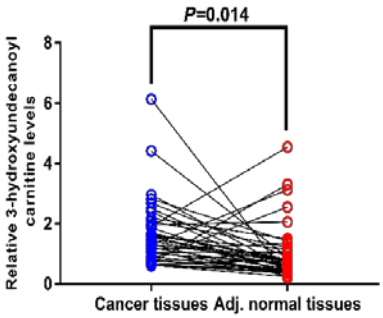

3-hydroxyl undecanoyl carnitine

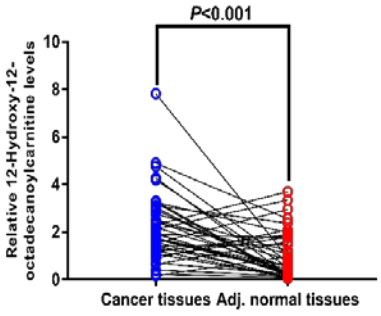

12-Hydroxy-12-octadecanoylcarnitine

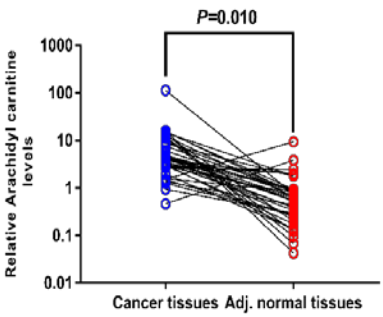

Arachidyl carnitine

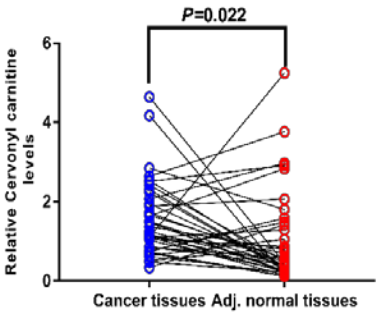

Cervonyl carnitine

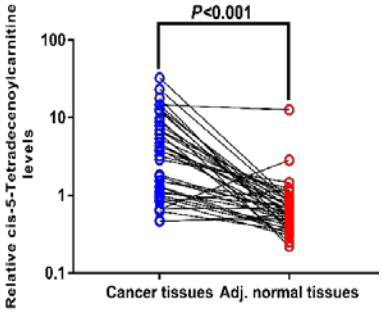

cis-5-Tetradecenoyl carnitine

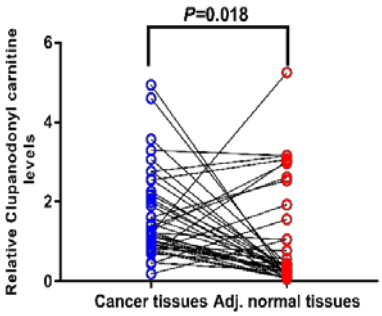

Clupanodonyl carnitine

Figure 5A

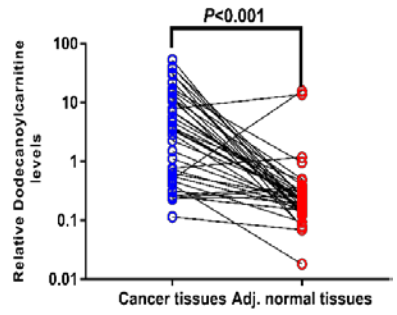

Dodecanoylcarnitine

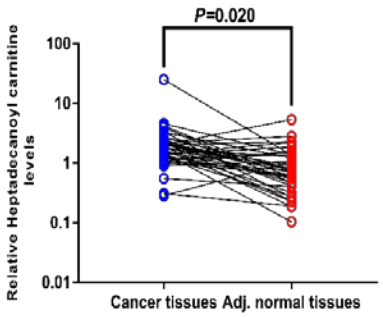

Heptadecanoyl carnitine

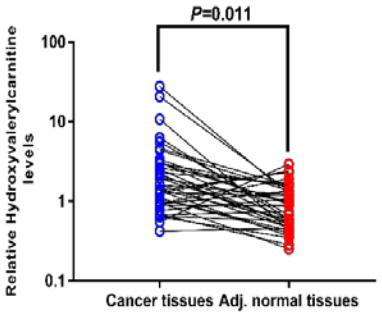

Hydroxyvaleryl carnitine

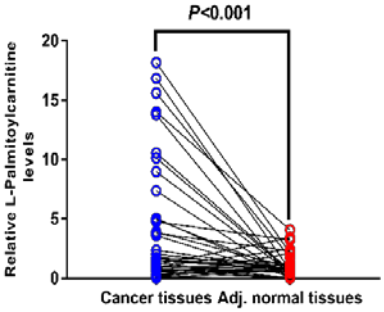

L-Palmitoylcarnitine

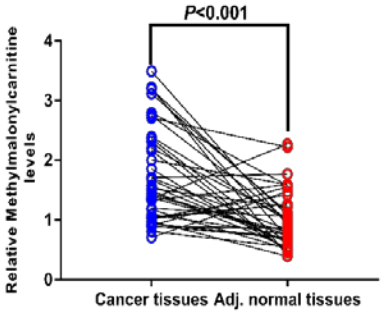

Methylmalonyl carnitine

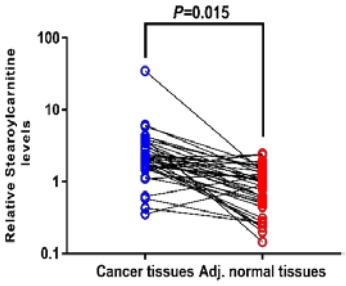

Stearoylcarnitine

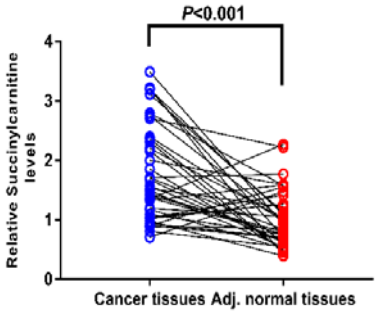

Succinylcarnitine

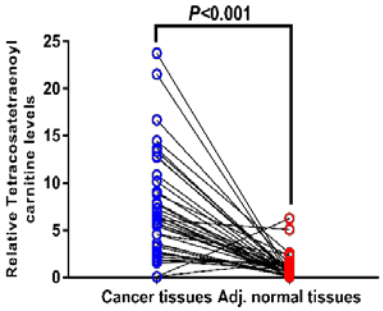

Tetracosatetraenoyl carnitine

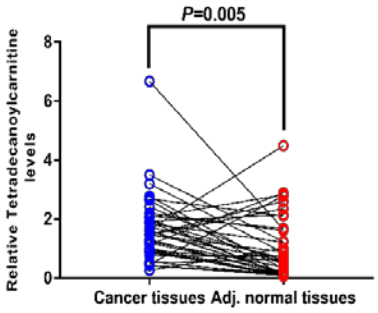

Tetradecanoyl carnitine

Figure 5B

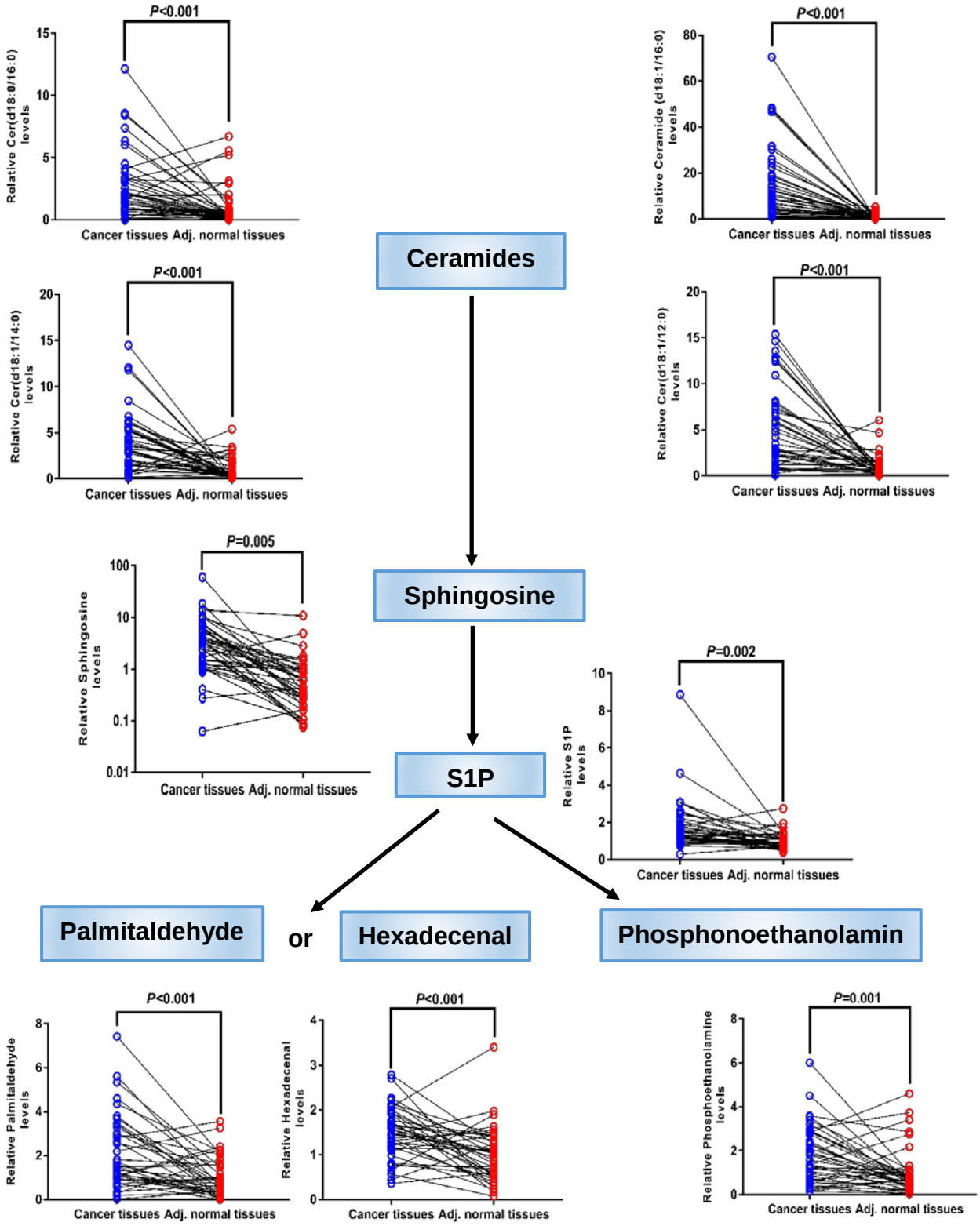
P<0.001
Relative Cer(d18:0/16:0) levels
Cancer tissues Adj. normal tissues
P<0.001
Relative Ceramide (d18:1/16:0) levels
Cancer tissues Adj. normal tissues
Ceramides
P<0.001
Relative Cer(d18:1/14:0) levels
Cancer tissues Adj. normal tissues
P<0.001
Relative Cer(d18:1/12:0) levels
Cancer tissues Adj. normal tissues
P=0.005
Relative Sphingosine levels
Cancer tissues Adj. normal tissues
Sphingosine
P=0.002
Relative S1P levels
Cancer tissues Adj. normal tissues
S1P
Palmitaldehyde
or
Hexadecenal
Phosphonoethanolamin
P<0.001
Relative Palmitaldehyde levels
Cancer tissues Adj. normal tissues
P<0.001
Relative Hexadecenal levels
Cancer tissues Adj. normal tissues
P=0.001
Relative Phosphoethanolamine levels
Cancer tissues Adj. normal tissues

Figure 6

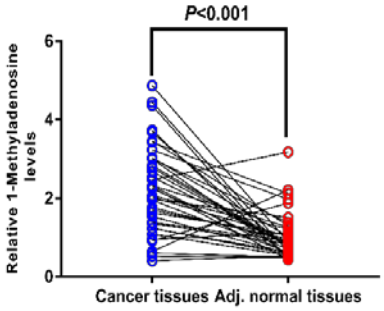

1-methyladenine

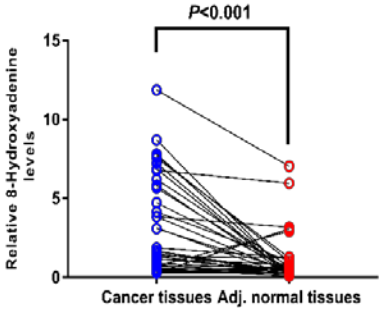

8-hydroxyadenine

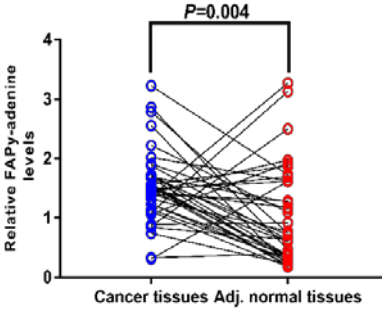

FAPy-adenine

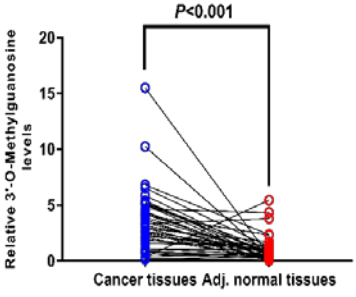

3'-O-methylguanine

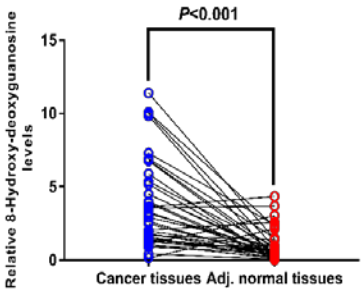

8-hydroxyguanine

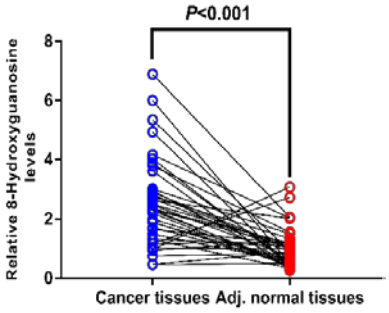

8-hydroxyl-deoguanine

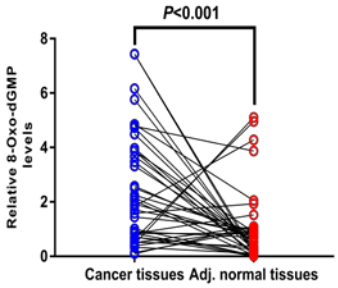

8-Oxo-dGMP

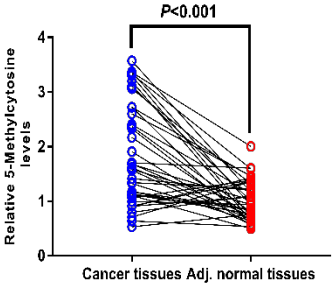

5-Methycytosine

Figure 7

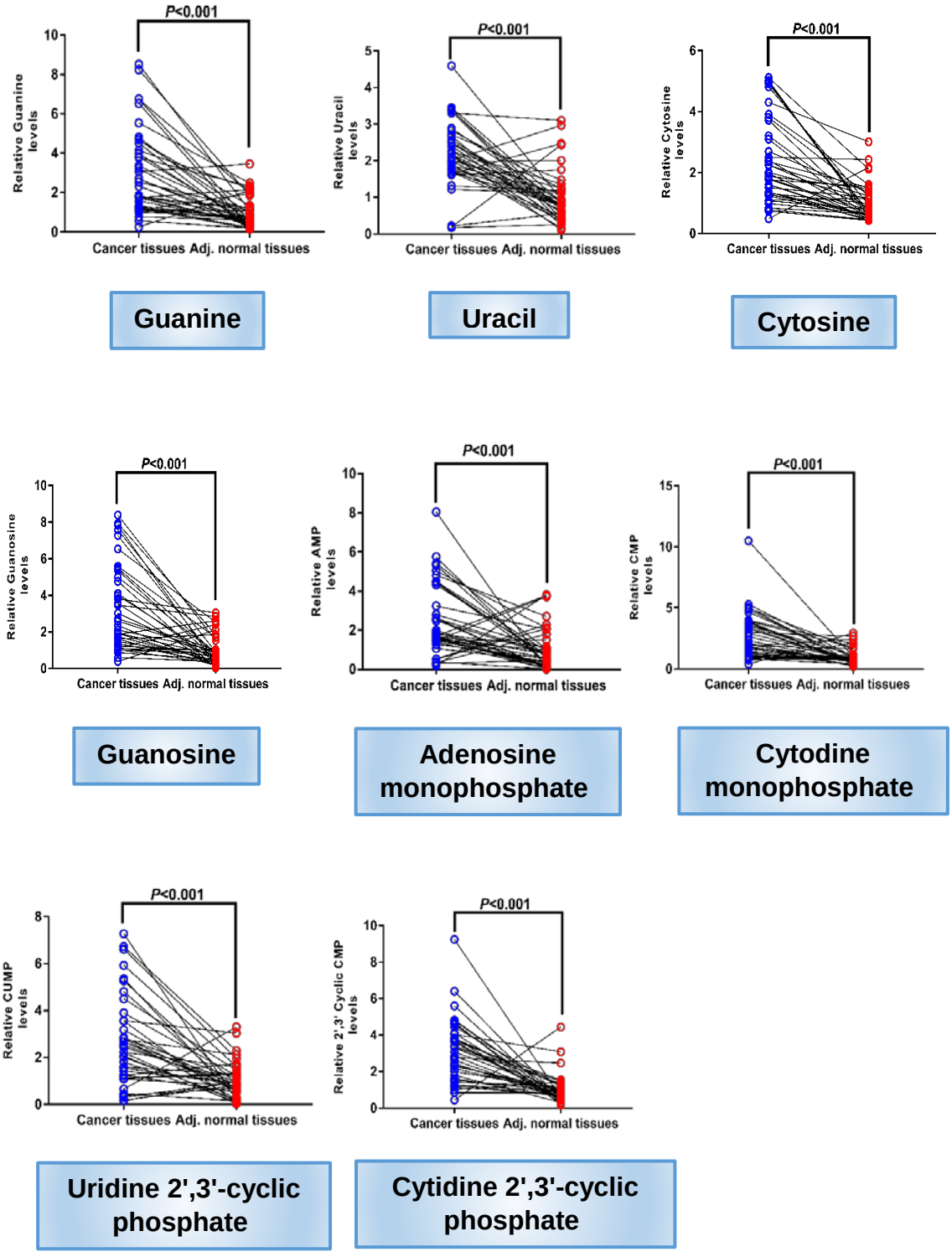
P<0.001
Relative Guanine levels
Cancer tissues Adj. normal tissues
Guanine
P<0.001
Relative Uracil levels
Cancer tissues Adj. normal tissues
Uracil
P<0.001
Relative Cytosine levels
Cancer tissues Adj. normal tissues
Cytosine
P<0.001
Relative Guanosine levels
Cancer tissues Adj. normal tissues
Guanosine
P<0.001
Relative AMP levels
Cancer tissues Adj. normal tissues
Adenosine monophosphate
P<0.001
Relative CMP levels
Cancer tissues Adj. normal tissues
Cytodine monophosphate
P<0.001
Relative CUMP levels
Cancer tissues Adj. normal tissues
Uridine 2',3'-cyclic phosphate
P<0.001
Relative 2',3' Cyclic CMP levels
Cancer tissues Adj. normal tissues
Cytidine 2',3'-cyclic phosphate

Figure 8

A

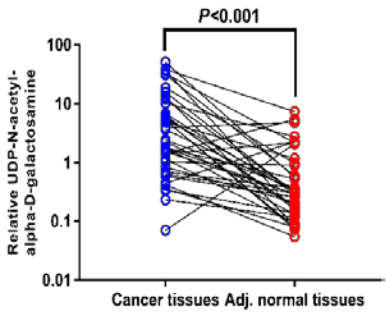

UDP-N-acetyl-alpha-D-galactosamine

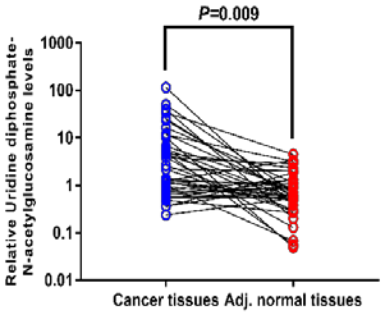

Uridine diphosphate-N-acetylglucosamine

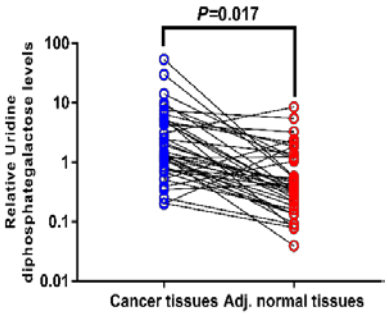

Uridine diphosphategalactose

B

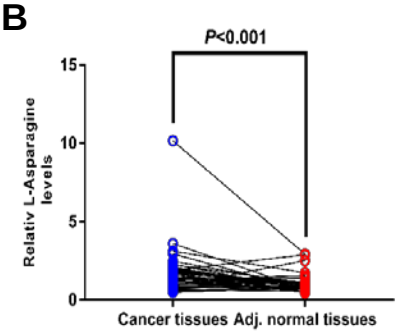

L-Asparagine

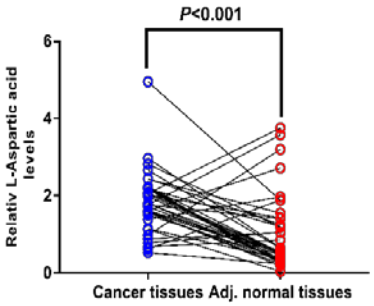

L-Aspartic acid

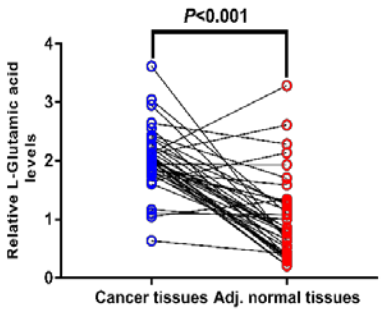

L-Glutamic acid

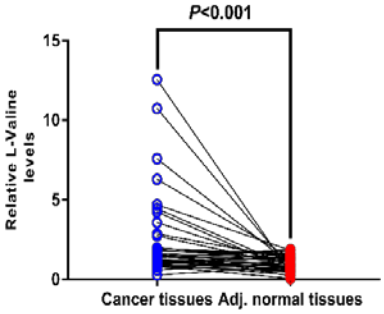

L-Valine

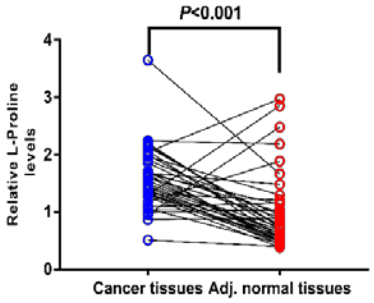

L-Proline

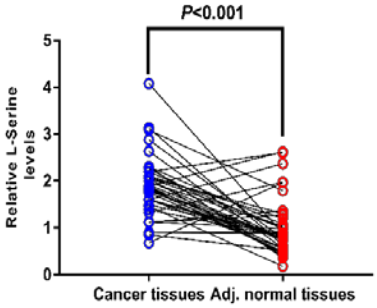

L-Serine

Figure 9

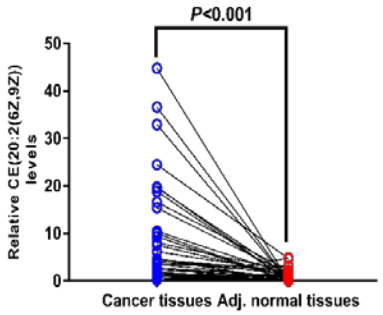

CE(20:2(6Z,9Z))

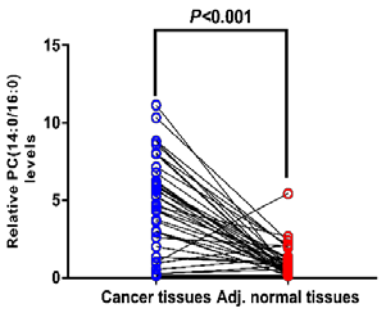

PC(14:0/16:0)

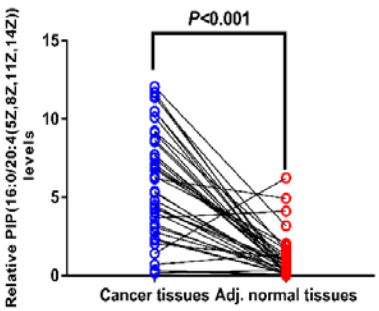

PIP(16:0/20:4(5Z,8Z, 11Z,14Z))

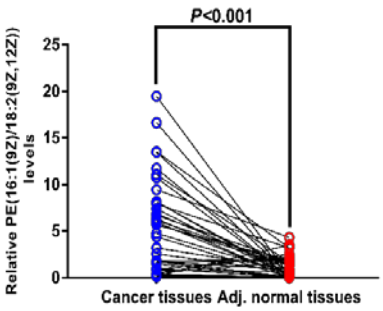

PE(16:1(9Z)/18:2 (9Z,12Z))

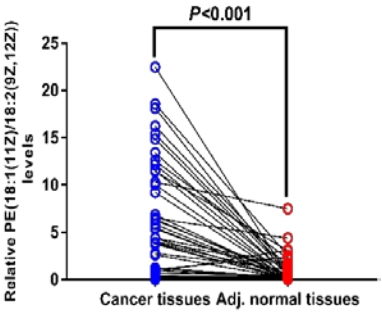

PE(18:1(11Z)/18:2 (9Z,12Z))

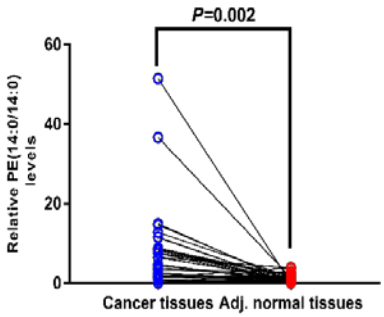

PE(14:0/14:0)

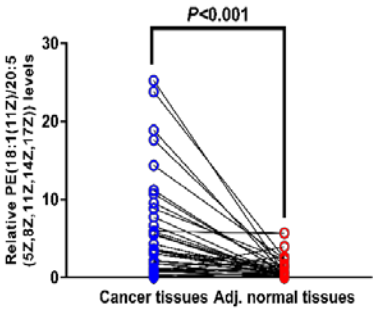

PE(18:1(11Z)/20:5 (5Z,8Z,11Z,14Z,17Z))

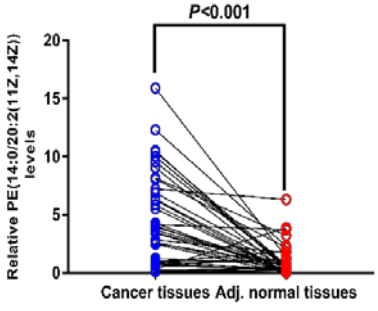

PE(14:0/20:2 (11Z,14Z))

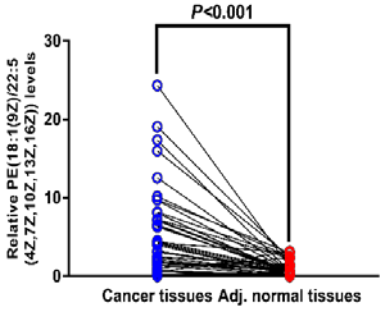

PE(18:1(9Z)/22:5(4Z, 7Z,10Z,13Z,16Z))

Figure 10

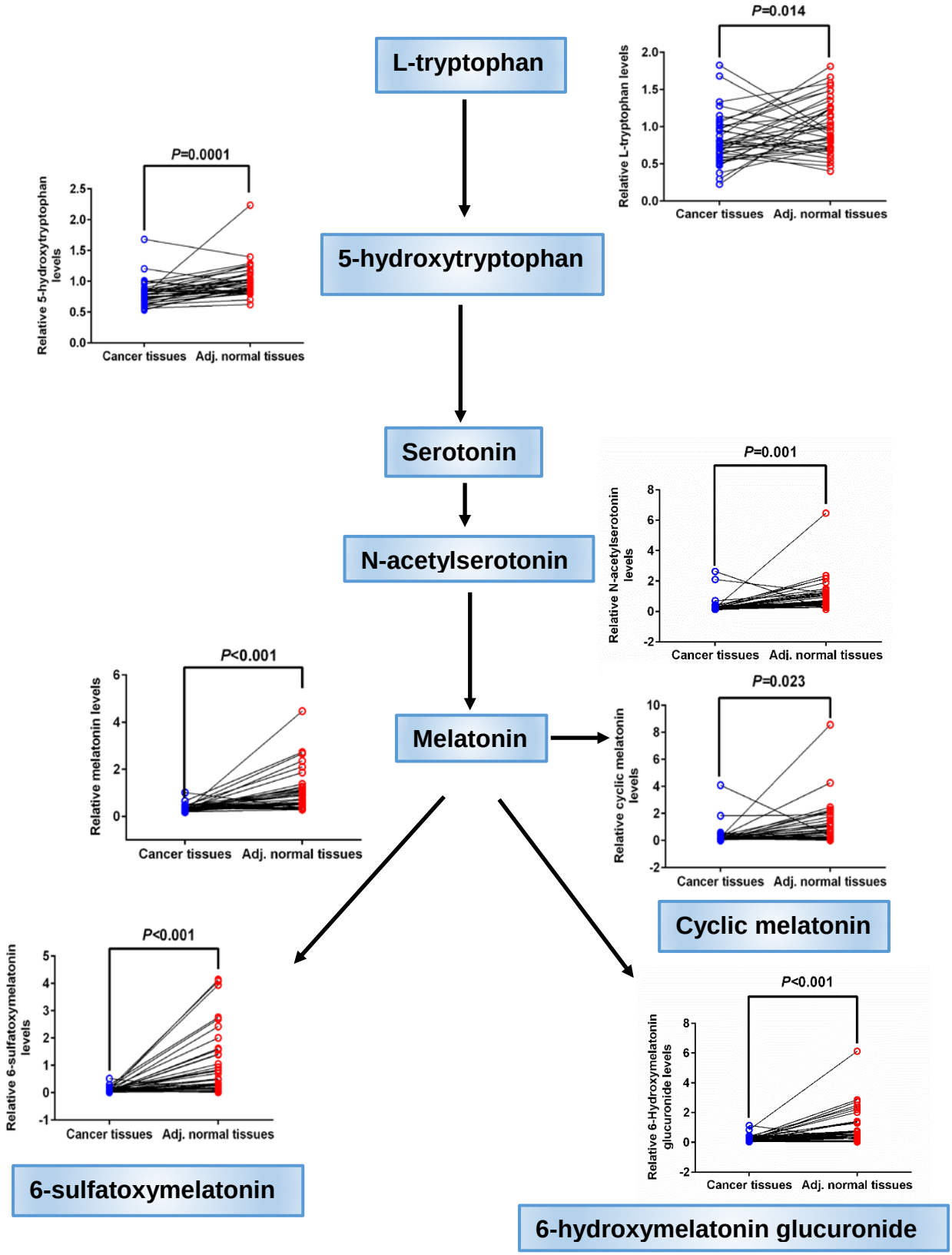
L-tryptophan
5-hydroxytryptophan
Serotonin
N-acetylserotonin
Melatonin
Cyclic melatonin
6-sulfatoxymelatonin
6-hydroxymelatonin glucuronide
P=0.014
Relative L-tryptophan levels
P=0.0001
Relative 5-hydroxytryptophan levels
P=0.001
Relative N-acetylserotonin levels
P<0.001
Relative melatonin levels
P=0.023
Relative cyclic melatonin levels
P<0.001
Relative 6-sulfatoxymelatonin levels
P<0.001
Relative 6-Hydroxymelatonin glucuronide levels
Cancer tissues
Adj. normal tissues

Figure 11

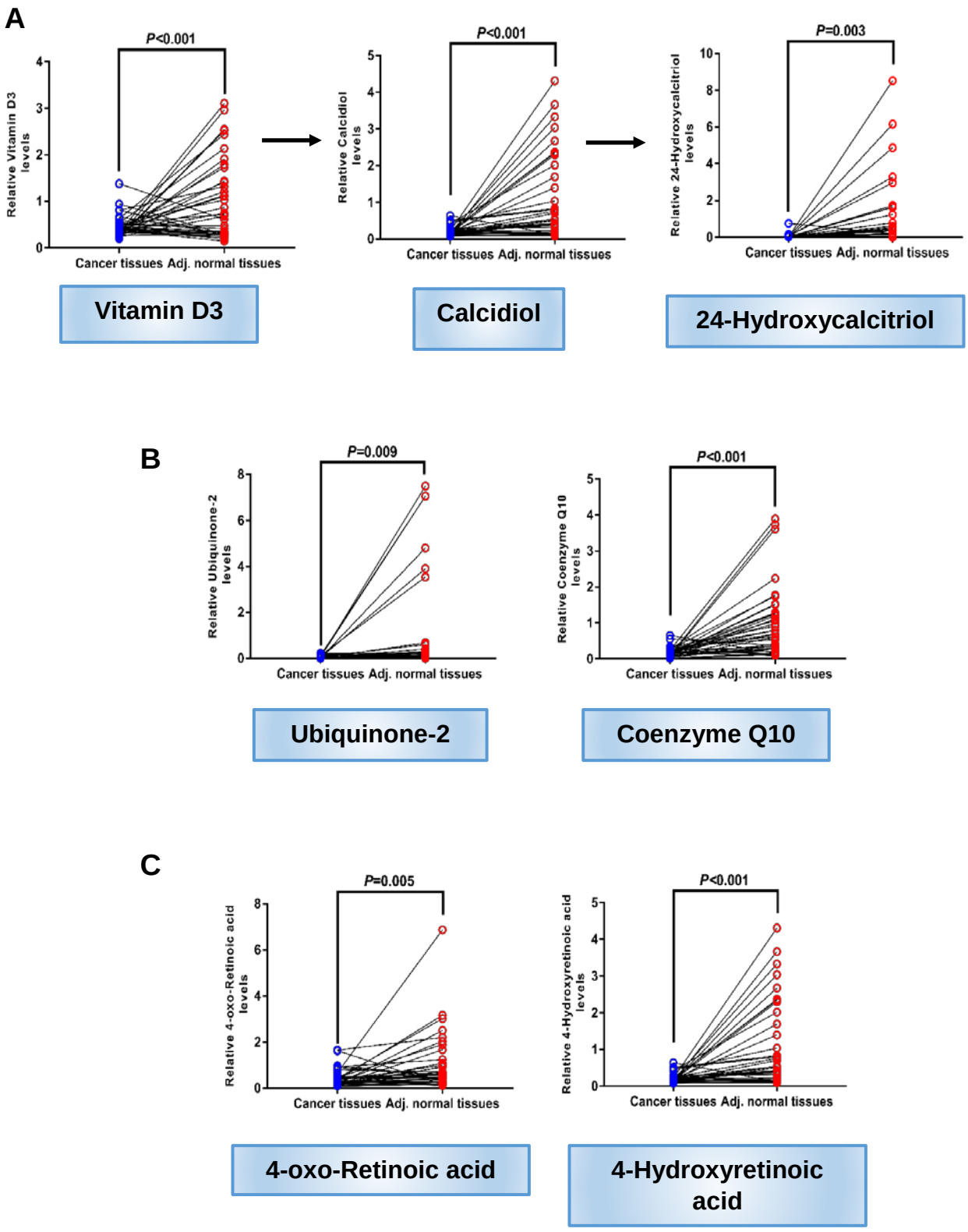
A
P<0.001
Relative Vitamin D3 levels
Cancer tissues Adj. normal tissues
Vitamin D3
P<0.001
Relative Calcidiol levels
Cancer tissues Adj. normal tissues
Calcidiol
P=0.003
Relative 24-Hydroxycalcitriol levels
Cancer tissues Adj. normal tissues
24-Hydroxycalcitriol
B
P=0.009
Relative Ubiquinone-2 levels
Cancer tissues Adj. normal tissues
Ubiquinone-2
P<0.001
Relative Coenzyme Q10 levels
Cancer tissues Adj. normal tissues
Coenzyme Q10
C
P=0.005
Relative 4-oxo-Retinoic acid levels
Cancer tissues Adj. normal tissues
4-oxo-Retinoic acid
P<0.001
Relative 4-Hydroxyretinoic acid levels
Cancer tissues Adj. normal tissues
4-Hydroxyretinoic acid

Figure 12

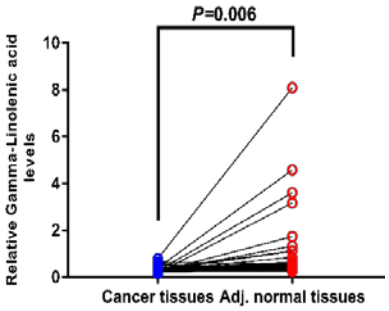

Gamma-Linolenic acid

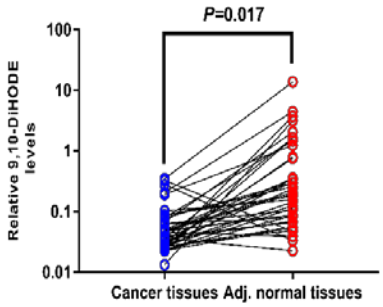

9,10-DiHODE

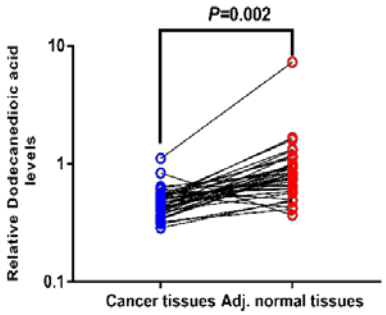

Dodecanedioic acid

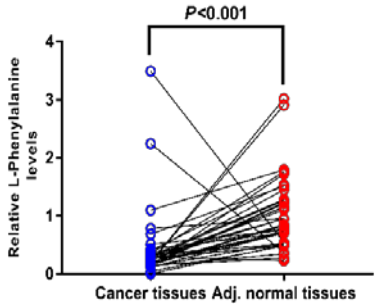

L-Phenylalanine

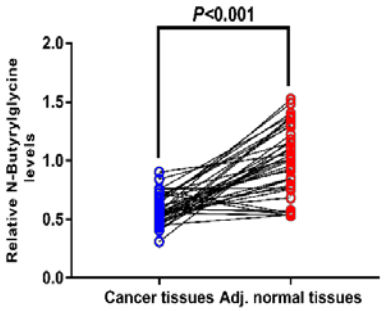

N-Butyrylglycine

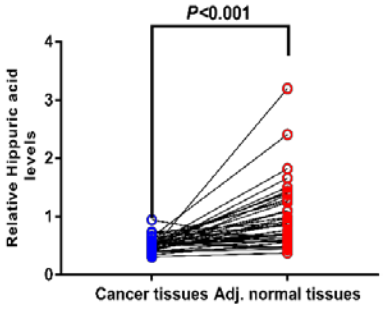

Hippuric acid

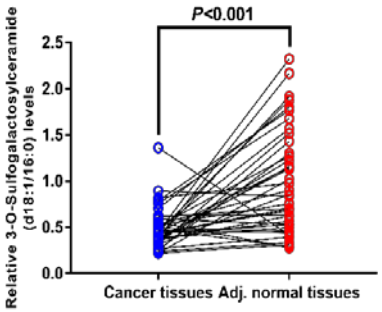

3-O-Sulfogalactosyl Ceramide (d18:1/16:0)

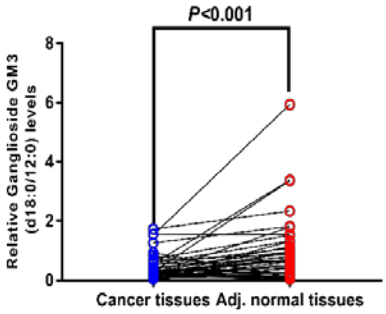

Ganglioside GM3 (d18:0/12:0)

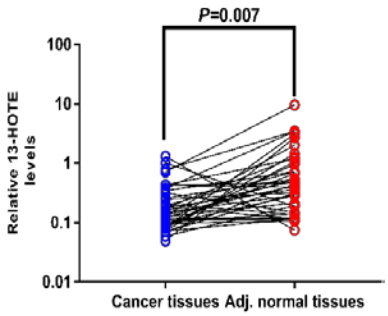

13-HOTE

Figure 13

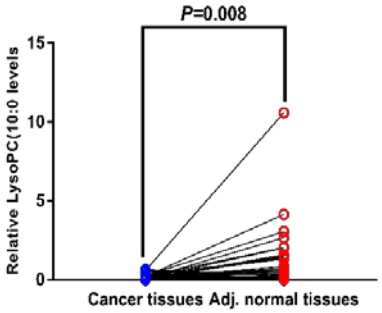

LysoPC(10:0)

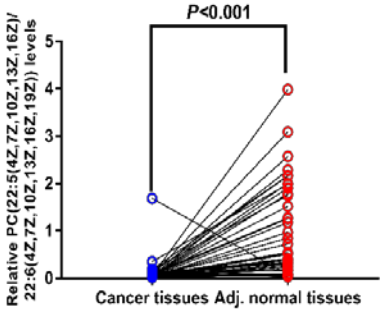

PC(22:5(4Z,7Z,10Z,13Z,16Z)/22:6(4Z,7Z,10Z,13Z,16Z,19Z)))

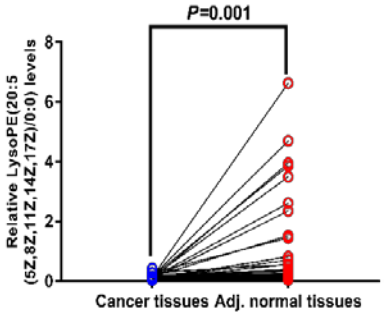

LysoPE(20:5(5Z,8Z,11Z,14Z,17Z)/0:0)

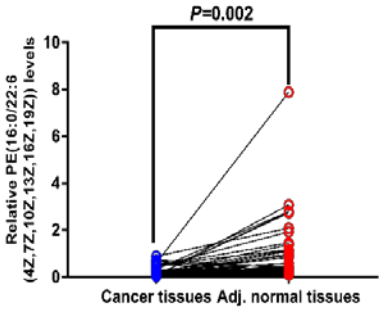

PE(16:0/22:6(4Z,7Z,10Z,13Z,16Z,19Z))

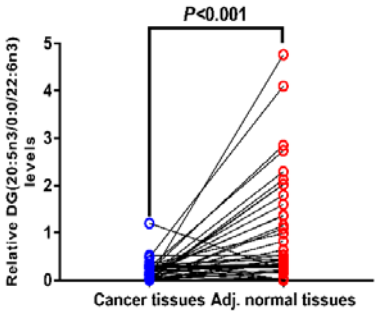

DG(20:5n3/0:0/22:6n3)

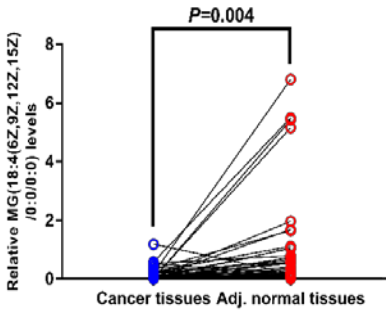

MG(18:4(6Z,9Z,12Z,15Z)/0:0/0:0)

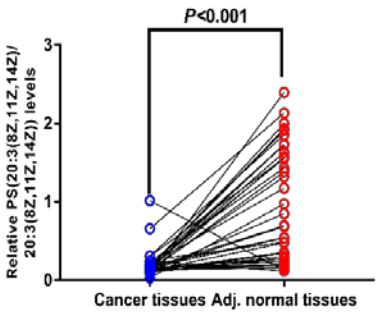

PS(20:3(8Z,11Z,14Z)/20:3(8Z,11Z,14Z))

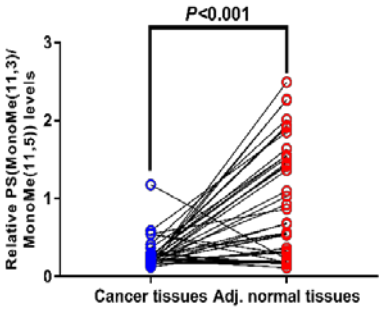

PS(MonoMe(11,3)/MonoMe(11,5))

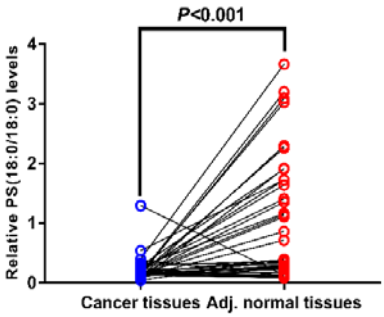

PS(18:0/18:0)

Figure 14

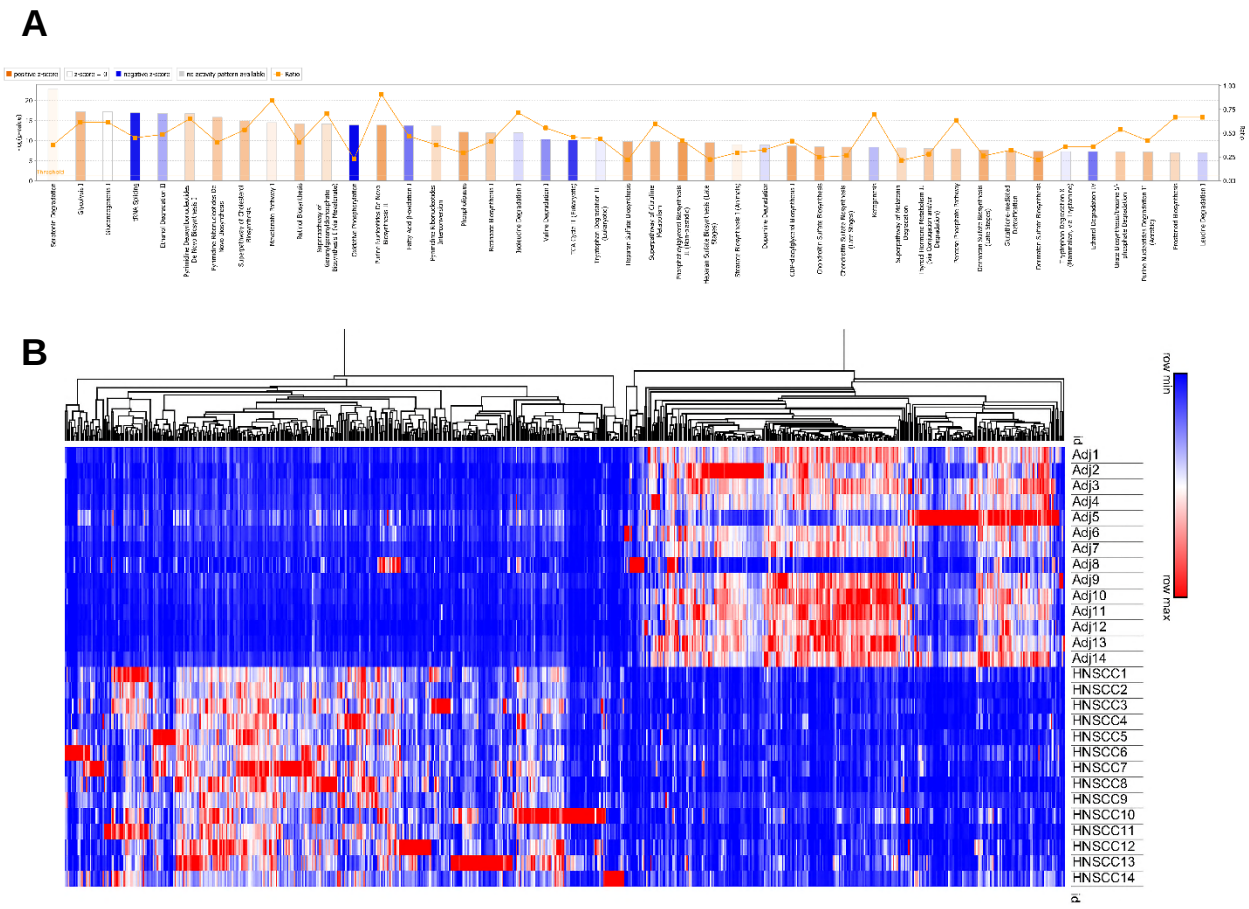
A
B
Adj1
Adj2
Adj3
Adj4
Adj5
Adj6
Adj7
Adj8
Adj9
Adj10
Adj11
Adj12
Adj13
Adj14
HNSCC1
HNSCC2
HNSCC3
HNSCC4
HNSCC5
HNSCC6
HNSCC7
HNSCC8
HNSCC9
HNSCC10
HNSCC11
HNSCC12
HNSCC13
HNSCC14

Figure 15

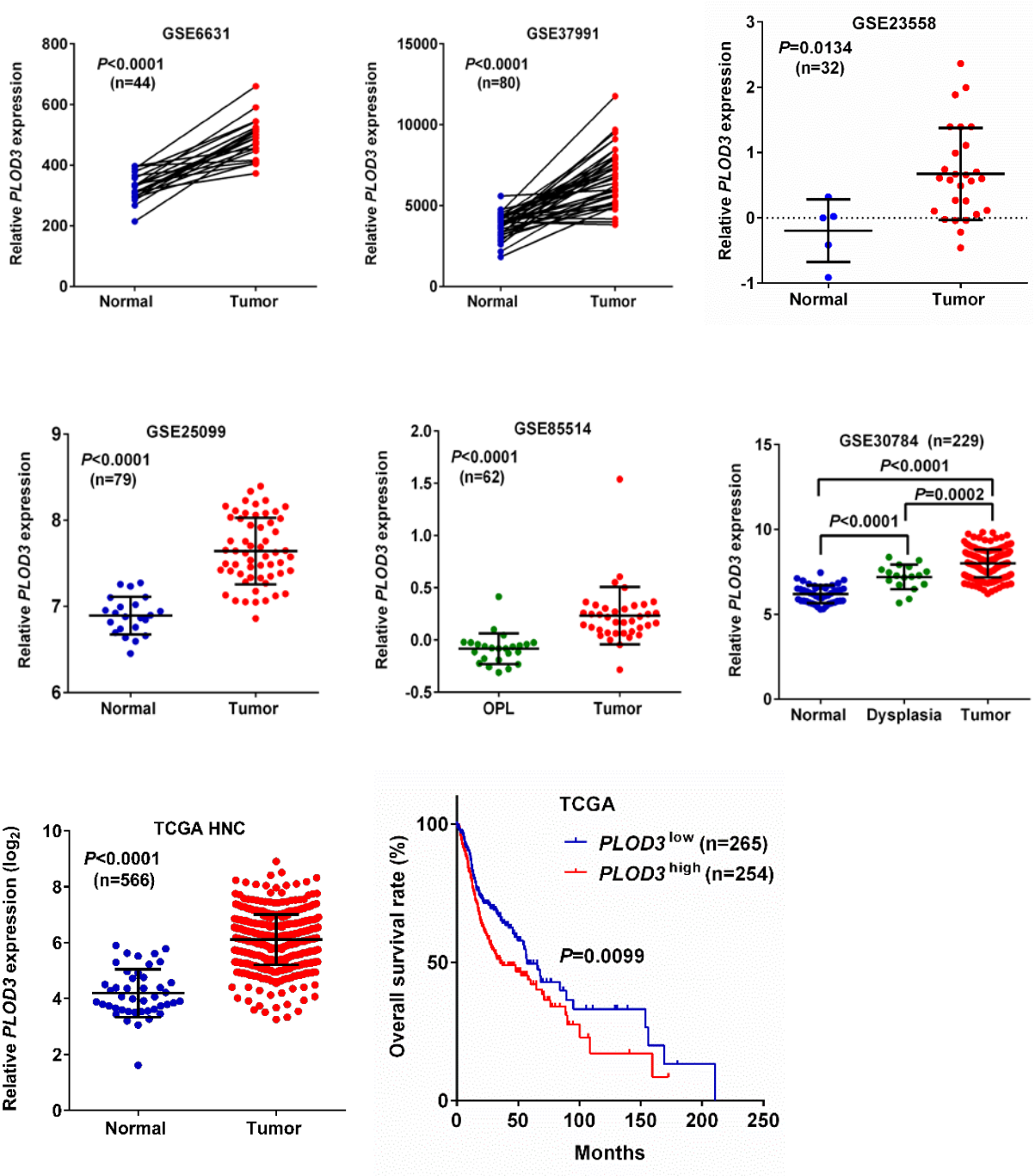
GSE6631
P<0.0001
(n=44)
Relative PLOD3 expression
Normal
Tumor
GSE37991
P<0.0001
(n=80)
GSE23558
P=0.0134
(n=32)
GSE25099
P<0.0001
(n=79)
GSE85514
P<0.0001
(n=62)
OPL
GSE30784 (n=229)
P<0.0001
P=0.0002
P<0.0001
Dysplasia
TCGA HNC
P<0.0001
(n=566)
Relative PLOD3 expression (log2)
TCGA
PLOD3 low (n=265)
PLOD3 high (n=254)
P=0.0099
Overall survival rate (%)
Months

Figure 16

A

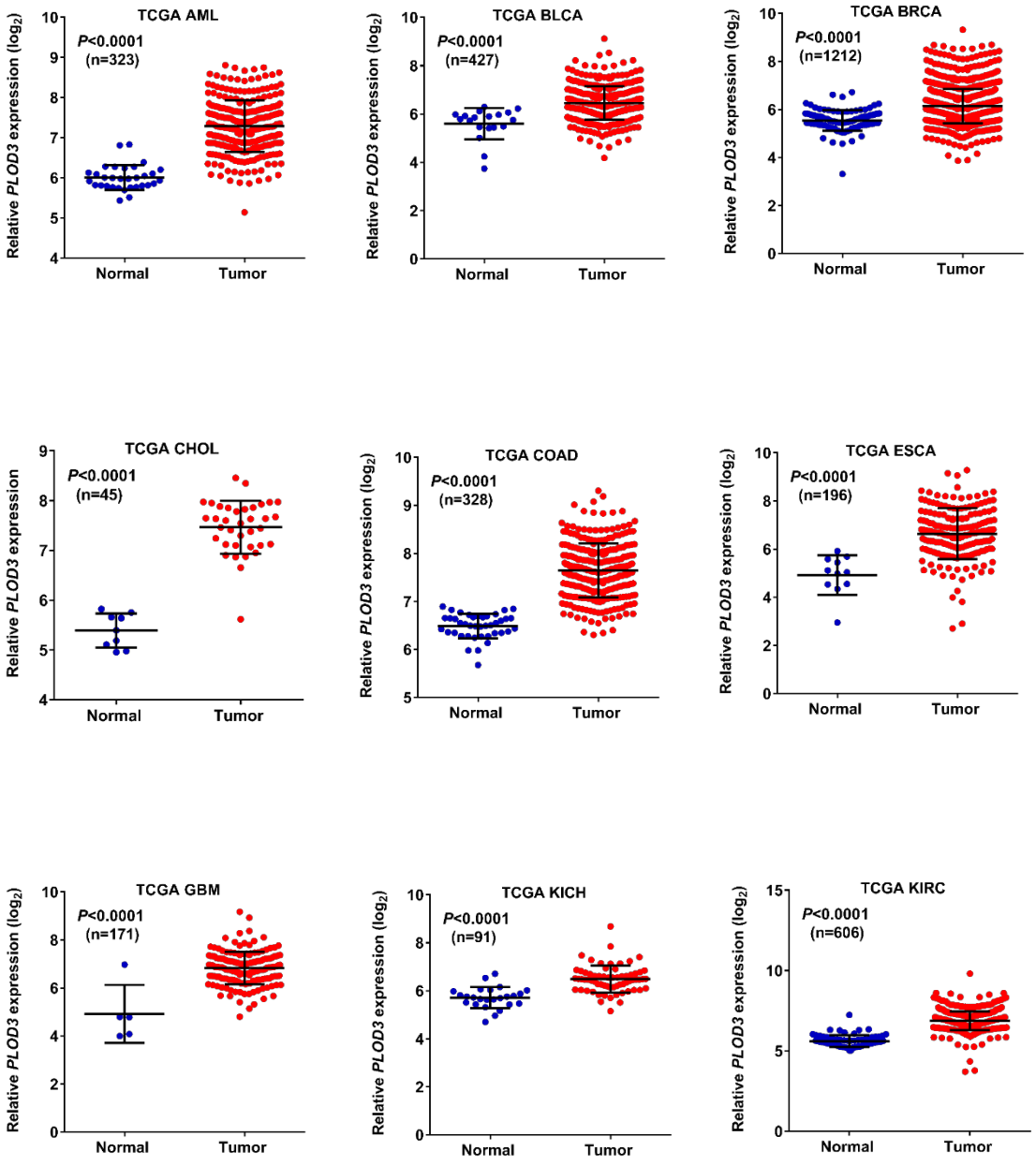
TCGA AML
P<0.0001
(n=323)
TCGA BLCA
P<0.0001
(n=427)
TCGA BRCA
P<0.0001
(n=1212)
TCGA CHOL
P<0.0001
(n=45)
TCGA COAD
P<0.0001
(n=328)
TCGA ESCA
P<0.0001
(n=196)
TCGA GBM
P<0.0001
(n=171)
TCGA KICH
P<0.0001
(n=91)
TCGA KIRC
P<0.0001
(n=606)
Relative PLOD3 expression (log2)
Normal
Tumor

Figure 17A

B

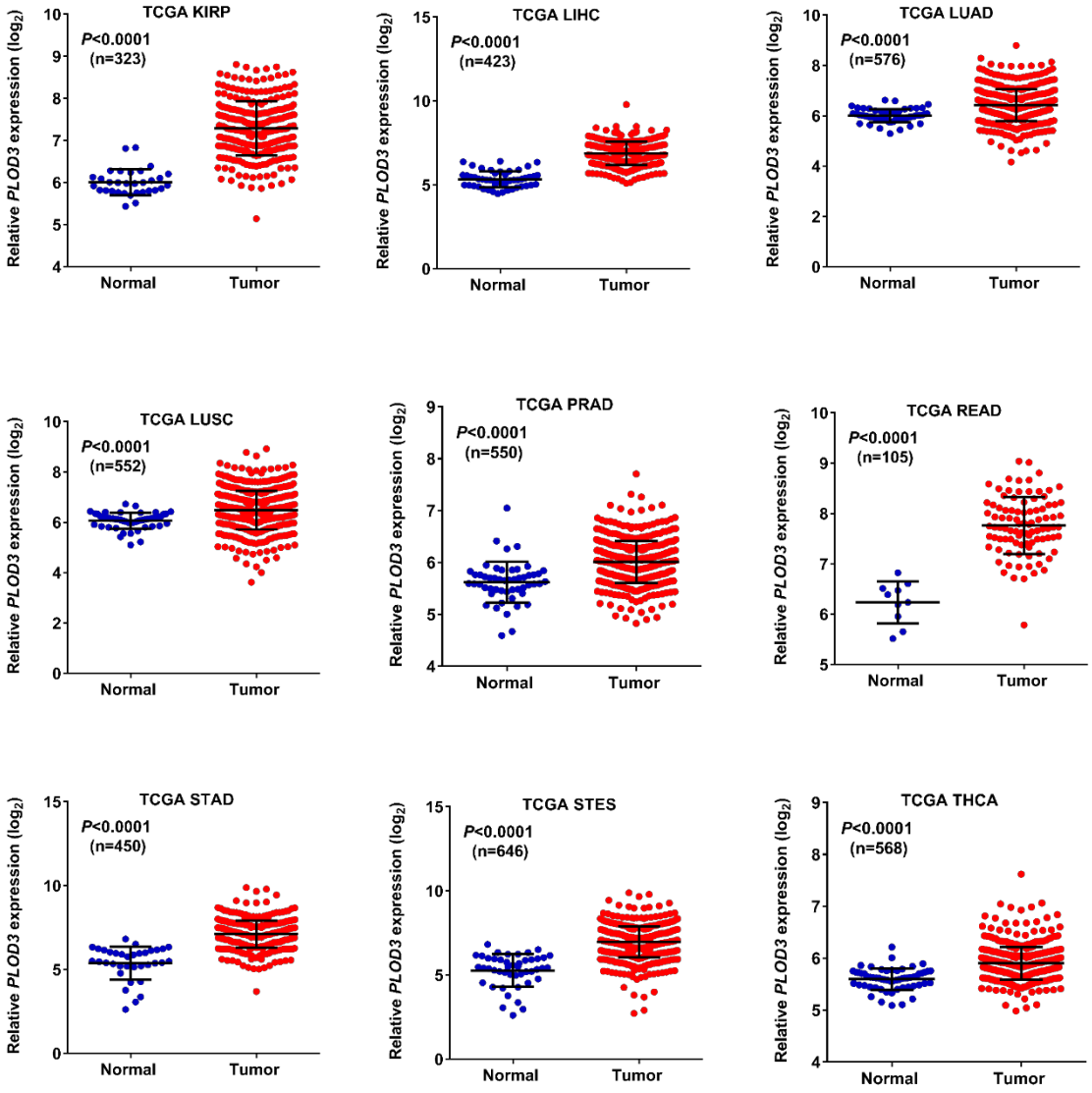
TCGA KIRP
P<0.0001
(n=323)
TCGA LIHC
P<0.0001
(n=423)
TCGA LUAD
P<0.0001
(n=576)
TCGA LUSC
P<0.0001
(n=552)
TCGA PRAD
P<0.0001
(n=550)
TCGA READ
P<0.0001
(n=105)
TCGA STAD
P<0.0001
(n=450)
TCGA STES
P<0.0001
(n=646)
TCGA THCA
P<0.0001
(n=568)
Relative PLOD3 expression (log2)
Normal
Tumor

Figure 17B

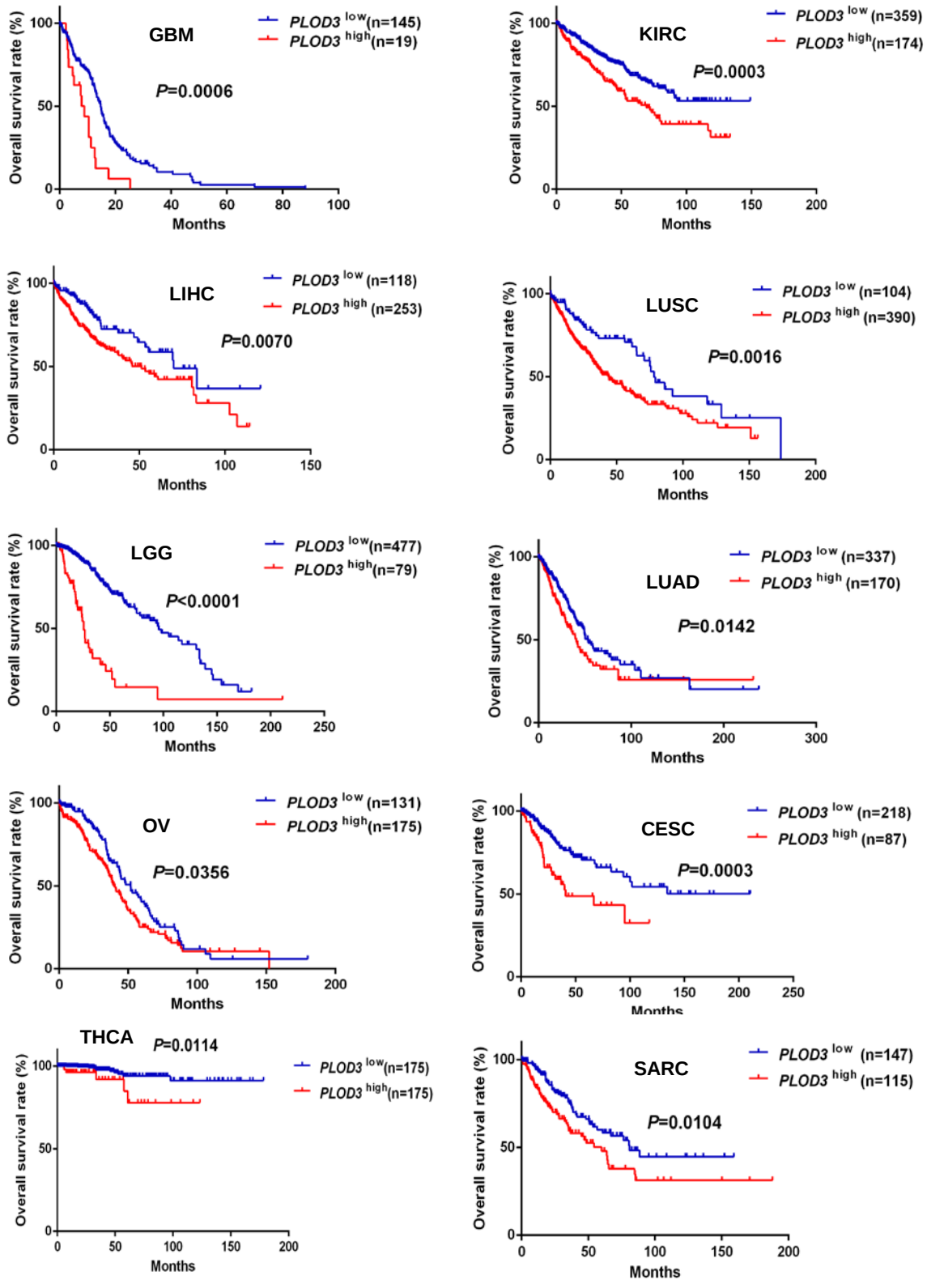
GBM
PLOD3 low(n=145)
PLOD3 high(n=19)
P=0.0006
KIRC
PLOD3 low (n=359)
PLOD3 high(n=174)
P=0.0003
LIHC
PLOD3 low (n=118)
PLOD3 high (n=253)
P=0.0070
LUSC
PLOD3 low (n=104)
PLOD3 high (n=390)
P=0.0016
LGG
PLOD3 low(n=477)
PLOD3 high(n=79)
P<0.0001
LUAD
PLOD3 low (n=337)
PLOD3 high (n=170)
P=0.0142
OV
PLOD3 low (n=131)
PLOD3 high(n=175)
P=0.0356
CESC
PLOD3 low (n=218)
PLOD3 high (n=87)
P=0.0003
THCA
P=0.0114
PLOD3 low(n=175)
PLOD3 high(n=175)
SARC
PLOD3 low (n=147)
PLOD3 high (n=115)
P=0.0104
Overall survival rate (%)
Months

Figure 18

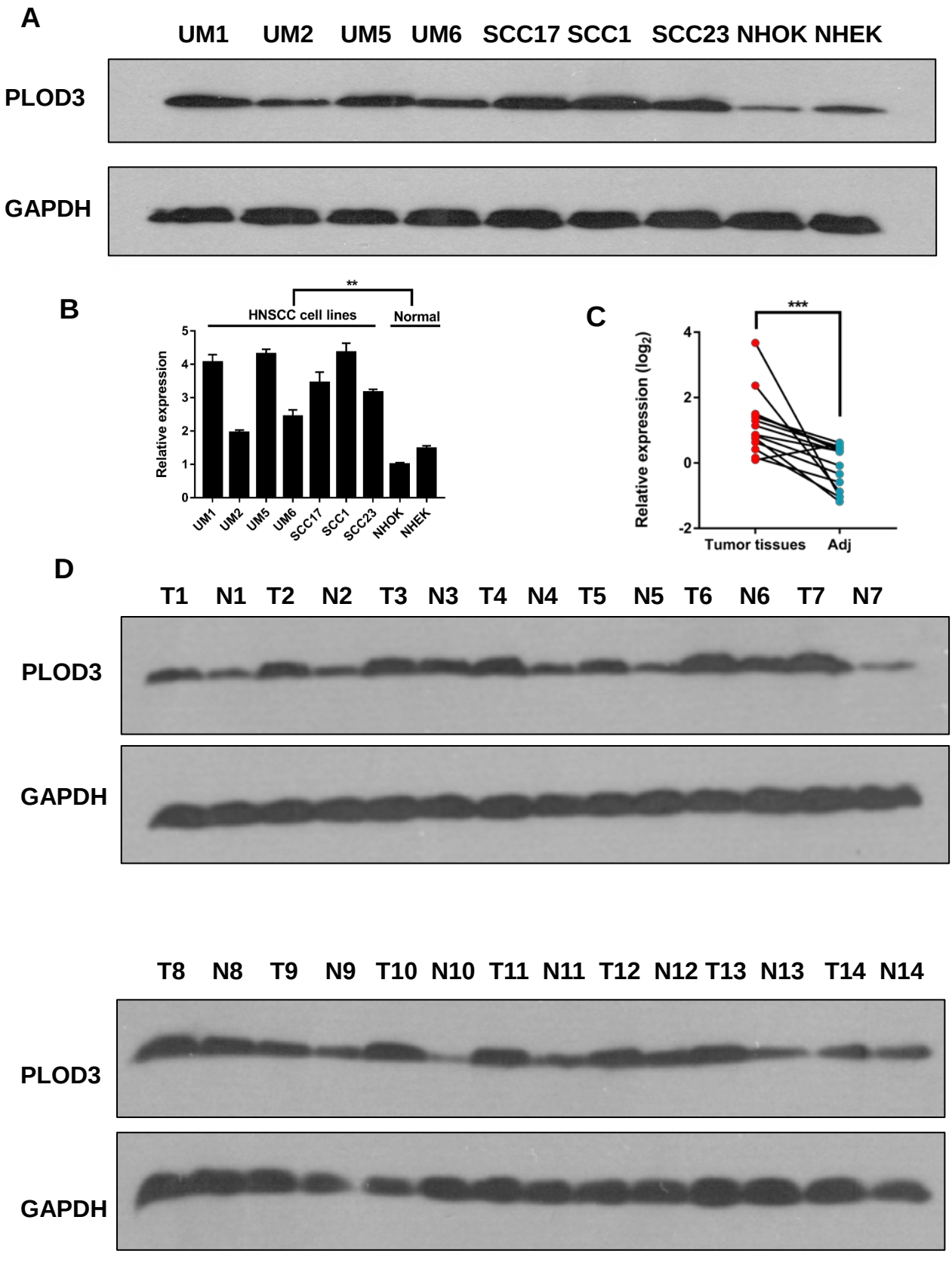
A
UM1 UM2 UM5 UM6 SCC17 SCC1 SCC23 NHOK NHEK
PLOD3
GAPDH
B
**
HNSCC cell lines
Normal
Relative expression
UM1 UM2 UM5 UM6 SCC17 SCC1 SCC23 NHOK NHEK
C
***
Relative expression (log2)
Tumor tissues
Adj
D
T1 N1 T2 N2 T3 N3 T4 N4 T5 N5 T6 N6 T7 N7
PLOD3
GAPDH
T8 N8 T9 N9 T10 N10 T11 N11 T12 N12 T13 N13 T14 N14
PLOD3
GAPDH

Figure 19

A

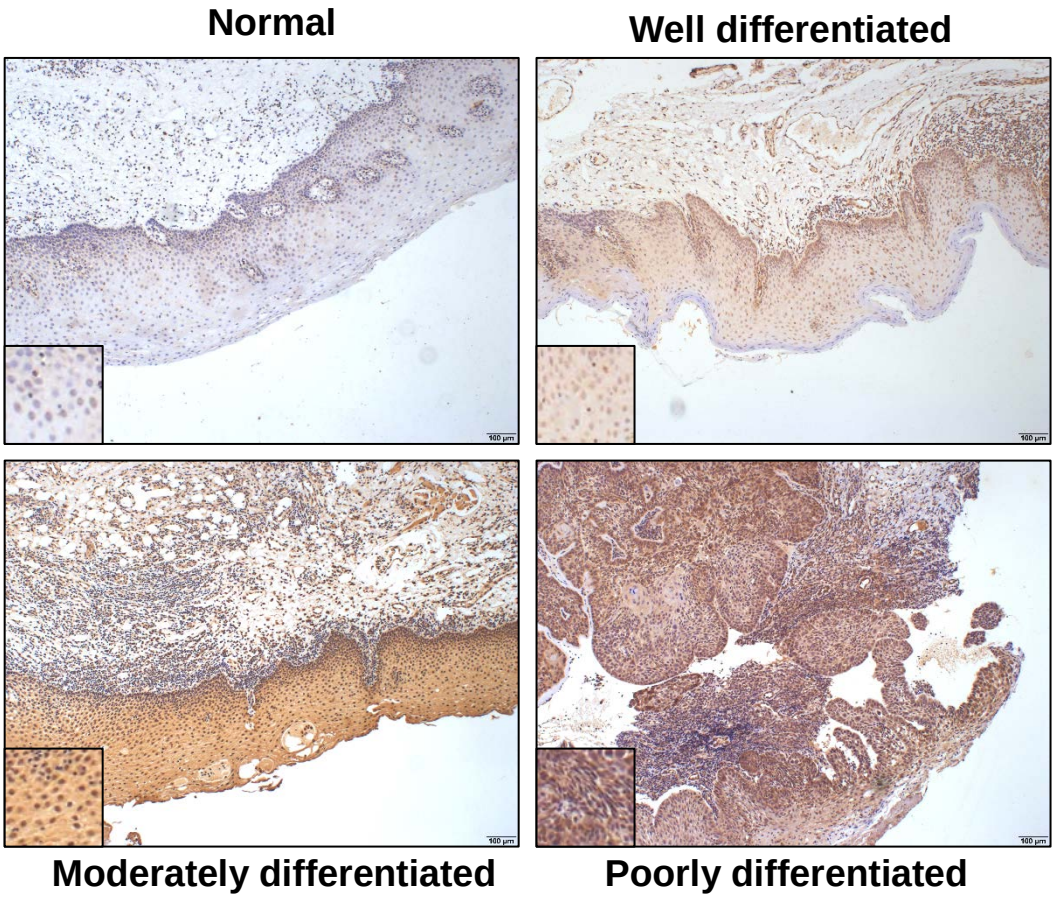
Normal
Well differentiated
Moderately differentiated
Poorly differentiated

B

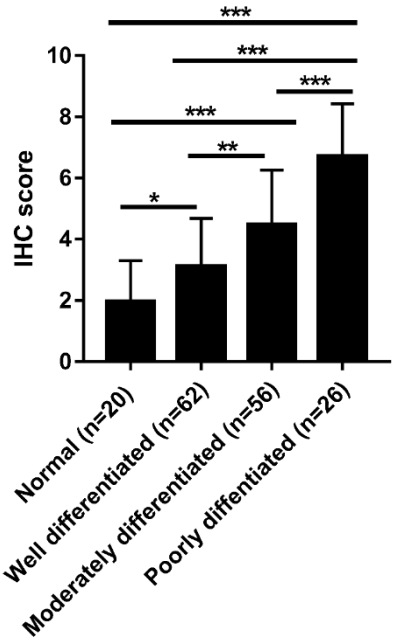
IHC score
0
2
4
6
8
10
*
**
***
***
***
***
Normal (n=20)
Well differentiated (n=62)
Moderately differentiated (n=56)
Poorly diffentiated (n=26)

Figure 20

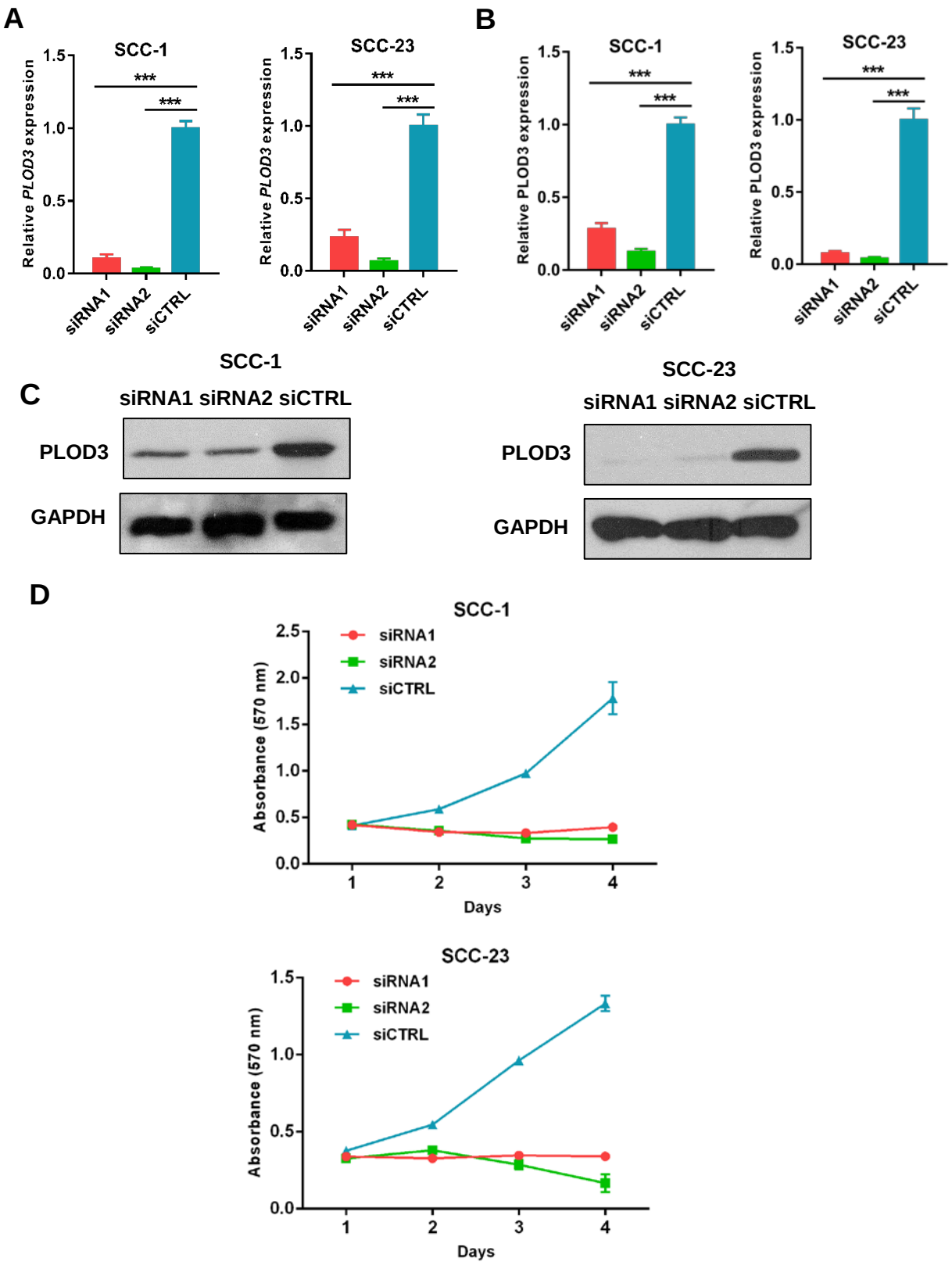

Figure 21A-21D

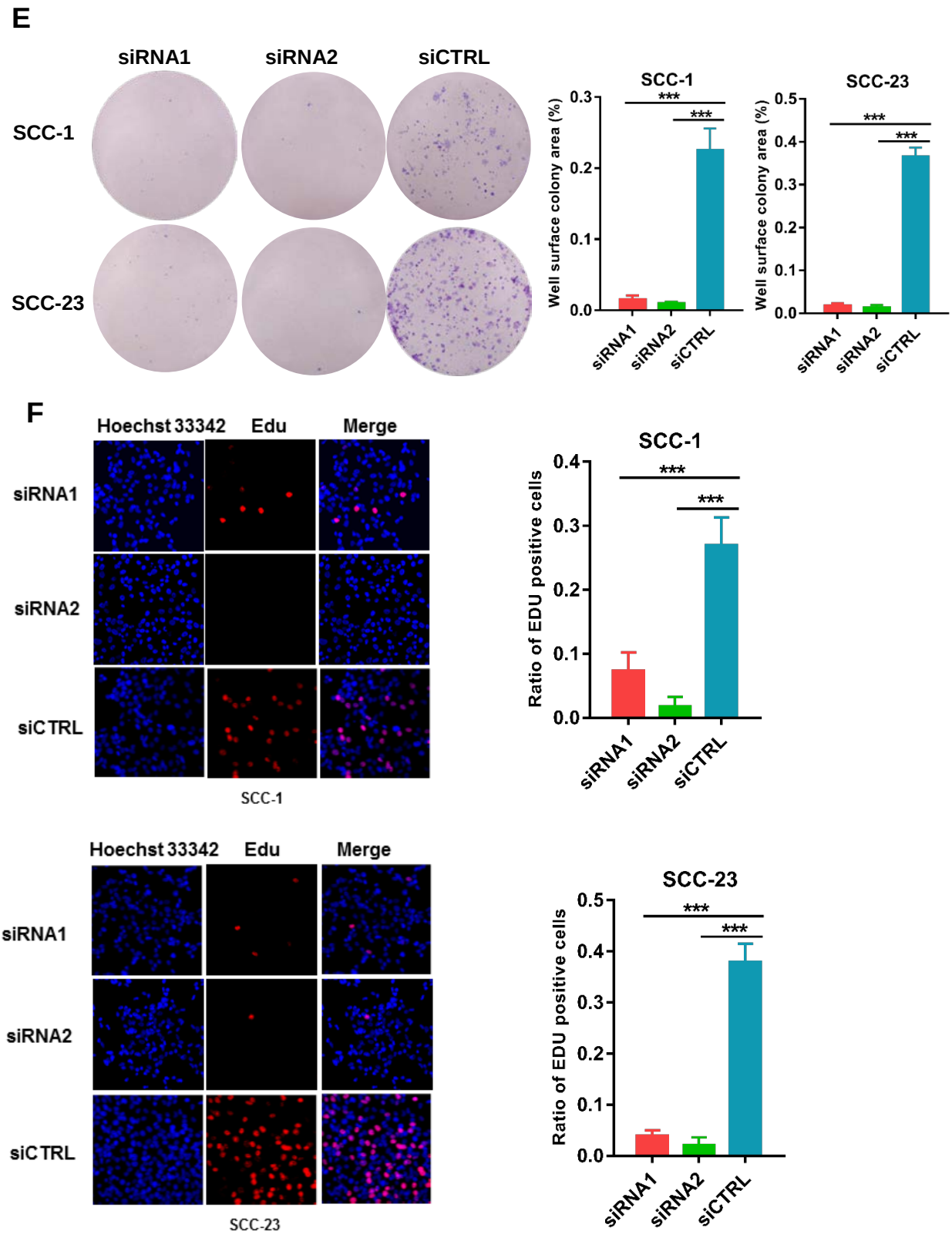

Figure 21E-21F

G

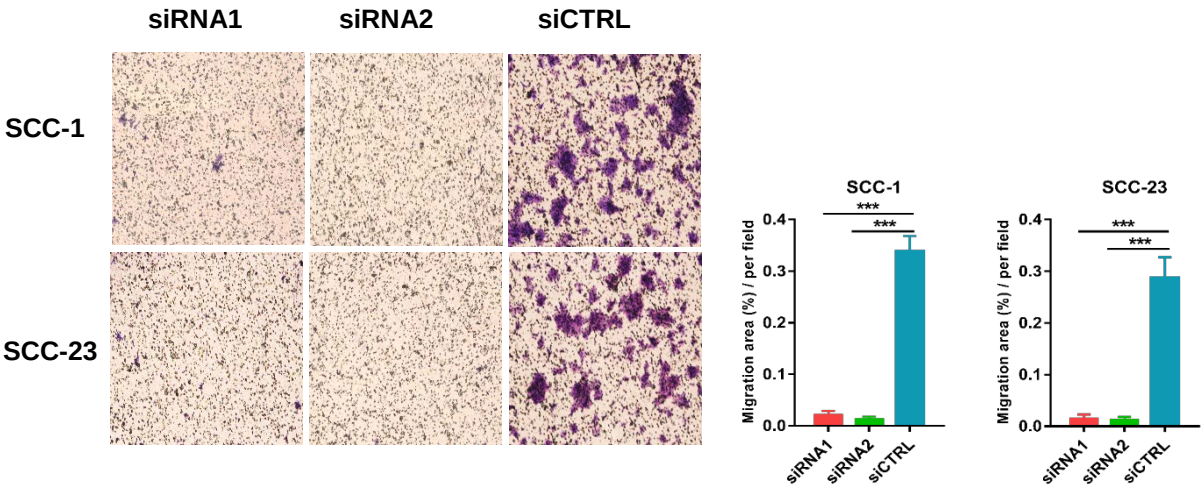

H

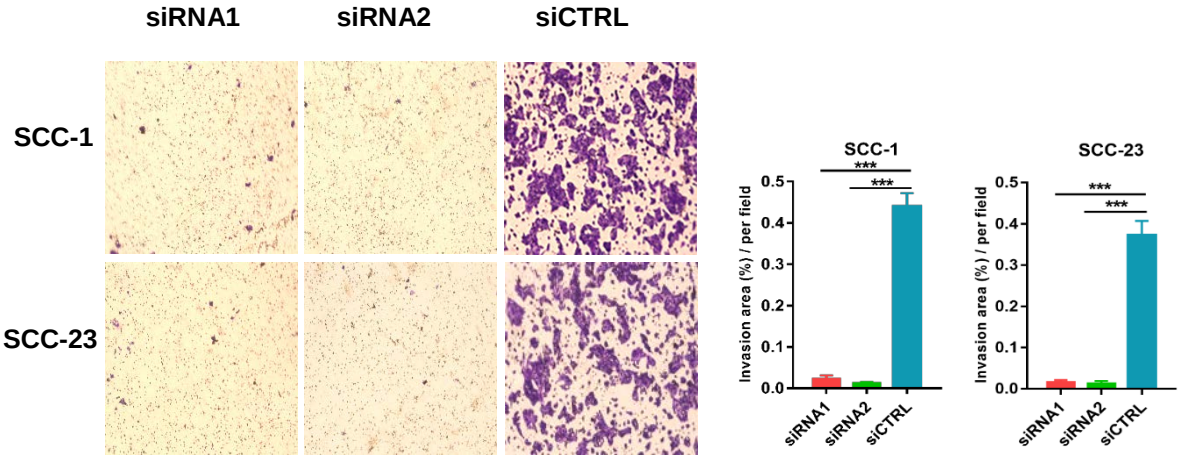

Figure 21G-21H

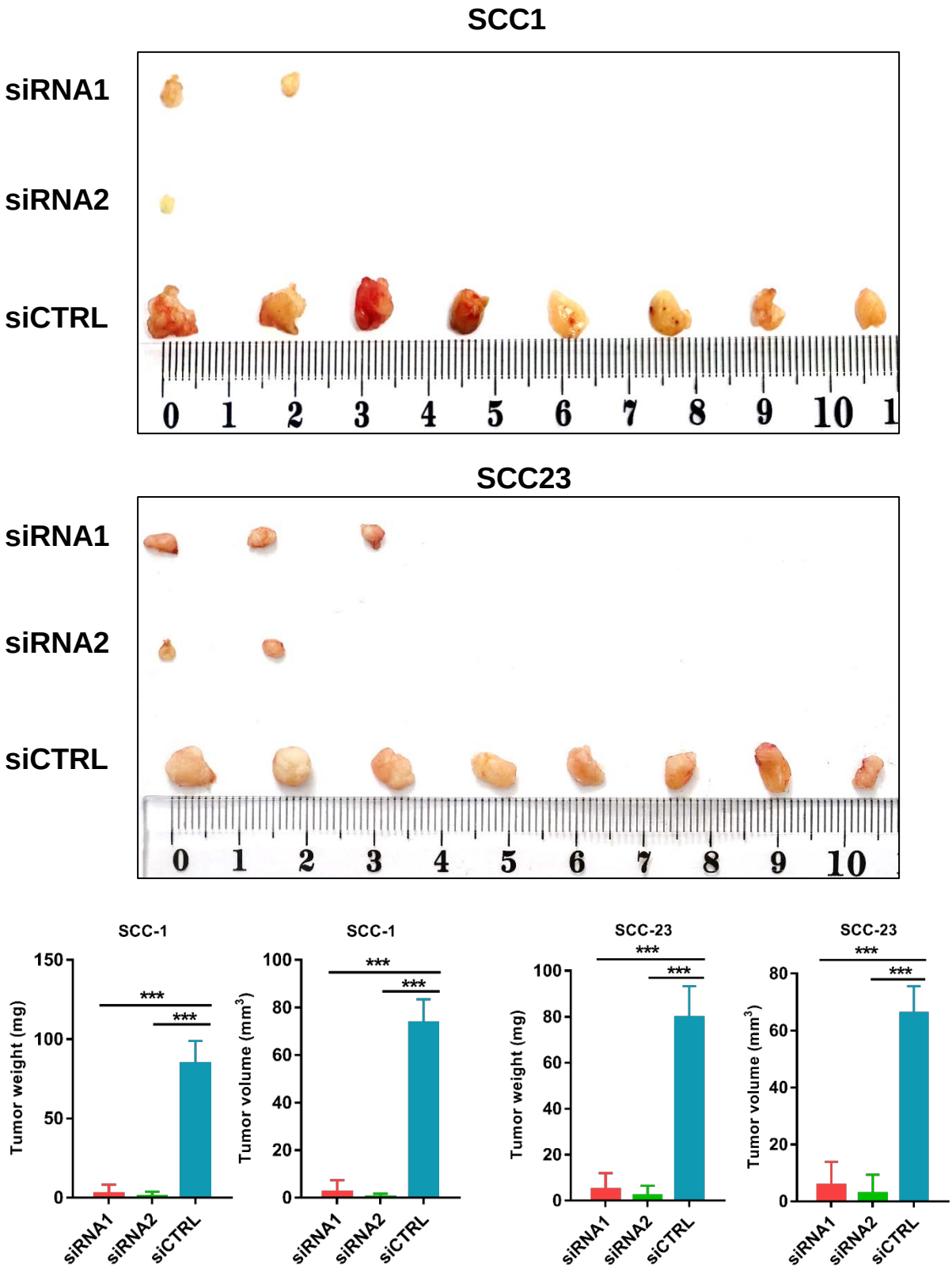
SCC1
siRNA1
siRNA2
siCTRL
0 1 2 3 4 5 6 7 8 9 10 1
SCC23
siRNA1
siRNA2
siCTRL
0 1 2 3 4 5 6 7 8 9 10
SCC-1
Tumor weight (mg)
150
100
50
0
***
***
siRNA1
siRNA2
siCTRL
SCC-1
Tumor volume (mm3)
100
80
60
40
20
0
***
***
siRNA1
siRNA2
siCTRL
SCC-23
Tumor weight (mg)
100
80
60
40
20
0
***
***
siRNA1
siRNA2
siCTRL
SCC-23
Tumor volume (mm3)
80
60
40
20
0
***
***
siRNA1
siRNA2
siCTRL

Figure 22

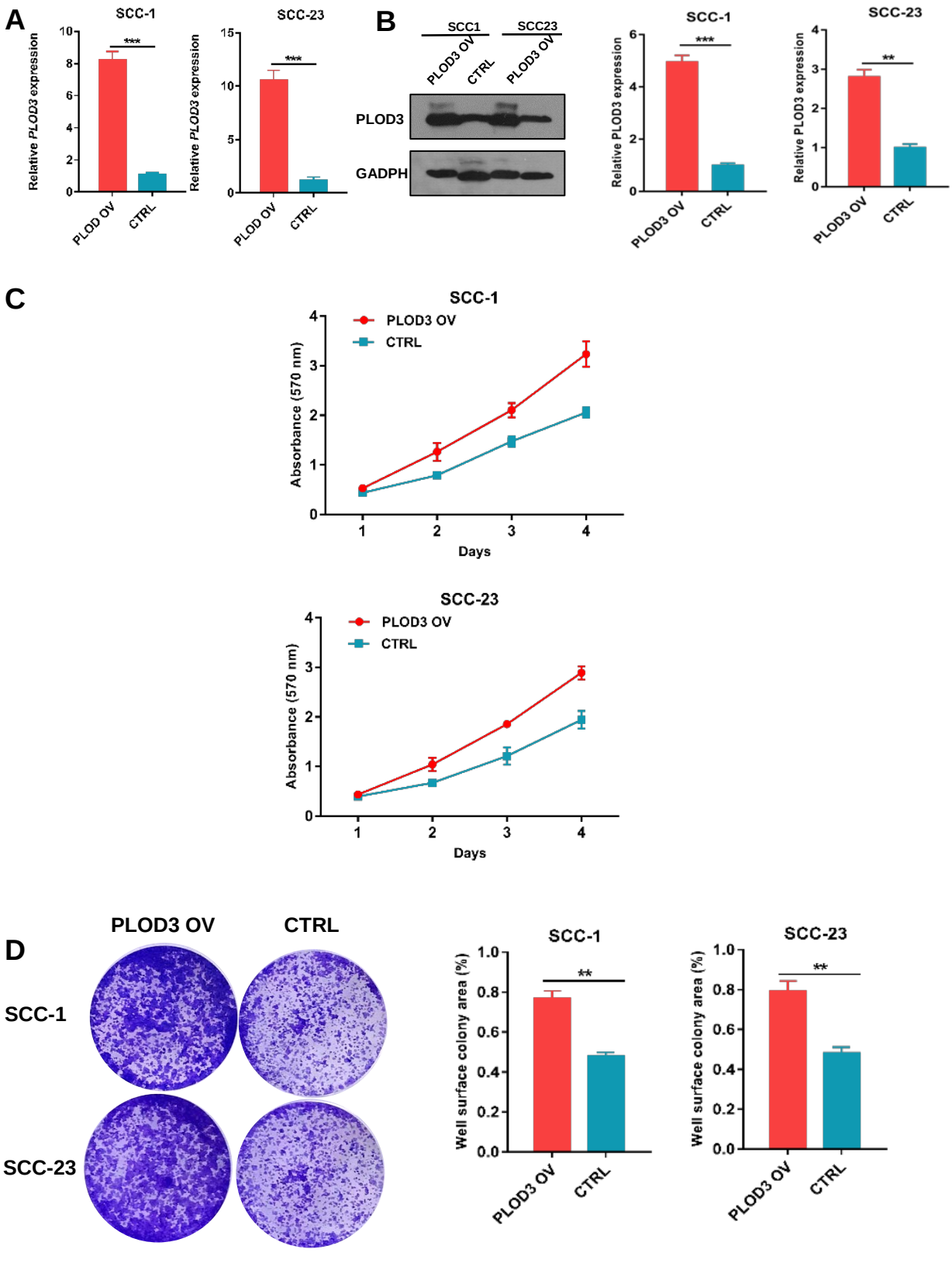

Figure 23A-23D

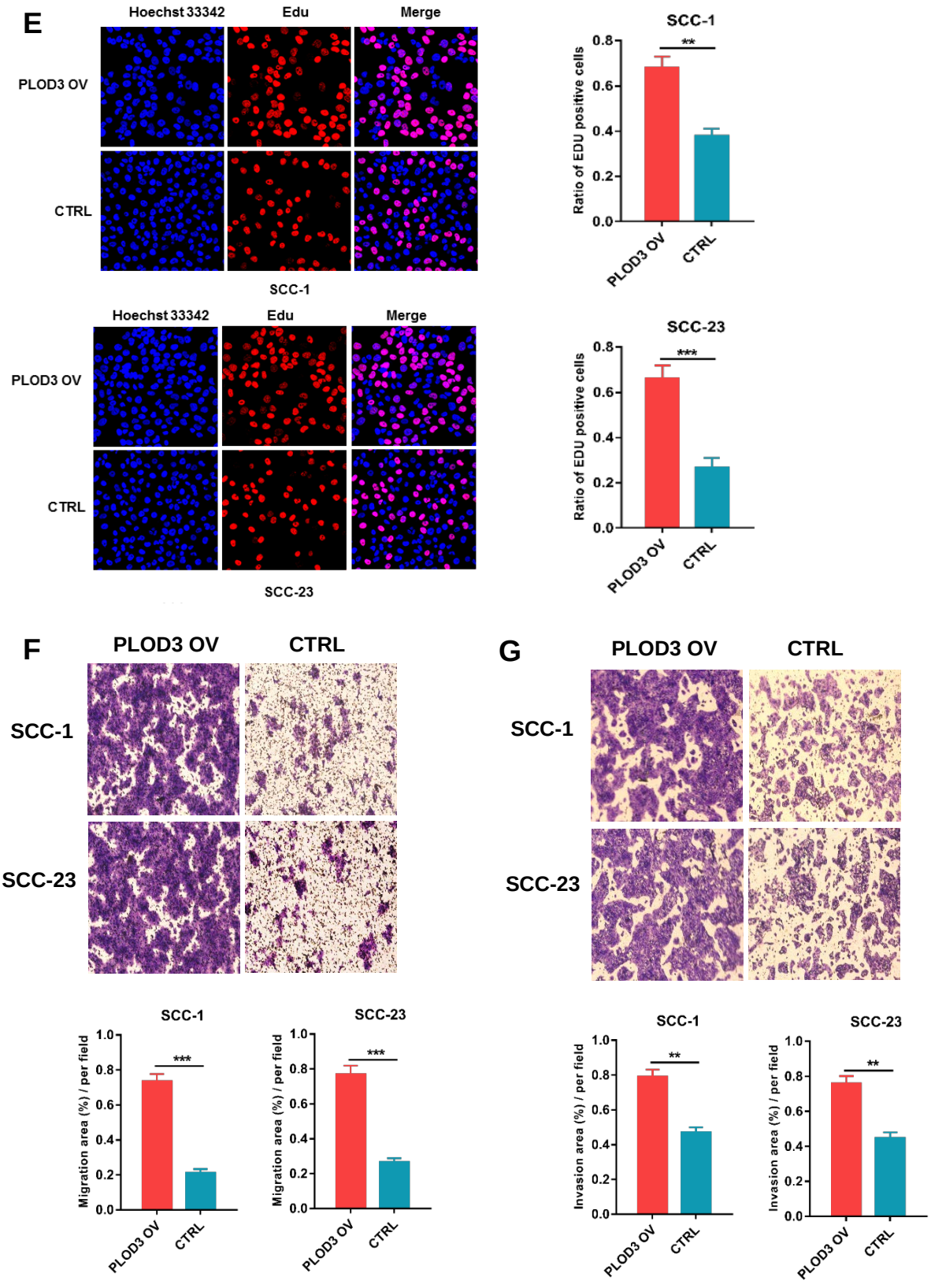

Figure 23E-23G

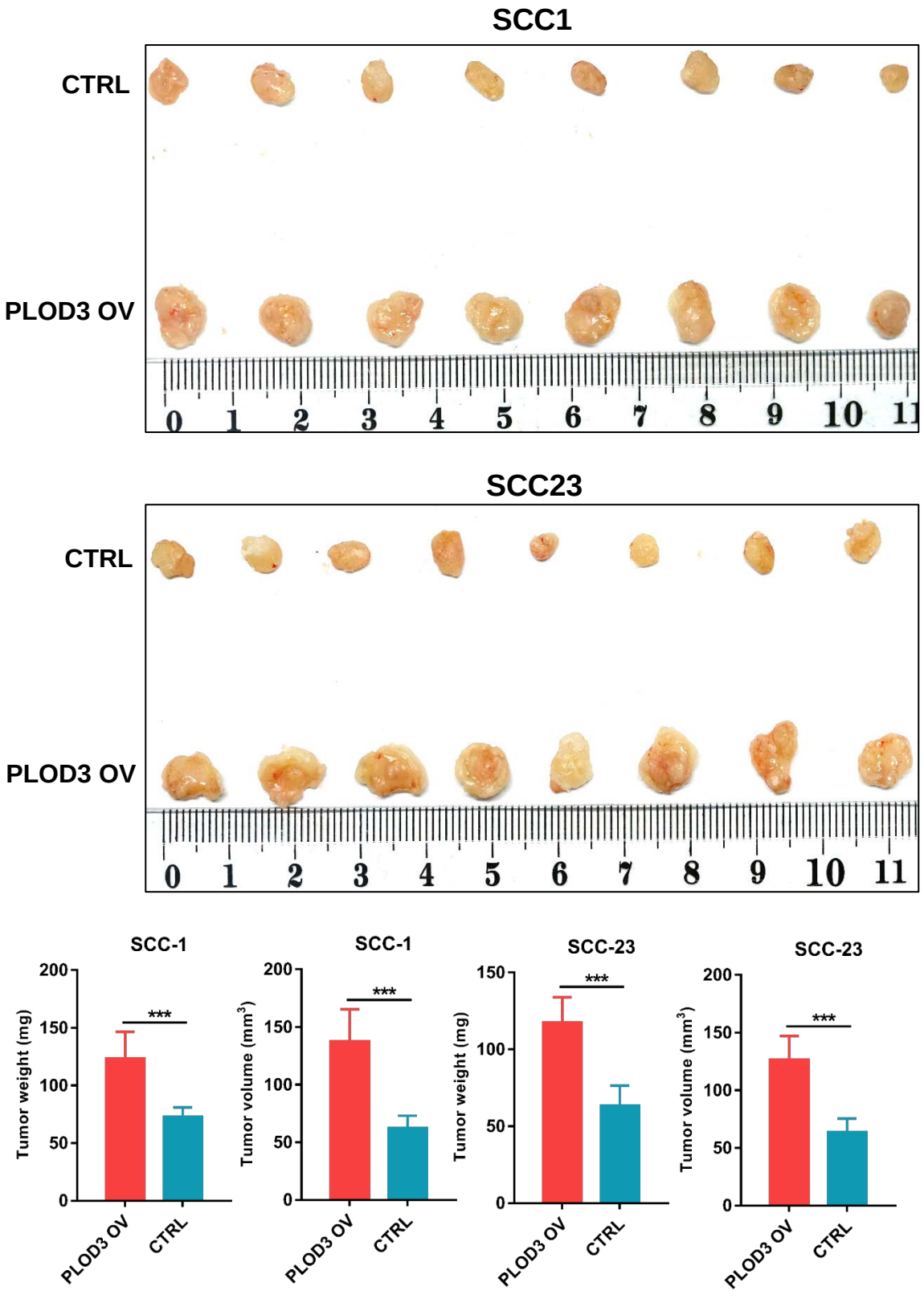
SCC1
CTRL
PLOD3 OV
0 1 2 3 4 5 6 7 8 9 10 11
SCC23
CTRL
PLOD3 OV
0 1 2 3 4 5 6 7 8 9 10 11
SCC-1
Tumor weight (mg)
200
150
100
50
0
***
PLOD3 OV
CTRL
SCC-1
Tumor volume (mm3)
200
150
100
50
0
***
PLOD3 OV
CTRL
SCC-23
Tumor weight (mg)
150
100
50
0
***
PLOD3 OV
CTRL
SCC-23
Tumor volume (mm3)
200
150
100
50
0
***
PLOD3 OV
CTRL

Figure 24

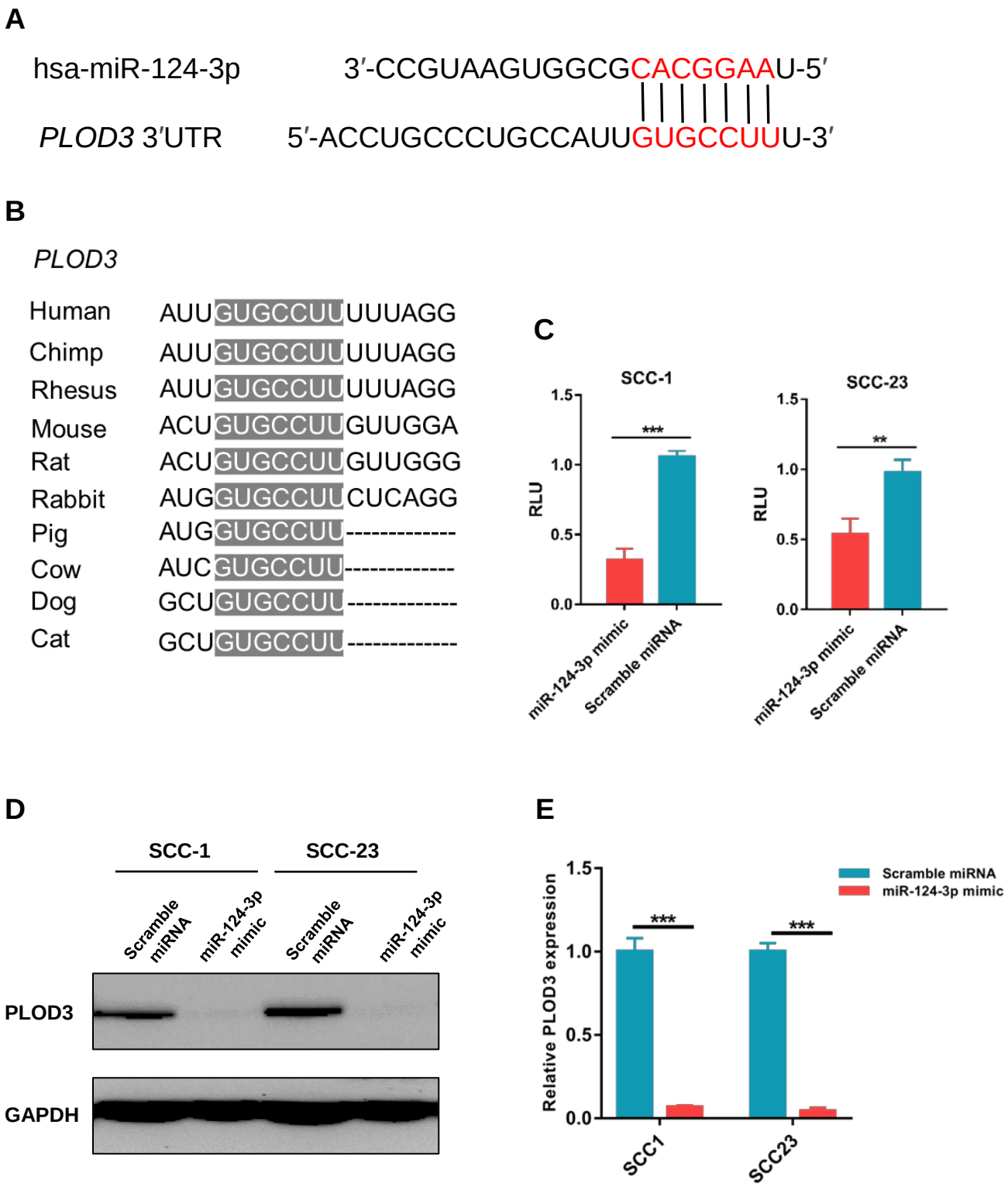
A
hsa-miR-124-3p
3′-CCGUAAGUGGCGCACGGAAU-5′
PLOD3 3′UTR
5′-ACCUGCCCUGCCAUUGUGCCUUU-3′
B
PLOD3
Human AUUGUGCCUUUUUAGG
Chimp AUUGUGCCUUUUUAGG
Rhesus AUUGUGCCUUUUUAGG
Mouse ACUGUGCCUUGUUGGA
Rat ACUGUGCCUUGUUGGG
Rabbit AUGGUGCCUUCUCAGG
Pig AUGGUGCCUU----------
Cow AUCGUGCCUU----------
Dog GCUGUGCCUU----------
Cat GCUGUGCCUU----------
C
SCC-1
SCC-23
RLU
1.5
1.0
0.5
0.0
***
**
miR-124-3p mimic
Scramble miRNA
D
SCC-1
SCC-23
Scramble miRNA
miR-124-3p mimic
PLOD3
GAPDH
E
Scramble miRNA
miR-124-3p mimic
Relative PLOD3 expression
SCC1
SCC23

Figure 25

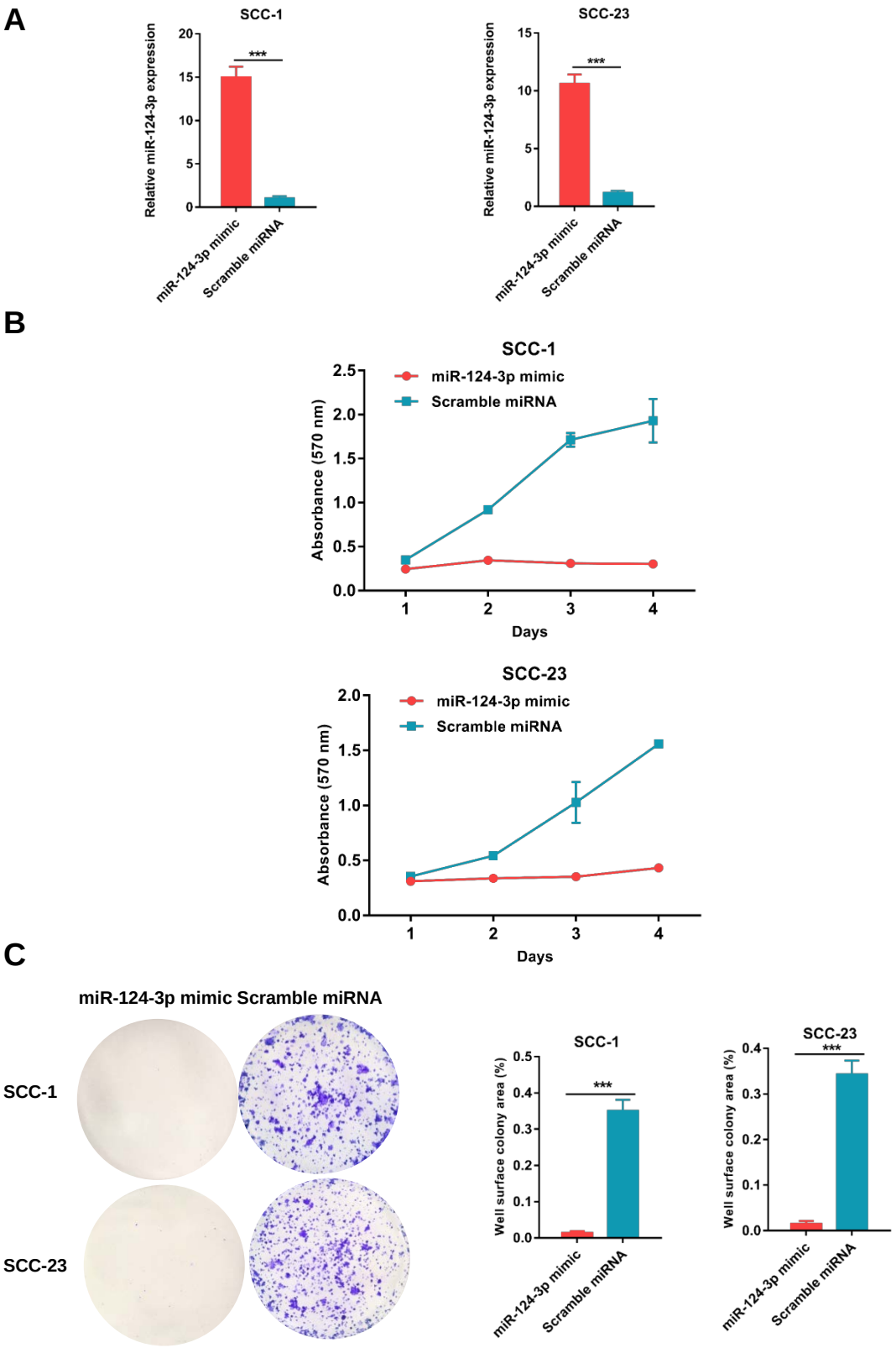

Figure 26A-26C

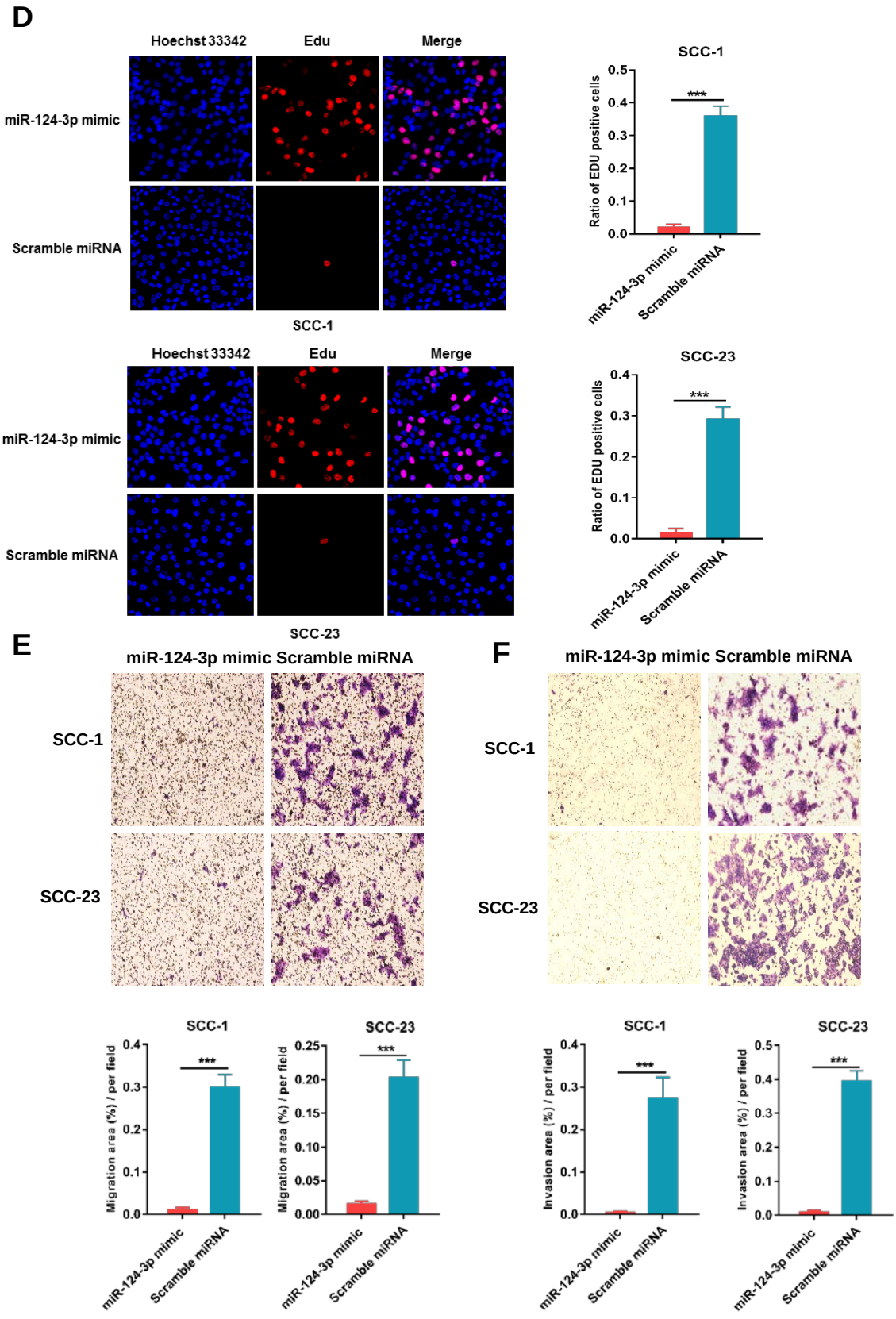

Figure 26D-26F

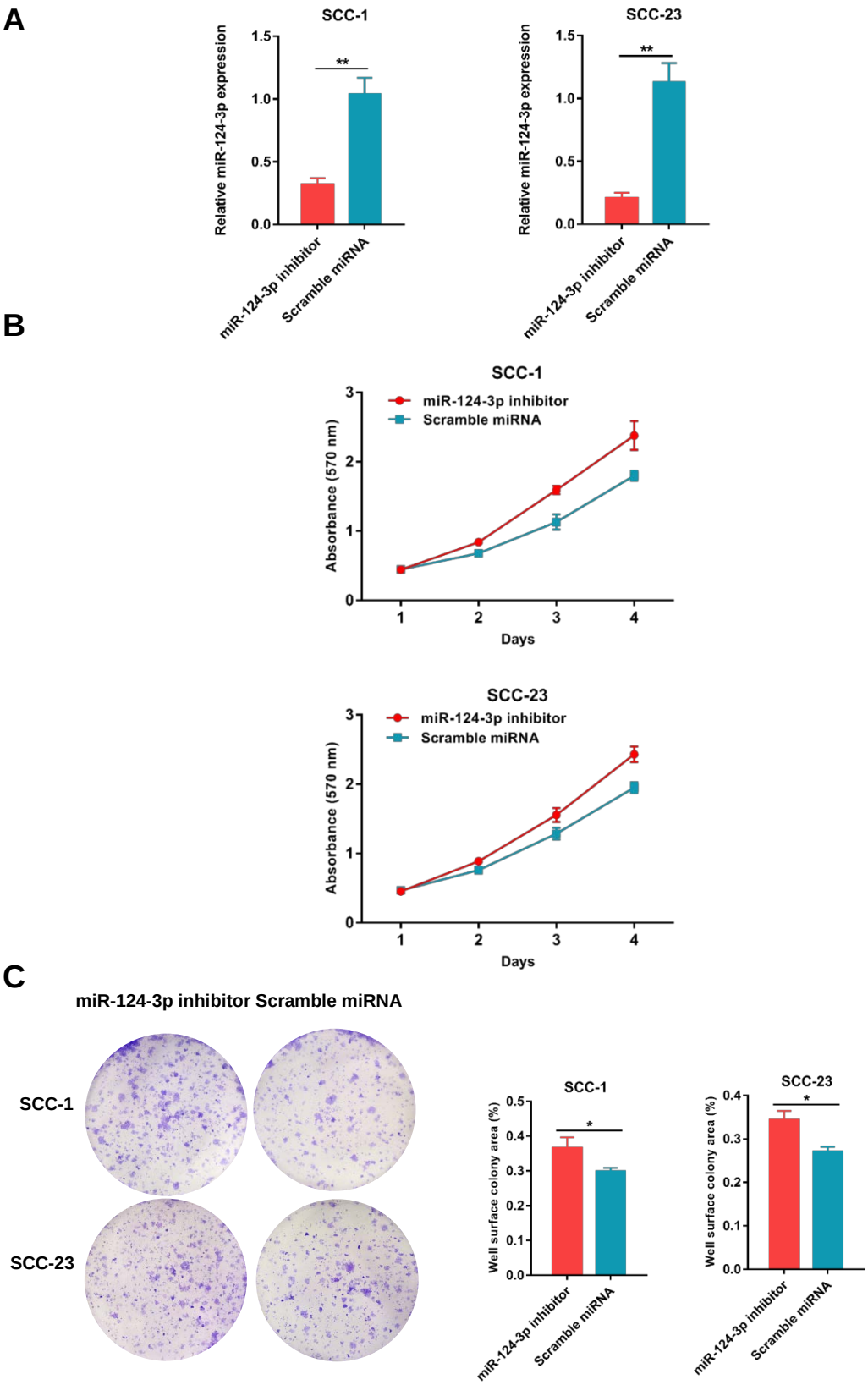

Figure 27A-2C

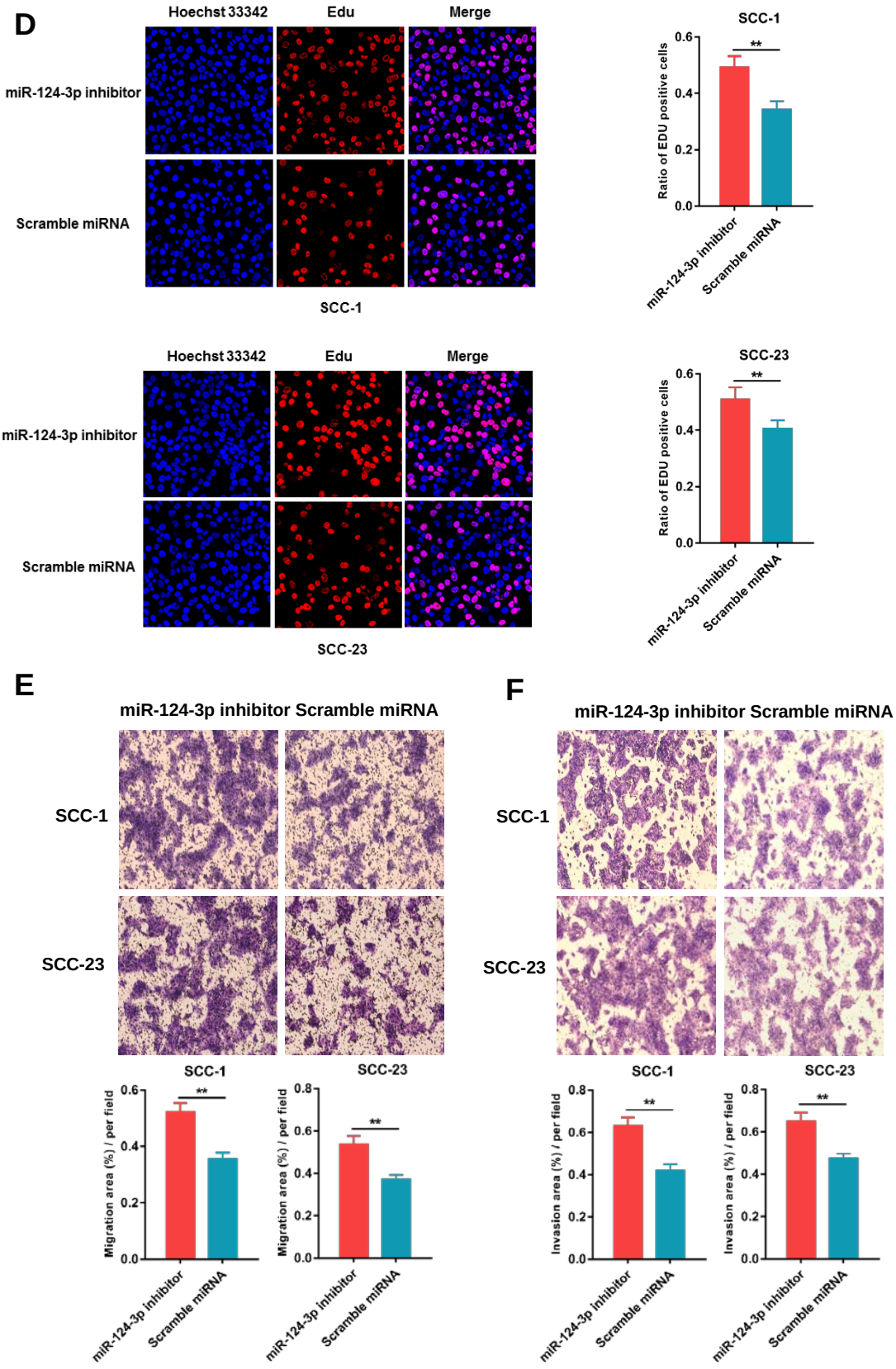

Figure 27D-27F

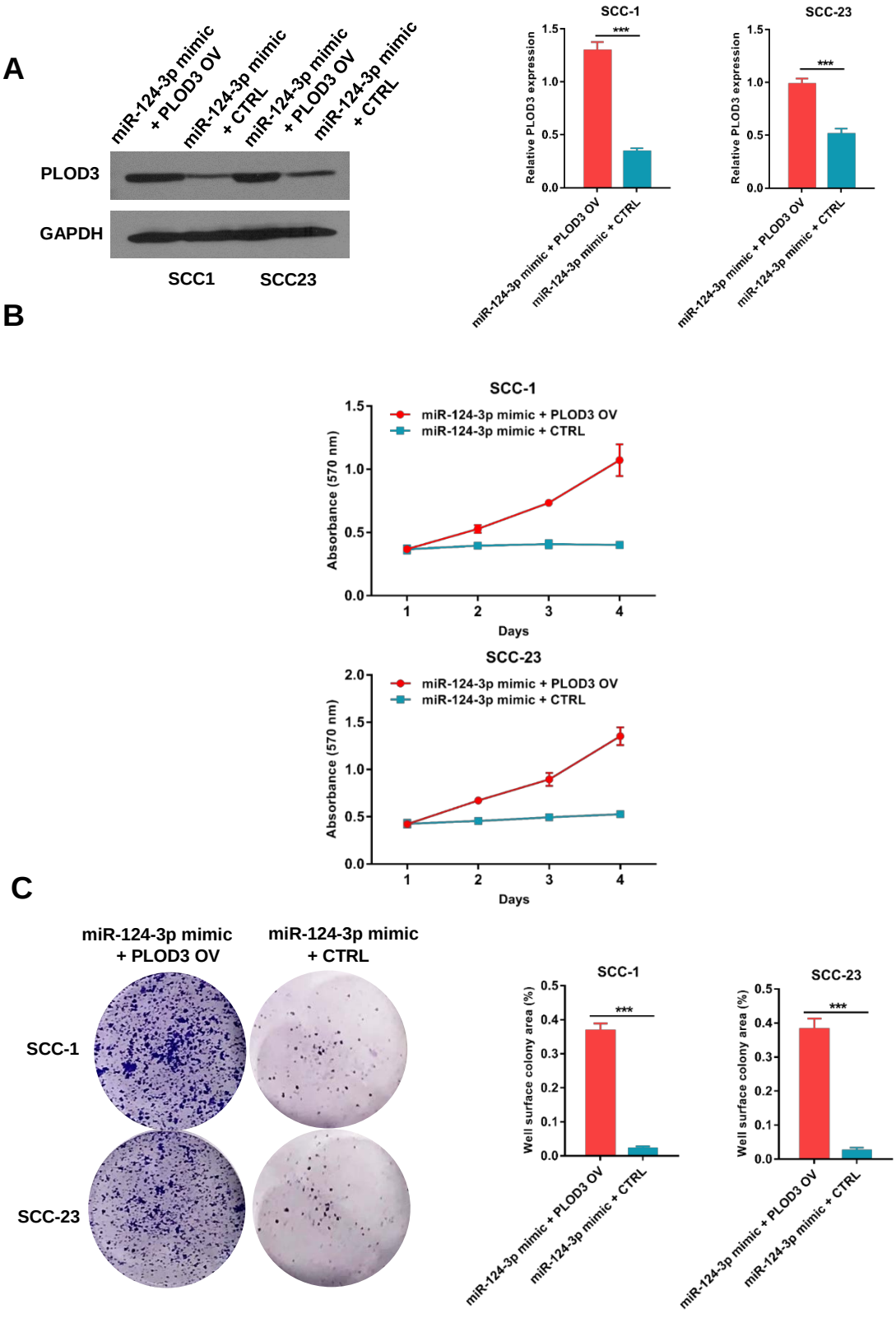

Figure 28A-28C

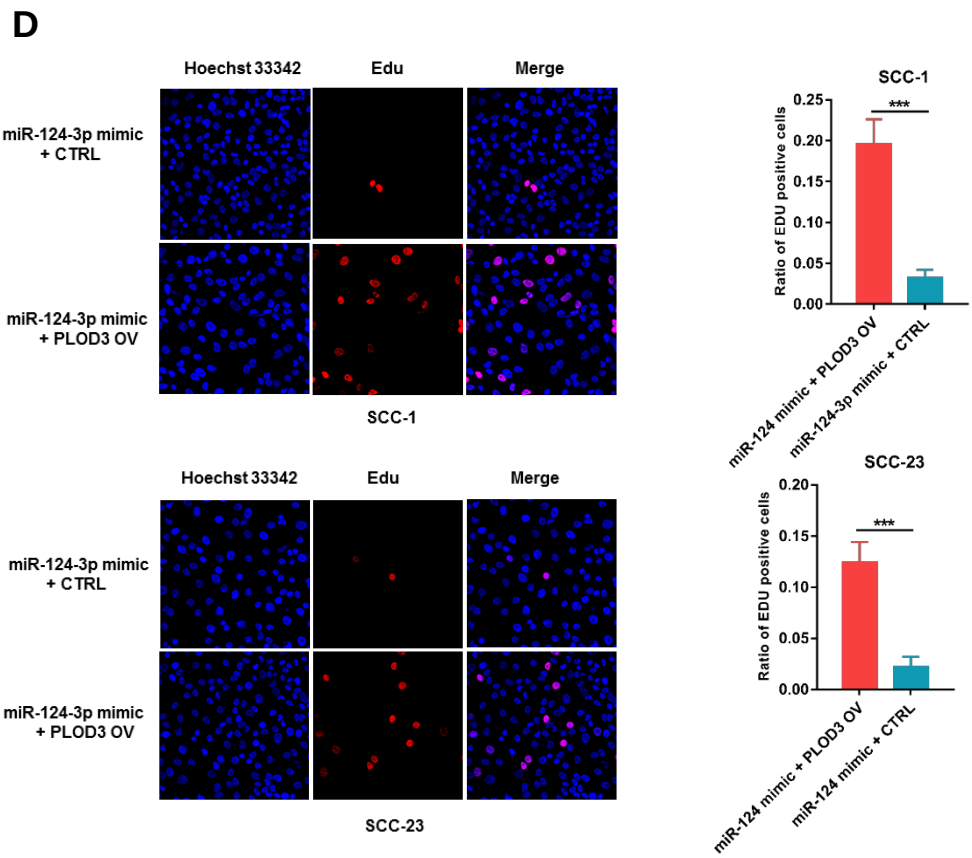

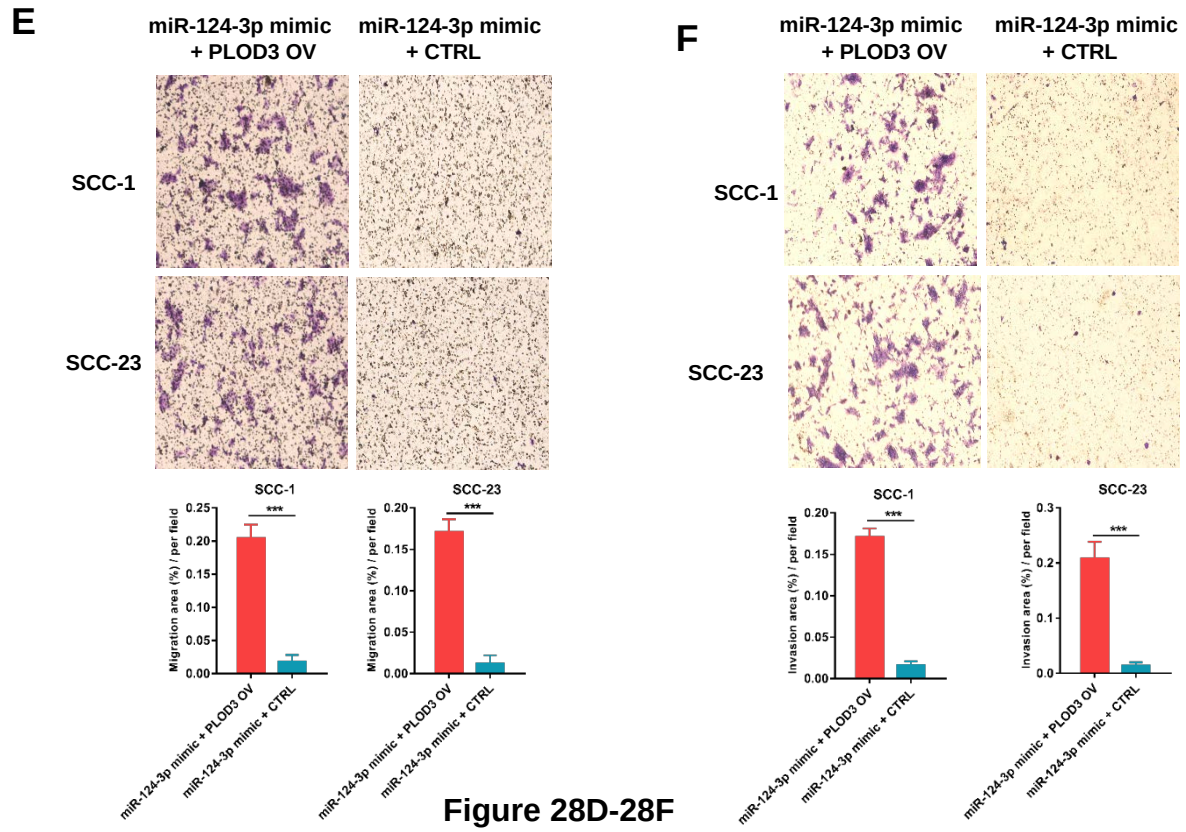

Figure 28D-28F

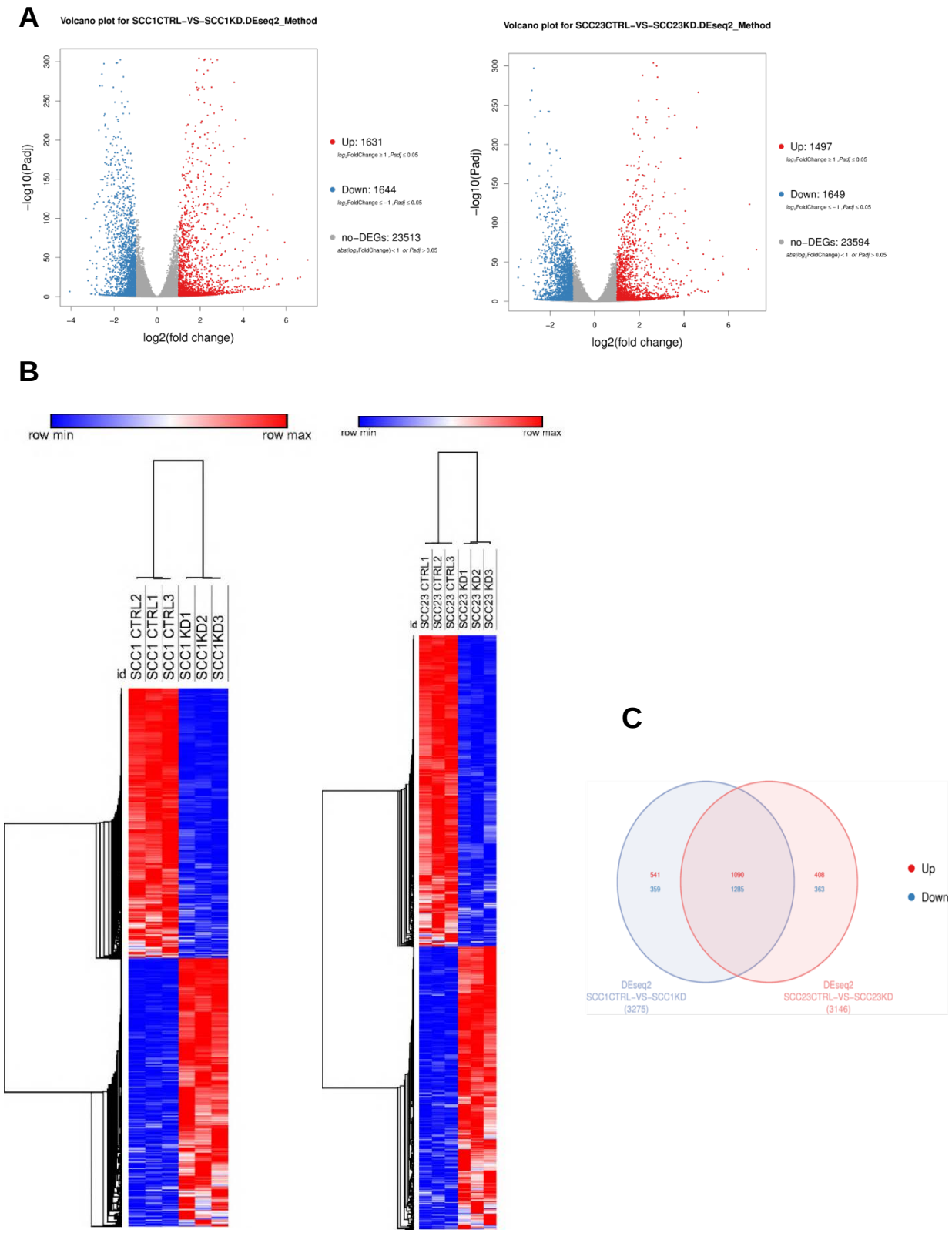
A
Volcano plot for SCC1CTRL−VS−SCC1KD.DEseq2_Method
−log10(Padj)
log2(fold change)
Up: 1631
Down: 1644
no−DEGs: 23513
Volcano plot for SCC23CTRL−VS−SCC23KD.DEseq2_Method
−log10(Padj)
log2(fold change)
Up: 1497
Down: 1649
no−DEGs: 23594
B
row min
row max
id
SCC1 CTRL2
SCC1 CTRL1
SCC1 CTRL3
SCC1 KD1
SCC1KD2
SCC1KD3
row min
row max
id
SCC23 CTRL1
SCC23 CTRL2
SCC23 CTRL3
SCC23 KD1
SCC23 KD2
SCC23 KD3
C
541
359
1090
1285
408
363
Up
Down
DEseq2
SCC1CTRL−VS−SCC1KD
(3275)
DEseq2
SCC23CTRL−VS−SCC23KD
(3146)

Figure 29

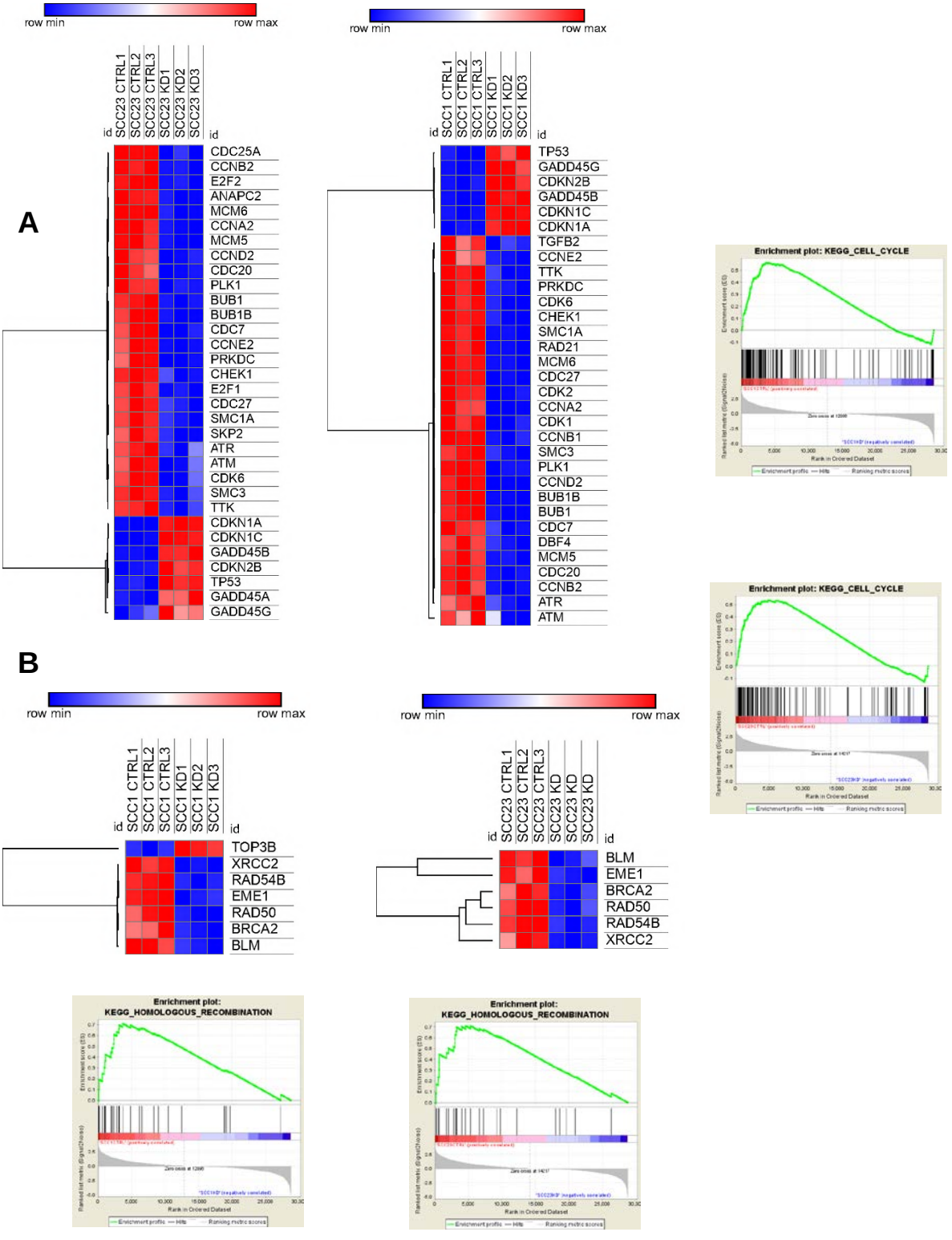

Figure 30A-30B

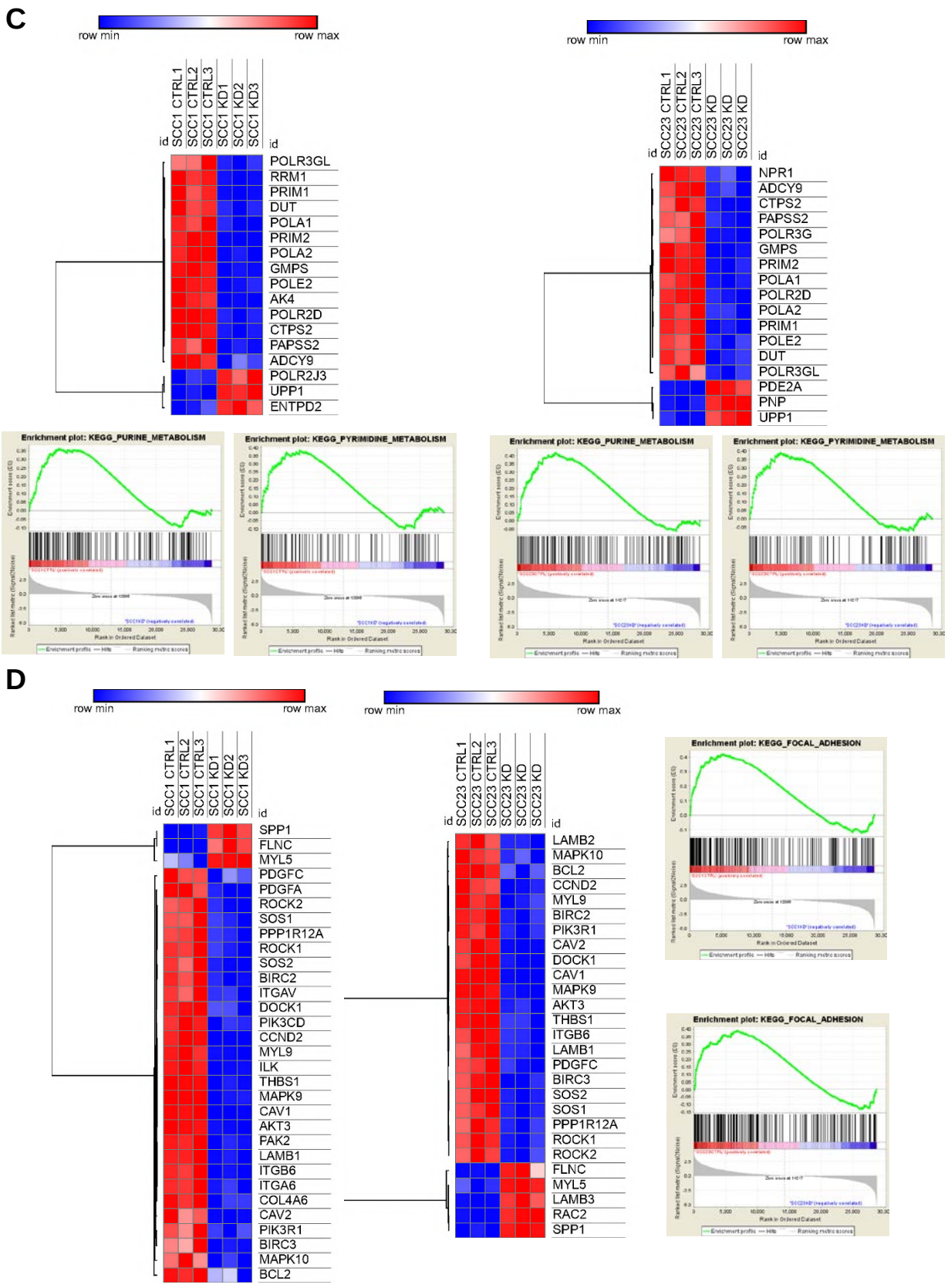

Figure 30C-30D

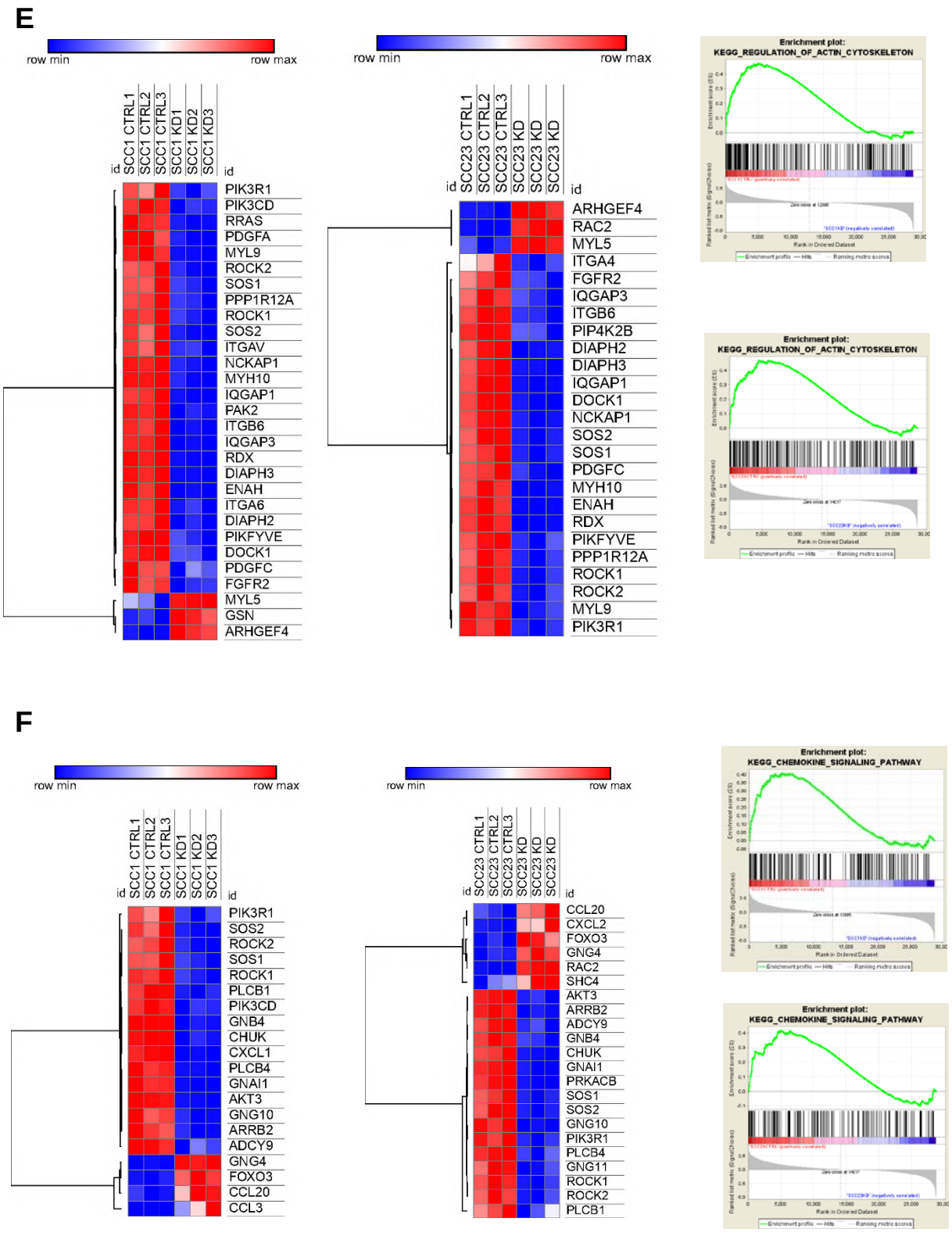

Figure 30E-30F

G

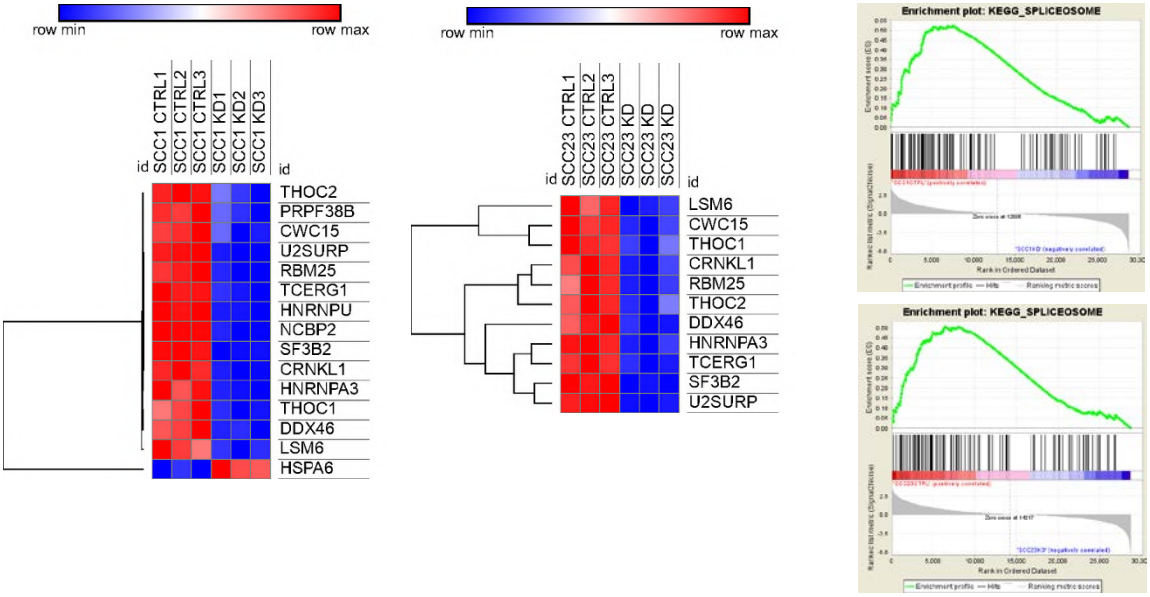

H

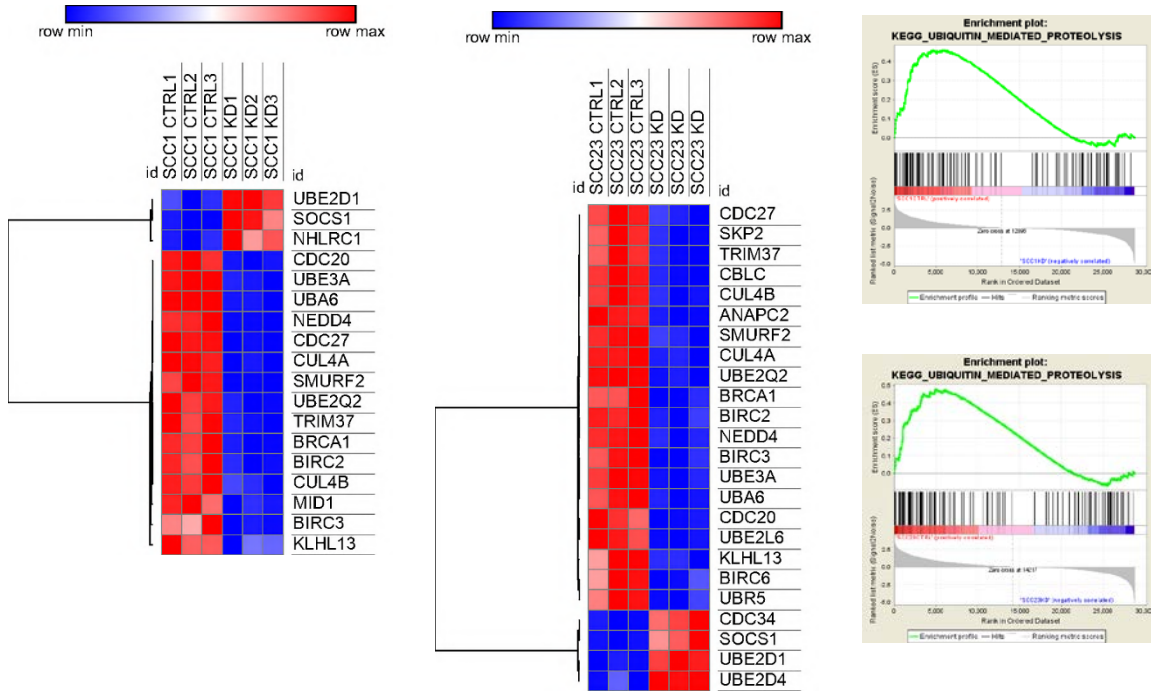

Figure 30G-30H

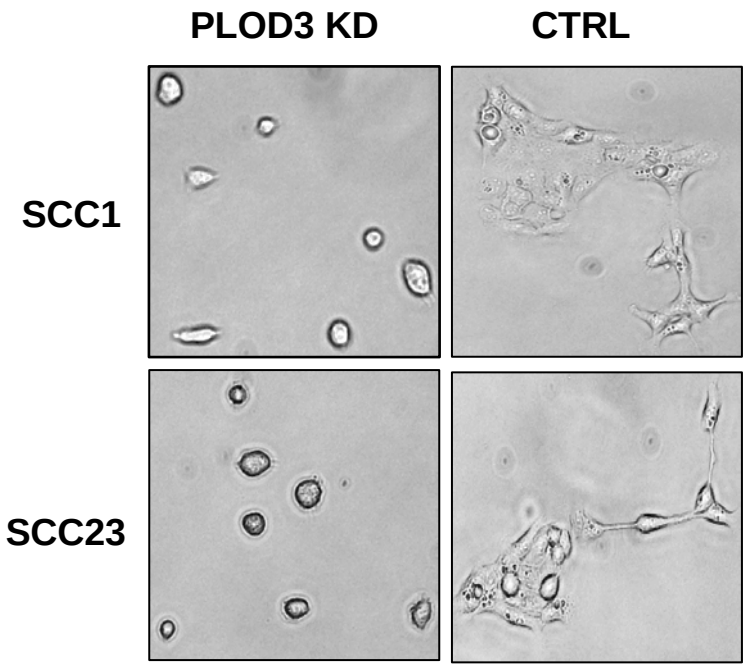

Figure 31

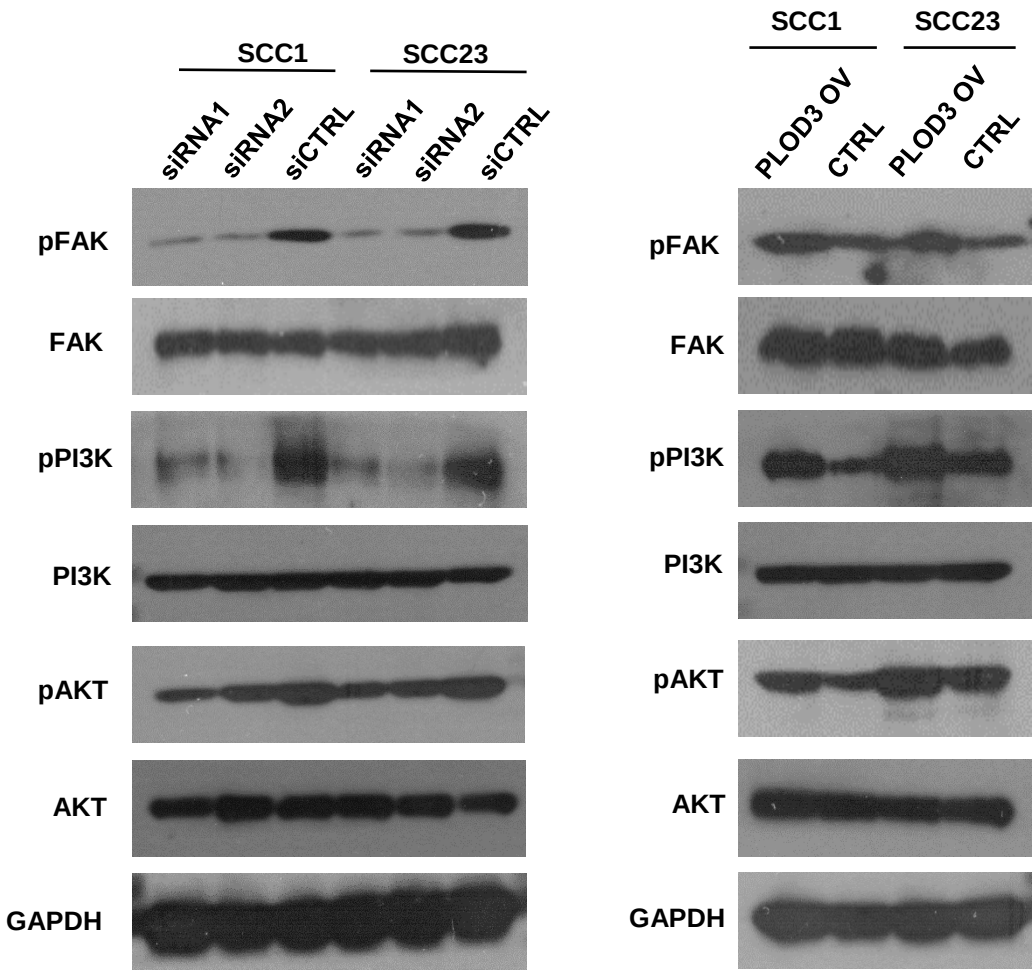
SCC1
SCC23
siRNA1
siRNA2
siCTRL
siRNA1
siRNA2
siCTRL
pFAK
FAK
pPI3K
PI3K
pAKT
AKT
GAPDH
SCC1
SCC23
PLOD3 OV
CTRL
PLOD3 OV
CTRL
pFAK
FAK
pPI3K
PI3K
pAKT
AKT
GAPDH

Figure 32

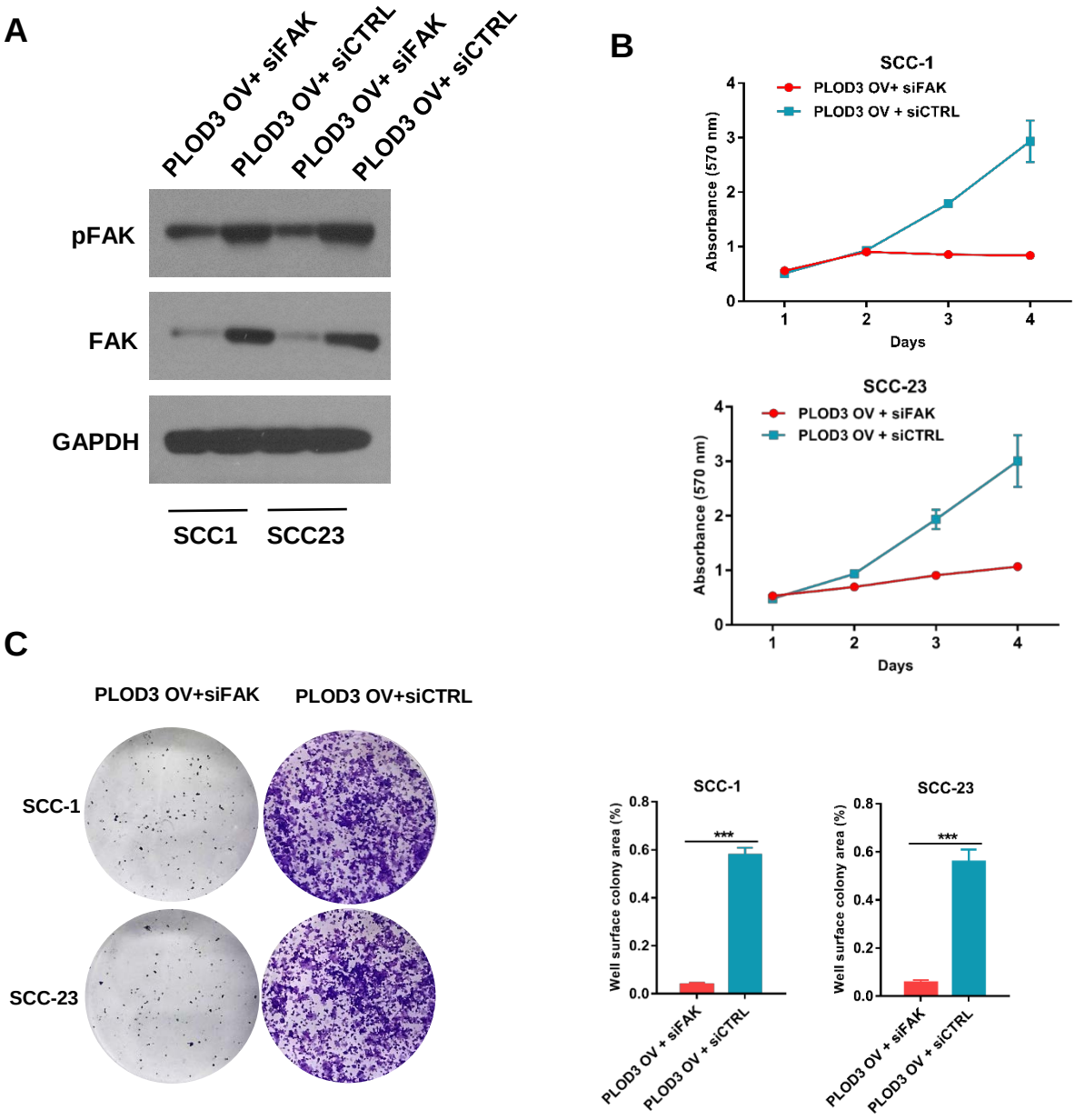

Figure 33A-33C

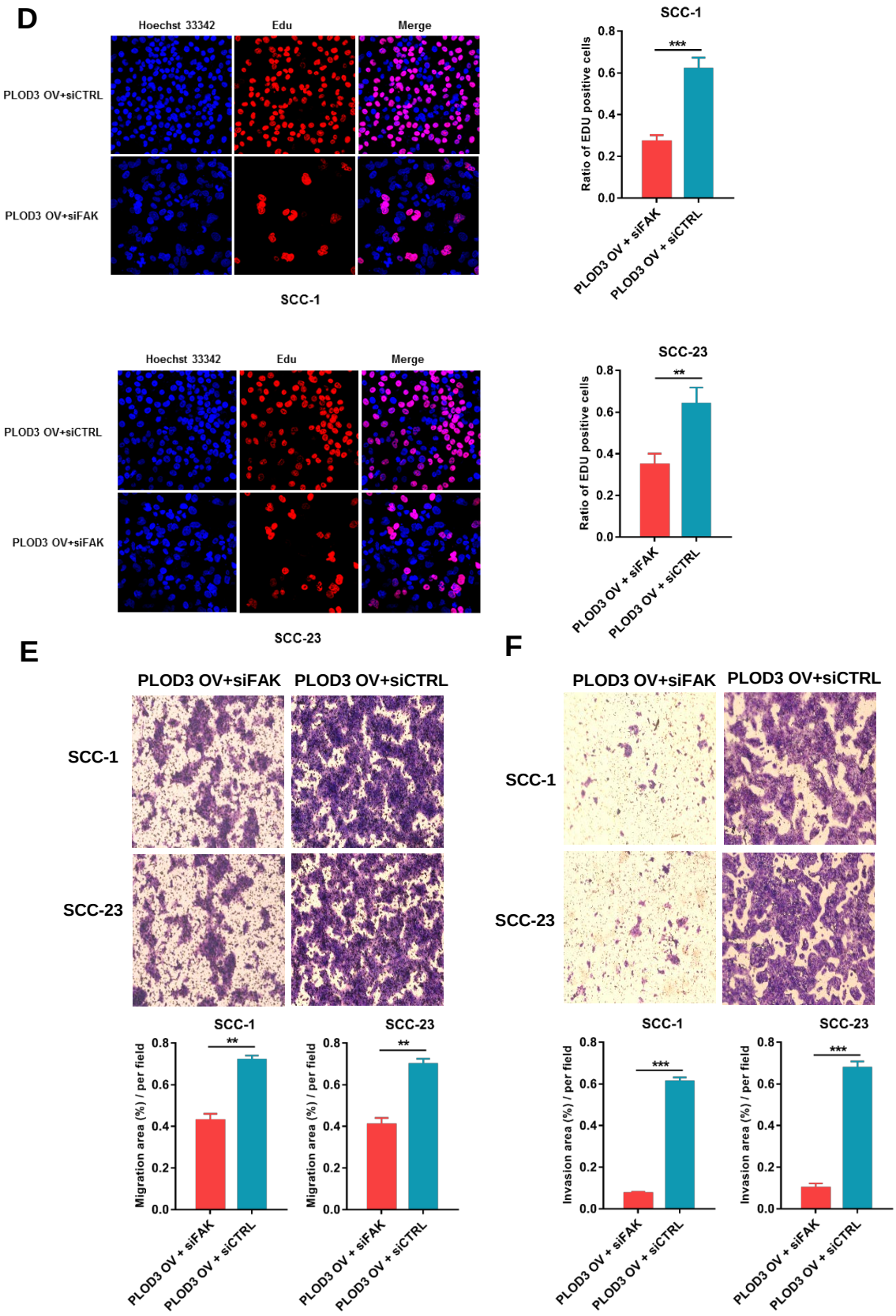

Figure 34D-34F

REFERENCES

1. Parkin, D.M., Bray, F., Ferlay, J. & Pisani, P. Global cancer statistics, 2002. *Ca-a Cancer Journal for Clinicians* **55**, 74-108 (2005).
2. Sanderson, R.J. & Ironside, J.A.D. Squamous cell carcinomas of the head and neck. *British Medical Journal* **325**, 822-827 (2002).
3. Kamangar, F., Dores, G.M. & Anderson, W.F. Patterns of cancer incidence, mortality, and prevalence across five continents: Defining priorities to reduce cancer disparities in different geographic regions of the world. *Journal of Clinical Oncology* **24**, 2137-2150 (2006).
4. Rezende, T.M.B., Freire, M.D. & Franco, O.L. Head and Neck Cancer Proteomic Advances and Biomarker Achievements. *Cancer* **116**, 4914-4925 (2010).
5. Zielinski, V. *et al.* ADAM8 in squamous cell carcinoma of the head and neck: a retrospective study. *Bmc Cancer* **12**(2012).
6. Mehanna, H., Paleri, V., West, C.M.L. & Nutting, C. Head and neck cancer-Part 1: Epidemiology, presentation, and prevention. *British Medical Journal* **341**(2010).
7. Sturgis, E.M. & Cinciripini, P.M. Trends in head and neck cancer incidence in relation to smoking prevalence - An emerging epidemic of human papillomavirus-associated cancers? *Cancer* **110**, 1429-1435 (2007).
8. Ramqvist, T. & Dalianis, T. Oropharyngeal cancer epidemic and human papillomavirus. *Emerg Infect Dis* **16**, 1671-7 (2010).
9. Pytynia, K.B., Dahlstrom, K.R. & Sturgis, E.M. Epidemiology of HPV-associated oropharyngeal cancer. *Oral Oncology* **50**, 380-386 (2014).

10. Vigneswaran, N. & Williams, M.D. Epidemiologic Trends in Head and Neck Cancer and Aids in Diagnosis. *Oral and Maxillofacial Surgery Clinics of North America* **26**, 123-+ (2014).

11. Gourin, C.G. & Podolsky, R.H. Racial disparities in patients with head and neck squamous cell carcinoma. *Laryngoscope* **116**, 1093-1106 (2006).

12. Nichols, A.C. & Bhattacharyya, N. Racial differences in stage and survival in head and neck squamous cell carcinoma. *Laryngoscope* **117**, 770-775 (2007).

13. Hashibe, M. *et al.* Alcohol drinking in never users of tobacco, cigarette smoking in never drinkers, and the risk of head and neck cancer: Pooled analysis in the international head and neck cancer epidemiology consortium. *Journal of the National Cancer Institute* **99**, 777-789 (2007).

14. Zhang, X.L. & Reichart, P.A. A review of betel quid chewing, oral cancer and precancer in Mainland China. *Oral Oncology* **43**, 424-430 (2007).

15. Argiris, A., Karamouzis, M.V., Raben, D. & Ferris, R.L. Head and neck cancer. *Lancet* **371**, 1695-1709 (2008).

16. Conway, D.I. *et al.* Enhancing epidemiologic research on head and neck cancer: INHANCE - The international head and neck cancer epidemiology consortium. *Oral Oncology* **45**, 743-746 (2009).

17. Liu, Y. *et al.* SOX4 Promotes Progression in OLP-Associated Squamous Cell Carcinoma. *Journal of Cancer* **7**, 1534-1540 (2016).

18. Huang, S.H. & O'Sullivan, B. Overview of the 8th Edition TNM Classification for Head and Neck Cancer. *Current Treatment Options in Oncology* **18**(2017).

19. Hanahan, D. & Weinberg, R.A. Hallmarks of Cancer: The Next Generation. *Cell* **144**, 646-674 (2011).

20. Yang, L.H. & Baker, N.E. Cell cycle withdrawal, progression, and cell survival regulation by EGFR and its effectors in the differentiating Drosophila eye. *Developmental Cell* **4**, 359-369 (2003).

21. Kalyankrishna, S. & Grandis, J.R. Epidermal growth factor receptor biology in head and neck cancer. *Journal of Clinical Oncology* **24**, 2666-2672 (2006).

22. Grandis, J.R. & Tweardy, D.J. Elevated Levels of Transforming Growth-Factor-Alpha and Epidermal Growth-Factor Receptor Messenger-Rna Are Early Markers of Carcinogenesis in Head and Neck-Cancer. *Cancer Research* **53**, 3579-3584 (1993).

23. Zhou, G., Liu, Z.Y. & Myers, J.N. TP53 Mutations in Head and Neck Squamous Cell Carcinoma and Their Impact on Disease Progression and Treatment Response. *Journal of Cellular Biochemistry* **117**, 2682-2692 (2016).

24. Chen, J.D. The Cell-Cycle Arrest and Apoptotic Functions of p53 in Tumor Initiation and Progression. *Cold Spring Harbor Perspectives in Medicine* **6**(2016).

25. Bieging, K.T., Mello, S.S. & Attardi, L.D. Unravelling mechanisms of p53-mediated tumour suppression. *Nature Reviews Cancer* **14**, 359-370 (2014).

26. Suh, Y., Amelio, I., Urbano, T.G. & Tavassoli, M. Clinical update on cancer: molecular oncology of head and neck cancer. *Cell Death & Disease* **5**(2014).

27. Bernstein, J.M., Bernstein, C.R., West, C.M.L. & Homer, J.J. Molecular and cellular processes underlying the hallmarks of head and neck cancer. *European Archives of Oto-Rhino-Laryngology* **270**, 2585-2593 (2013).

28. Blackburn, E.H., Greider, C.W. & Szostak, J.W. Telomeres and telomerase: the path from maize, Tetrahymena and yeast to human cancer and aging. *Nature Medicine* **12**, 1133-1138 (2006).

29. Boscolo-Rizzo, P. *et al.* Telomeres and telomerase in head and neck squamous cell carcinoma: from pathogenesis to clinical implications. *Cancer and Metastasis Reviews* **35**, 457-474 (2016).

30. Carla, C. *et al.* Angiogenesis in head and neck cancer: a review of the literature. *J Oncol* **2012**, 358472 (2012).

31. Kalluri, R. & Weinberg, R.A. The basics of epithelial-mesenchymal transition. *J Clin Invest* **119**, 1420-8 (2009).

32. Smith, A., Teknos, T.N. & Pan, Q. Epithelial to mesenchymal transition in head and neck squamous cell carcinoma. *Oral Oncol* **49**, 287-92 (2013).

33. DeBerardinis, R.J. & Chandel, N.S. Fundamentals of cancer metabolism. *Sci Adv* **2**, e1600200 (2016).

34. Yang, M., Soga, T. & Pollard, P.J. Oncometabolites: linking altered metabolism with cancer. *J Clin Invest* **123**, 3652-8 (2013).

35. Wang, J. *et al.* Metabolomic profiling of anionic metabolites in head and neck cancer cells by capillary ion chromatography with Orbitrap mass spectrometry. *Anal Chem* **86**, 5116-24 (2014).

36. Grandis, J.R. *et al.* Human leukocyte antigen class I allelic and haplotype loss in squamous cell carcinoma of the head and neck: clinical and immunogenetic consequences. *Clin Cancer Res* **6**, 2794-802 (2000).

37. Li, H. *et al.* Genomic analysis of head and neck squamous cell carcinoma cell lines and human tumors: a rational approach to preclinical model selection. *Mol Cancer Res* **12**, 571-82 (2014).

38. Coussens, L.M. & Werb, Z. Inflammation and cancer. *Nature* **420**, 860-7 (2002).

39. St John, M.A. *et al.* Proinflammatory mediators upregulate snail in head and neck squamous cell carcinoma. *Clin Cancer Res* **15**, 6018-27 (2009).

40. Marur, S. & Forastiere, A.A. Head and Neck Squamous Cell Carcinoma: Update on Epidemiology, Diagnosis, and Treatment. *Mayo Clin Proc* **91**, 386-96 (2016).

41. Bernier, J. *et al.* Postoperative irradiation with or without concomitant chemotherapy for locally advanced head and neck cancer. *New England Journal of Medicine* **350**, 1945-1952 (2004).

42. Galbiatti, A.L.S. *et al.* Head and neck cancer: causes, prevention and treatment. *Brazilian Journal of Otorhinolaryngology* **79**, 239-247 (2013).

43. Allison, K.H. & Sledge, G.W. Heterogeneity and Cancer. *Oncology-New York* **28**, 772-778 (2014).

44. Meacham, C.E. & Morrison, S.J. Tumour heterogeneity and cancer cell plasticity. *Nature* **501**, 328-337 (2013).

45. Tomczak, K., Czerwinska, P. & Wiznerowicz, M. The Cancer Genome Atlas (TCGA): an immeasurable source of knowledge. *Contemp Oncol (Pozn)* **19**, A68-77 (2015).

46. Zhang, J.J. *et al.* International Cancer Genome Consortium Data Portal-a one-stop shop for cancer genomics data. *Database-the Journal of Biological Databases and Curation* (2011).

47. Yu, K.H. & Snyder, M. Omics Profiling in Precision Oncology. *Molecular & Cellular Proteomics* **15**, 2525-2536 (2016).

48. Tran, B. *et al.* Cancer Genomics: Technology, Discovery, and Translation. *Journal of Clinical Oncology* **30**, 647-660 (2012).

49. He, Y.D. Genomic approach to biomarker identification and its recent applications. *Cancer Biomark* **2**, 103-33 (2006).

50. Jansson, M.D. & Lund, A.H. MicroRNA and cancer. *Mol Oncol* **6**, 590-610 (2012).

51. Prensner, J.R. & Chinnaiyan, A.M. The emergence of lncRNAs in cancer biology. *Cancer Discov* **1**, 391-407 (2011).

52. Kristensen, L.S., Hansen, T.B., Veno, M.T. & Kjems, J. Circular RNAs in cancer: opportunities and challenges in the field. *Oncogene* **37**, 555-565 (2018).

53. Shruthi, B.S., Vinodhkumar, P. & Selvamani. Proteomics: A new perspective for cancer. *Adv Biomed Res* **5**, 67 (2016).

54. Reymond, M.A. & Schlegel, W. Proteomics in cancer. *Adv Clin Chem* **44**, 103-42 (2007).

55. Pastwa, E., Somiari, S.B., Czyz, M. & Somiari, R.I. Proteomics in human cancer research. *Proteomics Clin Appl* **1**, 4-17 (2007).

56. Kuehnbaum, N.L. & Britz-McKibbin, P. New advances in separation science for metabolomics: resolving chemical diversity in a post-genomic era. *Chem Rev* **113**, 2437-68 (2013).

57. Aerts, J.T. *et al.* Patch clamp electrophysiology and capillary electrophoresis-mass spectrometry metabolomics for single cell characterization. *Anal Chem* **86**, 3203-8 (2014).

58. Hooton, K. & Li, L. Nonocclusive Sweat Collection Combined with Chemical Isotope Labeling LC-MS for Human Sweat Metabolomics and Mapping the Sweat Metabolomes at Different Skin Locations. *Analytical Chemistry* **89**, 7847-7851 (2017).

59. Subramanian, A. *et al.* Gene set enrichment analysis: A knowledge-based approach for interpreting genome-wide expression profiles. *Proceedings of the National Academy of Sciences of the United States of America* **102**, 15545-15550 (2005).

60. King, K.L. & Cidlowski, J.A. Cell cycle regulation and apoptosis. *Annual Review of Physiology* **60**, 601-617 (1998).

61. Lim, S.H. & Kaldis, P. Cdks, cyclins and CKIs: roles beyond cell cycle regulation. *Development* **140**, 3079-3093 (2013).

62. Malumbres, M. & Barbacid, M. Cell cycle, CDKs and cancer: a changing paradigm. *Nature Reviews Cancer* **9**, 153-166 (2009).

63. Dang, C.V. c-myc target genes involved in cell growth, apoptosis, and metabolism. *Molecular and Cellular Biology* **19**, 1-11 (1999).

64. Dang, C.V. MYC, Metabolism, Cell Growth, and Tumorigenesis. *Cold Spring Harbor Perspectives in Medicine* **3**(2013).

65. Liu, Z.X., Sun, Q.R. & Wang, X.S. PLK1, A Potential Target for Cancer Therapy. *Translational Oncology* **10**, 22-32 (2017).

66. Prindle, M.J. & Loeb, L.A. DNA polymerase delta in DNA replication and genome maintenance. *Environ Mol Mutagen* **53**, 666-82 (2012).

67. Stoimenov, I. & Helleday, T. PCNA on the crossroad of cancer. *Biochem Soc Trans* **37**, 605-13 (2009).

68. Bishop, A.J. & Schiestl, R.H. Homologous Recombination and Its Role in Carcinogenesis. *J Biomed Biotechnol* **2**, 75-85 (2002).

69. Yin, J. *et al.* Potential Mechanisms Connecting Purine Metabolism and Cancer Therapy. *Front Immunol* **9**, 1697 (2018).

70. Elamin, Y.Y., Rafee, S., Osman, N., KJ, O.B. & Gately, K. Thymidine Phosphorylase in Cancer; Enemy or Friend? *Cancer Microenviron* **9**, 33-43 (2016).

71. Meng, J.H. & Wang, J.F. Role of SNARE proteins in tumourigenesis and their potential as targets for novel anti-cancer therapeutics. *Biochimica Et Biophysica Acta-Reviews on Cancer* **1856**, 1-12 (2015).

72. Steinbichler, T.B., Dudas, J., Riechelmann, H. & Skvortsova, I.I. The role of exosomes in cancer metastasis. *Seminars in Cancer Biology* **44**, 170-181 (2017).

73. Ruiz-Martinez, M. *et al.* YKT6 expression, exosome release, and survival in non-small cell lung cancer. *Oncotarget* **7**, 51515-51524 (2016).

74. Wang, Z.F. & Burge, C.B. Splicing regulation: From a parts list of regulatory elements to an integrated splicing code. *Rna-a Publication of the Rna Society* **14**, 802-813 (2008).

75. van Alphen, R.J., Wiemer, E.A.C., Burger, H. & Eskens, F.A.L.M. The spliceosome as target for anticancer treatment. *British Journal of Cancer* **100**, 228-232 (2009).

76. He, X.L. & Zhang, P. Serine/arginine-rich splicing factor 3 (SRSF3) regulates homologous recombination-mediated DNA repair. *Molecular Cancer* **14**(2015).

77. Voorhees, P.M., Dees, E.C., O'Neil, B. & Orlowski, R.Z. The proteasome as a target for cancer therapy. *Clinical Cancer Research* **9**, 6316-6325 (2003).

78. Zhang, X. *et al.* Proteasome beta-4 subunit contributes to the development of melanoma and is regulated by miR-148b. *Tumour Biol* **39**, 1010428317705767 (2017).

79. Bhagwat, A.S. & Vakoc, C.R. Targeting Transcription Factors in Cancer. *Trends Cancer* **1**, 53-65 (2015).

80. Ribeiro, J.R., Lovasco, L.A., Vanderhyden, B.C. & Freiman, R.N. Targeting TBP-Associated Factors in Ovarian Cancer. *Front Oncol* **4**, 45 (2014).

81. Pinho, S.S. & Reis, C.A. Glycosylation in cancer: mechanisms and clinical implications. *Nat Rev Cancer* **15**, 540-55 (2015).

82. Tominaga, N. *et al.* RPN2-mediated glycosylation of tetraspanin CD63 regulates breast cancer cell malignancy. *Mol Cancer* **13**, 134 (2014).

83. Zheng, J. Energy metabolism of cancer: Glycolysis versus oxidative phosphorylation (Review). *Oncol Lett* **4**, 1151-1157 (2012).

84. Burnichon, N. *et al.* SDHA is a tumor suppressor gene causing paraganglioma. *Human Molecular Genetics* **19**, 3011-3020 (2010).

85. Oudijk, L. *et al.* SDHA mutations in adult and pediatric wild-type gastrointestinal stromal tumors. *Modern Pathology* **26**, 456-463 (2013).

86. Tretter, L., Patocs, A. & Chinopoulos, C. Succinate, an intermediate in metabolism, signal transduction, ROS, hypoxia, and tumorigenesis. *Biochimica Et Biophysica Acta-Bioenergetics* **1857**, 1086-1101 (2016).

87. Chen, W.C. *et al.* Systematic Analysis of Gene Expression Alterations and Clinical Outcomes for Long-Chain Acyl-Coenzyme A Synthetase Family in Cancer. *Plos One* **11**(2016).

88. Pozzi, A. *et al.* Peroxisomal proliferator-activated receptor-alpha-dependent inhibition of endothelial cell proliferation and tumorigenesis. *Journal of Biological Chemistry* **282**, 17685-17695 (2007).

89. Cui, C.C., Merritt, R., Fu, L.W. & Pan, Z. Targeting calcium signaling in cancer therapy. *Acta Pharmaceutica Sinica B* **7**, 3-17 (2017).

90. Bindels, L.B. *et al.* Gut microbiota-derived propionate reduces cancer cell proliferation in the liver. *British Journal of Cancer* **107**, 1337-1344 (2012).

91. Andresen, L. *et al.* Propionic Acid Secreted from Propionibacteria Induces NKG2D Ligand Expression on Human-Activated T Lymphocytes and Cancer Cells. *Journal of Immunology* **183**, 897-906 (2009).

92. Andriamihaja, M., Chaumontet, C., Tome, D. & Blachier, F. Butyrate Metabolism in Human Colon Carcinoma Cells: Implications Concerning Its Growth-Inhibitory Effect. *Journal of Cellular Physiology* **218**, 58-65 (2009).

93. Whitmore, S.E. & Lamont, R.J. Oral Bacteria and Cancer. *Plos Pathogens* **10**(2014).

94. Qu, Q., Zeng, F., Liu, X., Wang, Q.J. & Deng, F. Fatty acid oxidation and carnitine palmitoyltransferase I: emerging therapeutic targets in cancer. *Cell Death & Disease* **7**(2016).

95. Newgard, C.B. *et al.* A Branched-Chain Amino Acid-Related Metabolic Signature that Differentiates Obese and Lean Humans and Contributes to Insulin Resistance. *Cell Metabolism* **9**, 311-326 (2009).

96. Fujiwara, N. *et al.* CPT2 downregulation adapts HCC to lipid-rich environment and promotes carcinogenesis via acylcarnitine accumulation in obesity. *Gut* **67**, 1493-1504 (2018).

97. Ganti, S. *et al.* Urinary acylcarnitines are altered in human kidney cancer. *International Journal of Cancer* **130**, 2791-2800 (2012).

98. Pyne, N.J., El Buri, A., Adams, D.R. & Pyne, S. Sphingosine 1-phosphate and cancer. *Adv Biol Regul* **68**, 97-106 (2018).

99. Pyne, N.J. & Pyne, S. Sphingosine 1-phosphate and cancer. *Nat Rev Cancer* **10**, 489-503 (2010).

100. Hakem, R. DNA-damage repair; the good, the bad, and the ugly. *EMBO J* **27**, 589-605 (2008).

101. Yi, C. & He, C. DNA repair by reversal of DNA damage. *Cold Spring Harb Perspect Biol* **5**, a012575 (2013).

102. Lukey, M.J., Katt, W.P. & Cerione, R.A. Targeting amino acid metabolism for cancer therapy. *Drug Discov Today* **22**, 796-804 (2017).

103. Tsun, Z.Y. & Possemato, R. Amino acid management in cancer. *Semin Cell Dev Biol* **43**, 22-32 (2015).

104. Comelli, E.M. *et al.* A focused microarray approach to functional glycomics: transcriptional regulation of the glycome. *Glycobiology* **16**, 117-31 (2006).

105. Wice, B.M. *et al.* The Intracellular Accumulation of Udp-N-Acetylhexosamines Is Concomitant with the Inability of Human-Colon Cancer-Cells to Differentiate. *Journal of Biological Chemistry* **260**, 139-146 (1985).

106. Sasai, K., Ikeda, Y., Fujii, T., Tsuda, T. & Taniguchi, N. UDP-GlcNAc concentration is an important factor in the biosynthesis of beta 1,6-branched oligosaccharides: regulation based on the kinetic properties of N-acetylglucosaminyltransferase V. *Glycobiology* **12**, 119-127 (2002).

107. Rohrig, F. & Schulze, A. The multifaceted roles of fatty acid synthesis in cancer. *Nature Reviews Cancer* **16**, 732-749 (2016).

108. Santos, C.R. & Schulze, A. Lipid metabolism in cancer. *Febs Journal* **279**, 2610-2623 (2012).

109. Majidinia, M. *et al.* Melatonin: A pleiotropic molecule that modulates DNA damage response and repair pathways. *Journal of Pineal Research* **63**(2017).

110. Brzezinski, A. Melatonin in humans. *N Engl J Med* **336**, 186-95 (1997).

111. Feldman, D., Krishnan, A.V., Swami, S., Giovannucci, E. & Feldman, B.J. The role of vitamin D in reducing cancer risk and progression. *Nat Rev Cancer* **14**, 342-57 (2014).

112. Tuohimaa, P. *et al.* Calcidiol and prostate cancer. *J Steroid Biochem Mol Biol* **93**, 183-90 (2005).

113. Hodges, S., Hertz, N., Lockwood, K. & Lister, R. CoQ10: could it have a role in cancer management? *Biofactors* **9**, 365-70 (1999).

114. Das, B.C. *et al.* Retinoic acid signaling pathways in development and diseases. *Bioorg Med Chem* **22**, 673-83 (2014).

115. Van heusden, J. *et al.* All-trans-retinoic acid metabolites significantly inhibit the proliferation of MCF-7 human breast cancer cells in vitro. *Br J Cancer* **77**, 26-32 (1998).

116. Gjaltema, R.A.F. & Bank, R.A. Molecular insights into prolyl and lysyl hydroxylation of fibrillar collagens in health and disease. *Critical Reviews in Biochemistry and Molecular Biology* **52**, 74-95 (2017).

117. Myllyla, R. *et al.* Expanding the lysyl hydroxylase toolbox: new insights into the localization and activities of lysyl hydroxylase 3 (LH3). *J Cell Physiol* **212**, 323-9 (2007).

118. Valtavaara, M., Szpirer, C., Szpirer, J. & Myllyla, R. Primary structure, tissue distribution, and chromosomal localization of a novel isoform of lysyl hydroxylase (lysyl hydroxylase 3). *J Biol Chem* **273**, 12881-6 (1998).

119. Rautavuoma, K., Passoja, K., Helaakoski, T. & Kivirikko, K.I. Complete exon-intron organization of the gene for human lysyl hydroxylase 3 (LH3). *Matrix Biol* **19**, 73-9 (2000).

120. Ruotsalainen, H., Sipila, L., Kerkela, E., Pospiech, H. & Myllyla, R. Characterization of cDNAs for mouse lysyl hydroxylase 1, 2 and 3, their phylogenetic analysis and tissue-specific expression in the mouse. *Matrix Biol* **18**, 325-9 (1999).

121. Myllyharju, J. & Kivirikko, K.I. Collagens, modifying enzymes and their mutations in humans, flies and worms. *Trends in Genetics* **20**, 33-43 (2004).

122. Yamauchi, M. & Shiiba, M. Lysine hydroxylation and cross-linking of collagen. *Methods Mol Biol* **446**, 95-108 (2008).

123. Yamauchi, M. & Sricholpech, M. Lysine post-translational modifications of collagen. *Essays Biochem* **52**, 113-33 (2012).

124. Heikkinen, J. *et al.* Dimerization of human lysyl hydroxylase 3 (LH3) is mediated by the amino acids 541-547. *Matrix Biology* **30**, 27-33 (2011).

125. Ruotsalainen, H. *et al.* Glycosylation catalyzed by lysyl hydroxylase 3 is essential for basement membranes. *Journal of Cell Science* **119**, 625-635 (2006).

126. Sipila, L. *et al.* Secretion and assembly of type IV and VI collagens depend on glycosylation of hydroxylysines. *Journal of Biological Chemistry* **282**, 33381-33388 (2007).

127. Ihme, A. *et al.* Ehlers-Danlos Syndrome Type-Vi - Collagen Type Specificity of Defective Lysyl Hydroxylation in Various Tissues. *Journal of Investigative Dermatology* **83**, 161-165 (1984).

128. Sricholpech, M. *et al.* Lysyl Hydroxylase 3 Glucosylates Galactosylhydroxylysine Residues in Type I Collagen in Osteoblast Culture. *Journal of Biological Chemistry* **286**, 8846-8856 (2011).

129. Sricholpech, M. *et al.* Lysyl Hydroxylase 3-mediated Glucosylation in Type I Collagen MOLECULAR LOCI AND BIOLOGICAL SIGNIFICANCE. *Journal of Biological Chemistry* **287**, 22998-23009 (2012).

130. Uzawa, K. *et al.* Differential expression of human lysyl hydroxylase genes, lysine hydroxylation, and cross-linking of type I collagen during osteoblastic differentiation in vitro. *Journal of Bone and Mineral Research* **14**, 1272-1280 (1999).

131. Risteli, M. *et al.* Reduction of Lysyl Hydroxylase 3 Causes Deleterious Changes in the Deposition and Organization of Extracellular Matrix. *Journal of Biological Chemistry* **284**, 28204-28211 (2009).

132. Wang, C.G. *et al.* Identification of amino acids important for the catalytic activity of the collagen glucosyltransferase associated with the multifunctional lysyl hydroxylase 3 (LH3). *Journal of Biological Chemistry* **277**, 18568-18573 (2002).

133. Ruotsalainen, H. *et al.* The Activities of Lysyl Hydroxylase 3 (LH3) Regulate the Amount and Oligomerization Status of Adiponectin. *Plos One* **7**(2012).

134. Risteli, M. *et al.* Lysyl Hydroxylase 3 Modifies Lysine Residues to Facilitate Oligomerization of Mannan-Binding Lectin. *Plos One* **9**(2014).

135. Salo, A.M. *et al.* Lysyl hydroxylase 3 (LH3) modifies proteins in the extracellular space, a novel mechanism for matrix remodeling. *Journal of Cellular Physiology* **207**, 644-653 (2006).

136. Wang, C.G., Ristiluoma, M.M., Salo, A.M., Eskelinen, S. & Myllyla, R. Lysyl hydroxylase 3 is secreted from cells by two pathways. *Journal of Cellular Physiology* **227**, 668-675 (2012).

137. Rautavuoma, K. *et al.* Premature aggregation of type IV collagen and early lethality in lysyl hydroxylase 3 null mice. *Proceedings of the National Academy of Sciences of the United States of America* **101**, 14120-14125 (2004).

138. Isaacman-Beck, J., Schneider, V., Franzini-Armstrong, C. & Granato, M. The lh3 Glycosyltransferase Directs Target-Selective Peripheral Nerve Regeneration. *Neuron* **88**, 691-703 (2015).

139. Banerjee, S., Isaacman-Beck, J., Schneider, V.A. & Granato, M. A Novel Role for Lh3 Dependent ECM Modifications during Neural Crest Cell Migration in Zebrafish. *Plos One* **8**(2013).

140. Dayer, C. & Stamenkovic, I. Recruitment of Matrix Metalloproteinase-9 (MMP-9) to the Fibroblast Cell Surface by Lysyl Hydroxylase 3 (LH3) Triggers Transforming Growth Factor-beta (TGF-beta) Activation and Fibroblast Differentiation. *Journal of Biological Chemistry* **290**, 13763-13778 (2015).

141. Amodio, G. *et al.* Identification of a microRNA (miR-663a) induced by ER stress and its target gene PLOD3 by a combined microRNome and proteome approach. *Cell Biology and Toxicology* **32**, 285-303 (2016).

142. Watt, S.A. *et al.* Lysyl Hydroxylase 3 Localizes to Epidermal Basement Membrane and Is Reduced in Patients with Recessive Dystrophic Epidermolysis Bullosa. *Plos One* **10**(2015).

143. Salo, A.M. *et al.* A Connective Tissue Disorder Caused by Mutations of the Lysyl Hydroxylase 3 Gene. *American Journal of Human Genetics* **83**, 495-503 (2008).

144. Cheng, L. *et al.* Identification of genes with a correlation between copy number and expression in gastric cancer. *Bmc Medical Genomics* **5**(2012).

145. Nicastri, A. *et al.* N-Glycoprotein Analysis Discovers New Up-Regulated Glycoproteins in Colorectal Cancer Tissue. *Journal of Proteome Research* **13**, 4932-4941 (2014).

146. Schiarea, S. *et al.* Secretome Analysis of Multiple Pancreatic Cancer Cell Lines Reveals Perturbations of Key Functional Networks. *Journal of Proteome Research* **9**, 4376-4392 (2010).

147. Tsai, C.K. *et al.* Overexpression of PLOD3 promotes tumor progression and poor prognosis in gliomas. *Oncotarget* **9**, 15705-15720 (2018).

148. Zhao, X.Y., Sun, S.Y., Zeng, X.Q. & Cui, L. Expression profiles analysis identifies a novel three-mRNA signature to predict overall survival in oral squamous cell carcinoma. *American Journal of Cancer Research* **8**, 450-461 (2018).

149. Molinolo, A.A. *et al.* Dysregulated molecular networks in head and neck carcinogenesis. *Oral Oncology* **45**, 324-334 (2009).

150. Barrett, T. & Edgar, R. Mining microarray data at NCBI's Gene Expression Omnibus (GEO)*. *Methods Mol Biol* **338**, 175-90 (2006).

151. Clough, E. & Barrett, T. The Gene Expression Omnibus Database. *Methods Mol Biol* **1418**, 93-110 (2016).

152. Lee, J.S. Exploring cancer genomic data from the cancer genome atlas project. *BMB Rep* **49**, 607-611 (2016).

153. Nilsson, R. *et al.* Metabolic enzyme expression highlights a key role for MTHFD2 and the mitochondrial folate pathway in cancer. *Nat Commun* **5**, 3128 (2014).

154. Shen, Q. *et al.* Barrier to autointegration factor 1, procollagen-lysine, 2-oxoglutarate 5-dioxygenase 3, and splicing factor 3b subunit 4 as early-stage cancer decision markers and drivers of hepatocellular carcinoma. *Hepatology* **67**, 1360-1377 (2018).

155. Liu, W., Zhang, T., Guo, L., Wang, Y. & Yang, Y. Lysyl hydroxylases are transcription targets for GATA3 driving lung cancer cell metastasis. *Sci Rep* **8**, 11905 (2018).

156. Yun, H.S. *et al.* Radiotherapy diagnostic biomarkers in radioresistant human H460 lung cancer stem-like cells. *Cancer Biol Ther* **17**, 208-18 (2016).

157. Acunzo, M., Romano, G., Wernicke, D. & Croce, C.M. MicroRNA and cancer--a brief overview. *Adv Biol Regul* **57**, 1-9 (2015).

158. Wightman, B., Ha, I. & Ruvkun, G. Posttranscriptional regulation of the heterochronic gene lin-14 by lin-4 mediates temporal pattern formation in C. elegans. *Cell* **75**, 855-62 (1993).

159. Lee, R.C., Feinbaum, R.L. & Ambros, V. The C. elegans heterochronic gene lin-4 encodes small RNAs with antisense complementarity to lin-14. *Cell* **75**, 843-54 (1993).

160. Bartel, D.P. MicroRNAs: genomics, biogenesis, mechanism, and function. *Cell* **116**, 281-97 (2004).

161. Krol, J., Loedige, I. & Filipowicz, W. The widespread regulation of microRNA biogenesis, function and decay. *Nat Rev Genet* **11**, 597-610 (2010).

162. Hayes, J., Peruzzi, P.P. & Lawler, S. MicroRNAs in cancer: biomarkers, functions and therapy. *Trends Mol Med* **20**, 460-9 (2014).

163. Rodriguez, A., Griffiths-Jones, S., Ashurst, J.L. & Bradley, A. Identification of mammalian microRNA host genes and transcription units. *Genome Res* **14**, 1902-10 (2004).

164. Lin, S.L., Kim, H. & Ying, S.Y. Intron-mediated RNA interference and microRNA (miRNA). *Front Biosci* **13**, 2216-30 (2008).

165. Denli, A.M., Tops, B.B., Plasterk, R.H., Ketting, R.F. & Hannon, G.J. Processing of primary microRNAs by the Microprocessor complex. *Nature* **432**, 231-5 (2004).

166. Cullen, B.R. Transcription and processing of human microRNA precursors. *Mol Cell* **16**, 861-5 (2004).

167. Felekkis, K., Touvana, E., Stefanou, C. & Deltas, C. microRNAs: a newly described class of encoded molecules that play a role in health and disease. *Hippokratia* **14**, 236-240 (2010).

168. Farazi, T.A., Hoell, J.I., Morozov, P. & Tuschl, T. MicroRNAs in Human Cancer. *Microrna Cancer Regulation: Advanced Concepts, Bioinformatics and Systems Biology Tools* **774**, 1-20 (2013).

169. Huang, Y. *et al.* Biological functions of microRNAs: a review. *J Physiol Biochem* **67**, 129-39 (2011).

170. Huang, Y., Shen, X.J., Zou, Q. & Zhao, Q.L. Biological functions of microRNAs. *Bioorg Khim* **36**, 747-52 (2010).

171. Ardekani, A.M. & Naeini, M.M. The Role of MicroRNAs in Human Diseases. *Avicenna J Med Biotechnol* **2**, 161-79 (2010).

172. Sayed, D. & Abdellatif, M. MicroRNAs in development and disease. *Physiol Rev* **91**, 827-87 (2011).

173. Rosenfeld, N. *et al.* MicroRNAs accurately identify cancer tissue origin. *Nat Biotechnol* **26**, 462-9 (2008).

174. Bissey, P.A. *et al.* Dysregulation of the MiR-449b target TGFBI alters the TGF beta pathway to induce cisplatin resistance in nasopharyngeal carcinoma. *Oncogenesis* **7**(2018).

175. Ziebarth, J.D., Bhattacharya, A. & Cui, Y. Integrative Analysis of Somatic Mutations Altering MicroRNA Targeting in Cancer Genomes. *Plos One* **7**(2012).

176. Blondal, T. *et al.* Assessing sample and miRNA profile quality in serum and plasma or other biofluids. *Methods* **59**, S1-S6 (2013).

177. Mitchell, P.S. *et al.* Circulating microRNAs as stable blood-based markers for cancer detection. *Proceedings of the National Academy of Sciences of the United States of America* **105**, 10513-10518 (2008).

178. Hung, K.F. *et al.* MicroRNA-31 upregulation predicts increased risk of progression of oral potentially malignant disorder. *Oral Oncology* **53**, 42-47 (2016).

179. Liu, C.J. *et al.* miR-134 induces oncogenicity and metastasis in head and neck carcinoma through targeting WWOX gene. *International Journal of Cancer* **134**, 811-821 (2014).

180. Zhang, L., Sun, Z.J., Bian, Y.S. & Kulkarni, A.B. MicroRNA-135b acts as a tumor promoter by targeting the hypoxia-inducible factor pathway in genetically defined mouse model of head and neck squamous cell carcinoma. *Cancer Letters* **331**, 230-238 (2013).

181. Nohata, N. *et al.* Tumour-suppressive microRNA-874 contributes to cell proliferation through targeting of histone deacetylase 1 in head and neck squamous cell carcinoma. *British Journal of Cancer* **108**, 1648-1658 (2013).

182. Nakanishi, H. *et al.* Loss of miR-125b-1 contributes to head and neck cancer development by dysregulating TACSTD2 and MAPK pathway. *Oncogene* **33**, 702-712 (2014).

183. Pylayeva, Y. *et al.* Ras- and PI3K-dependent breast tumorigenesis in mice and humans requires focal adhesion kinase signaling. *Journal of Clinical Investigation* **119**, 252-266 (2009).

184. Schaller, M.D. Cellular functions of FAK kinases: insight into molecular mechanisms and novel functions. *Journal of Cell Science* **123**, 1007-1013 (2010).

185. Lee, B.Y., Timpson, P., Horvath, L.G. & Daly, R.J. FAK signaling in human cancer as a target for therapeutics. *Pharmacology & Therapeutics* **146**, 132-149 (2015).

186. Schaller, M.D. *et al.* Autophosphorylation of the Focal Adhesion Kinase, Pp125(Fak), Directs Sh2 Dependent Binding of Pp60(Src). *Molecular and Cellular Biology* **14**, 1680-1688 (1994).

187. Schlaepfer, D.D., Hanks, S.K., Hunter, T. & Vandergeer, P. Integrin-Mediated Signal-Transduction Linked to Ras Pathway by Grb2 Binding to Focal Adhesion Kinase. *Nature* **372**, 786-791 (1994).

188. Infante, J.R. *et al.* Safety, Pharmacokinetic, and Pharmacodynamic Phase I Dose-Escalation Trial of PF-00562271, an Inhibitor of Focal Adhesion Kinase, in Advanced Solid Tumors. *Journal of Clinical Oncology* **30**, 1527-1533 (2012).

189. Soria, J.C. *et al.* A phase I, pharmacokinetic and pharmacodynamic study of GSK2256098, a focal adhesion kinase inhibitor, in patients with advanced solid tumors. *Annals of Oncology* **27**, 2268-2274 (2016).

190. Skinner, H.D. *et al.* Proteomic Profiling Identifies PTK2/FAK as a Driver of Radioresistance in HPV-negative Head and Neck Cancer. *Clinical Cancer Research* **22**, 4643-4650 (2016).

191. Simpson, D.R., Mell, L.K. & Cohen, E.E.W. Targeting the PI3K/AKT/mTOR pathway in squamous cell carcinoma of the head and neck. *Oral Oncology* **51**, 291-298 (2015).

192. Garzon, R., Marcucci, G. & Croce, C.M. Targeting microRNAs in cancer: rationale, strategies and challenges. *Nature Reviews Drug Discovery* **9**, 775-789 (2010).

193. Kwak, P.B., Iwasaki, S. & Tomari, Y. The microRNA pathway and cancer. *Cancer Science* **101**, 2309-2315 (2010).

194. Lagos-Quintana, M. *et al.* Identification of tissue-specific microRNAs from mouse. *Current Biology* **12**, 735-739 (2002).

195. Neo, W.H. *et al.* MicroRNA miR-124 Controls the Choice between Neuronal and Astrocyte Differentiation by Fine-tuning Ezh2 Expression. *Journal of Biological Chemistry* **289**, 20788-20801 (2014).

196. Clark, A.M. *et al.* The microRNA miR-124 controls gene expression in the sensory nervous system of Caenorhabditis elegans. *Nucleic Acids Research* **38**, 3780-3793 (2010).

197. Sanuki, R. *et al.* miR-124a is required for hippocampal axogenesis and retinal cone survival through Lhx2 suppression. *Nature Neuroscience* **14**, 1125-U177 (2011).

198. Yoo, A.S. *et al.* MicroRNA-mediated conversion of human fibroblasts to neurons. *Nature* **476**, 228-U123 (2011).

199. Mondanizadeh, M. *et al.* MicroRNA-124 Regulates Neuronal Differentiation of Mesenchymal Stem Cells by Targeting Sp1 mRNA. *Journal of Cellular Biochemistry* **116**, 943-953 (2015).

200. Santos, M.C.T. *et al.* miR-124,-128, and-137 Orchestrate Neural Differentiation by Acting on Overlapping Gene Sets Containing a Highly Connected Transcription Factor Network. *Stem Cells* **34**, 220-232 (2016).

201. Choe, N. *et al.* The microRNA miR-124 inhibits vascular smooth muscle cell proliferation by targeting S100 calcium-binding protein A4 (S100A4). *Febs Letters* **591**, 1041-1052 (2017).

202. Qadir, A.S. *et al.* miR-124 Negatively Regulates Osteogenic Differentiation and In vivo Bone Formation of Mesenchymal Stem Cells. *Journal of Cellular Biochemistry* **116**, 730-742 (2015).

203. Qadir, A.S. *et al.* MiR-124 Inhibits Myogenic Differentiation of Mesenchymal Stem Cells Via Targeting Dlx5. *Journal of Cellular Biochemistry* **115**, 1572-1581 (2014).

204. Sun, Y. *et al.* MicroRNA-124 mediates the cholinergic anti-inflammatory action through inhibiting the production of pro-inflammatory cytokines. *Cell Research* **23**, 1270-1283 (2013).

205. Qin, Z., Wang, P.Y., Su, D.F. & Liu, X. miRNA-124 in Immune System and Immune Disorders. *Frontiers in Immunology* **7**(2016).

206. Zhao, Y. *et al.* MiR-124 acts as a tumor suppressor by inhibiting the expression of sphingosine kinase 1 and its downstream signaling in head and neck squamous cell carcinoma. *Oncotarget* **8**, 25005-25020 (2017).

207. Li, X., Fan, Q.Q., Li, J.Y., Song, J. & Gu, Y.C. MiR-124 down-regulation is critical for cancer associated fibroblasts-enhanced tumor growth of oral carcinoma. *Experimental Cell Research* **351**, 100-108 (2017).

208. Wang, X.S. *et al.* miR-124 exerts tumor suppressive functions on the cell proliferation, motility and angiogenesis of bladder cancer by fine-tuning UHRF1. *Febs Journal* **282**, 4376-4388 (2015).

209. Cai, W.L. *et al.* microRNA-124 inhibits bone metastasis of breast cancer by repressing Interleukin-11. *Molecular Cancer* **17**(2018).

210. Zhang, G.L. *et al.* miRNA-124-3p/neuropilin-1(NRP-1) axis plays an important role in mediating glioblastoma growth and angiogenesis. *International Journal of Cancer* **143**, 635-644 (2018).

211. Bishop, A.J.R. & Schiestl, R.H. Role of homologous recombination in carcinogenesis. *Experimental and Molecular Pathology* **74**, 94-105 (2003).

212. Nyhan, W.L. Disorders of purine and pyrimidine metabolism. *Molecular Genetics and Metabolism* **86**, 25-33 (2005).

213. Lane, A.N. & Fan, T.W.M. Regulation of mammalian nucleotide metabolism and biosynthesis. *Nucleic Acids Research* **43**, 2466-2485 (2015).

214. Cukierman, E., Pankov, R., Stevens, D.R. & Yamada, K.M. Taking cell-matrix adhesions to the third dimension. *Science* **294**, 1708-1712 (2001).

215. Chatzizacharias, N.A., Kouraklis, G.P. & Theocharis, S.E. Clinical significance of FAK expression in human neoplasia. *Histology and Histopathology* **23**, 629-650 (2008).

216. Hembruff, S.L. & Cheng, N. Chemokine signaling in cancer: Implications on the tumor microenvironment and therapeutic targeting. *Cancer Ther* **7**, 254-267 (2009).

217. Ciechanover, A., Orian, A. & Schwartz, A.L. Ubiquitin-mediated proteolysis: biological regulation via destruction. *Bioessays* **22**, 442-451 (2000).

218. Peng, X. & Guan, J.L. Focal Adhesion Kinase: From In Vitro Studies to Functional Analyses In Vivo. *Current Protein & Peptide Science* **12**, 52-67 (2011).

219. Yoon, H., Dehart, J.P., Murphy, J.M. & Lim, S.T.S. Understanding the Roles of FAK in Cancer: Inhibitors, Genetic Models, and New Insights. *Journal of Histochemistry & Cytochemistry* **63**, 114-128 (2015).

220. Engelman, J.A. Targeting PI3K signalling in cancer: opportunities, challenges and limitations. *Nature Reviews Cancer* **9**, 550-562 (2009).

221. Luo, J., Manning, B.D. & Cantley, L.C. Targeting the PI3K-Akt pathway in human cancer: Rationale and promise. *Cancer Cell* **4**, 257-262 (2003).